Transmission of broadband acoustic signals through saturated granular media.

Thomas, P. R.

Award date:
1978

Awarding institution:
University of Bath

TRANSMISSION OF BROADBAND ACOUSTIC SIGNALS THROUGH SATURATED GRANULAR MEDIA

Submitted by P.R. Thomas, B.Sc.

for the degree of Ph.D.

of the University of Bath

1978

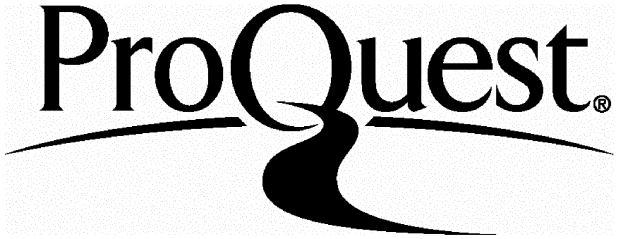

ABSTRACT

A correlation technique is developed which enables acoustic transmission measurements to be made in a laboratory tank on air-free samples of real and artificial marine sediments. Measurements of acoustic velocity and transmission loss are presented over a frequency range of 80 kHz to 320 kHz for water saturated granular materials having mean grain diameters ranging from 50 μ to 8000 μs.

The transmission loss figures are converted into a surface transmission loss, which is shown to be frequency independent and a volume transmission loss, which is shown to be linearly dependent on frequency over the range where the wavelength of the acoustic energy is greater than the particle size. The acoustic velocity, the surface transmission loss and the volume transmission loss are related to the physical properties of the samples, the mean grain size, phi-deviation, porosity, permeability and solid density. Velocity is shown to be directly related to mean grain size, porosity and phi-deviation and inter-grain friction is shown to be the dominant attenuation mechanism.

ACKNOWLEDGEMENTS

I should like to express my sincere gratitude to Professor W.D. Chesterman and to Dr. N.G. Pace for their invaluable guidance and encouragement throughout the duration of this project.

I should also like to thank Mr. R. Ceen for some enlightening discussions and for his practical assistance in the design and construction of equipment.

I am also indebted to Mr. B. Ring and the physics technicians for their expertise and guidance.

My thanks also go to Miss J.A. Lindquist and Miss L.M. Cox for their assistance in typing and collating this thesis.

The work was supported by a Research Studentship from the Natural Environment Research Council.

CONTENTS

Chapter 1

THE ACOUSTIC PROPERTIES OF SATURATED GRANULAR MATERIALS

1.1. Introduction

The transmission of acoustic energy through water saturated granular materials and the relationship between the acoustic and physical properties of such structures have been studied using different techniques for several decades with varying degrees of success.

Before discussing the techniques developed here in detail it is of value to look at the reasons behind such studies and to note the important parameters.

1.2. Why are acoustic properties important?

The majority of methods used to make studies of the sea-bed or other underwater structures rely on the analysis of an acoustic signal that has been either reflected from the surface of a "target" or has been transmitted through it. The acoustic signal used for such studies is usually in the form of a short pulse, the length of which limits the definition of the system.

The analysis of the return signal can provide information on the acoustic properties of the target object, including:-

(1) The velocity of sound propagation through the target.

(2) The attenuation of sound on transmission through the target.

(3) The backscattering coefficient

(4) The acoustic impedence of the target.

These measured acoustic properties are then used to either identify the structure, or, more specifically, to classify its physical properties.

This study is aimed at determining the relationships between the acoustic and physical properties of water-saturated granular materials simulating the first few centimetres of the sea-bed. The relationships are very important as they dictate the reliability with which marine sediments can be distinguished. The work is concerned with the transmission of acoustic signals and therefore has particular relevance to sub-bottom profiling and significant implications to all marine survey systems where transmissions through unconsolidated sediments on the sea-bed are observed.

The identification of marine sediments by the analysis of reflected acoustic signals presupposes a knowledge of the relationships between the acoustic and physical properties of the material. This can be done directly or may, in some cases, be done indirectly by comparison with 'known' data.

The acoustic properties that are discussed here are the propagation velocity and the attenuation as a function of frequency between 80 and 320 KHz. The main physical properties of interest are the grain size and size distribution, the porosity of the matrix, the permeability and the packing structure.

1.3. Explanation of terms

To avoid any confusion it is worth, at this stage, defining some of the terms that will be used during the subsequent discussion.

(i) Saturated porous granular medium

Saturated porous granular medium defines a medium composed of two constituents, one solid, one fluid. The 'framework', or part of the medium which would remain if the pore filler were removed, is composed of individual solid grains that are not bonded together. The pores are totally filled with the saturating medium, no air pockets or bubbles being present.

(ii) Porosity

Porosity is the ratio of the volume of the pore-filler to the total volume of the medium.

(iii) Attenuation

Throughout this work, attenuation will be used to define energy loss in the medium. This includes energy loss due to scattering and energy loss due to absorption or internal dissipation in the medium.

Attenuation is usually defined in terms of the attenuation coefficient (Heuter and Bolt, 1955) which together with the sound velocity, c, describes the propagation of plane waves in an attenuating medium.

$$A_x = A_o e^{jw(t - \frac{x}{c})} e^{-\alpha x} \qquad 1.1$$

where A_o = amplitude at x = o

w = the angular frequency

c = the velocity of propagation of compressional waves in the medium

α = the spatial attenuation coefficient

All equations showing the dependence of attenuation on frequency are expressed in the form

$$\alpha = kf^n \qquad 1.2$$

where k = constant

f = the frequency in KHz

n = the exponent of frequency

Chapter 2

INVESTIGATIONS INTO THE TRANSMISSION OF ACOUSTIC ENERGY THROUGH SATURATED GRANULAR MEDIA

2.1. Introduction

The work that has already been carried out in this field can best be divided into three categories.

(1) Theoretical studies

(2) Laboratory experimental studies

(3) Experimental studies of in situ real sediments

The principal objective of this work was to consider the practical aspects of the problem and hence only limited reference will be made to the theoretical side. This chapter will discuss briefly some of the available literature on the first category mentioned and will look in greater detail at references considering the two practical categories.

2.2. Theoretical Studies

The ideal theoretical solution to the problem would be a simple mathematical model which could describe the propagation of compressional waves in terms of the physical properties of the sediment through which the wave is being transmitted. Because of the complex and irregular structure of marine sediments, however, it is impossible to describe perfectly such a system in terms of one simple model, and any attempts to do so can only be approximations. The main problems in creating such a model are:-

1. What are the shapes of the individual grains and how are they arranged

spatially?

2. What happens at the grain to grain boundaries? What are the forces involved, does slipping occur?
3. Should the particles be considered to be moving or stationary with respect to the fluid? What is the degree of coupling between solid and fluid motions?

Nolle (1963) discusses the question of particle movement and shows that if the particles are at rest then the sound velocity is given by

$$C = (B/\rho_m)^{\frac{1}{2}} \qquad 2.1$$

where B = bulk modulus of the mixture

ρ_m = effective density of the liquid

The bulk modulus of the mixture being defined such that when unit hydrostatic pressure is applied to unit volume of the mixture the volume decrease is the sum of the decreases of the sand and liquid. That is

$$\frac{1}{B} = \frac{h}{B_l} + \frac{(1 - h)}{B_s} \qquad 2.2$$

where B_l = bulk modulus of liquid

B_s = bulk modulus of solid

h = porosity of the sediment matrix

This assumes no elastic behaviour of the sand skeleton which is in keeping with Gassman's (1951) studies of acoustical properties of glass spheres.

An effective density is used to account for the irregularities of flow through the sediment. Indirect paths through the sand prevent flow everywhere being in the direction of wave propagation causing some pockets to be virtually stagnant.

This effective density is obtained by dividing the true density by the effective porosity.

$$\rho_m = \frac{\rho}{(h/k)} \quad \text{(Where K is a constant.)} \qquad 2.3$$

The value of (k/h) was evaluated by Ferrero and Sacerdote (1951) in their studies of the acoustic properties of airfilled sands and shown to be approximately 4.3.

If this value for the constant is used in equations 2.1, 2.2 and 2.3, then the speed of sound in the mixture comes out to be less than the velocity in the water, a result not normally observed experimentally indicating, probably, that the assumption of stationary particles was incorrect.

Urick (1947) pointed out that if the particles are small compared to the wave length and move with the fluid, the sound velocity in the sediment may be calculated using the ordinary relationship for a fluid, equation 2.1, using the composite value for the bulk modulus and the total mass of solid and fluid per unit volume of the density. Nolle showed that this gives an answer for the velocity through water-filled packed sand of $1.64 \times 10^3 m.s.^{-1}$ which is in much better agreement with practically observed figures.

If it is therefore accepted that the particles are mobile it is then necessary to know to what extent they follow the motion of the fluid.

Morse (1952) in order to account for the large acoustic attenuation computed the velocity of acoustic wave propagation on the basis of particles moving with the fluid, and then computed an attenuation figure on the basis of a relative velocity between the two and an associated resistance coefficient.

Some of the best theoretical papers on the subject were written by Biot (1955 & 1956). Biot considered the problems of propagation of elastic waves through a porous elastic solid saturated by a viscous fluid in two sections, the low frequency range where Pouseille flow is valid, and the higher frequency region where the assumption breaks down. The limiting frequency at which point the Poiseuille flow breaks down was shown by Kirchoff to be dependant on the kinematic viscosity of the fluid and the size of the pores through which the flow is occurring.

In his approach Biot derived the macroscopic stress-strain relation of the medium by assuming the existence of a strain energy density function. The degree of coupling between the solid matrix and the fluid was taken into consideration in the kinetic energy of the system by introducing a mass coupling parameter and the damping effect of the containing fluid was considered in the dissipation energy. This dissipation energy was expressed in terms of the relative velocity between the fluid and the solid.

Biot's theory predicts the existence of two attenuated dilational waves and one attenuated rotational wave. With the exception of Patterson, (1956) experimental investigation on the wave motions in fluid saturated porous media do not agree with this result.

Yew and Jogi (1976) used a sonic pulse technique to observe velocity and attenuation in a fluid saturated porous specimen sandwiched between a pair of resonant-frequency matched piezoelectric crystal discs. (figure 2.1)

Consistent with the experimental arrangement Yew and Jogi solved Biot's equation using a Laplace transformation and, by comparison of the theoretically predicted result and the practical observations showed that the measured waves were the fast waves. The slow waves were shown to decay in amplitude much faster than the higher velocity waves indicating that it would be very difficult to observe both waves unless a very short specimen was used.

It was also shown that although the fast waves exhibit little or no dispersion, the slow waves are highly dispersive, the phase velocity, however, reaching a constant value at high frequencies.

2.3. Dissipation of compressional wave energy

Compressional wave energy can be lost from a plane wave travelling through a water-saturated sediment by three distinct mechanisms

(1) Rayleigh scattering

(2) Solid friction losses (particle-particle losses)

(3) Viscous losses (particle-fluid losses)

When the wavelength of the acoustic signal is much greater than the particle size Rayleigh scattering is not an important loss mechanism. At higher frequencies or larger particle size, however, this becomes a major loss factor giving rise to an amplitude loss proportional to the

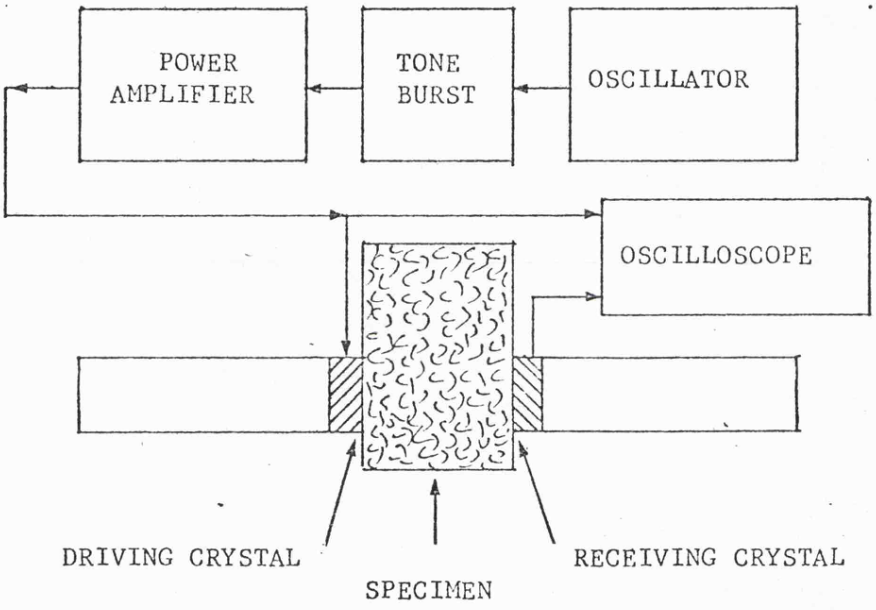

Figure 2.1 Experimental arrangement used by Yew and Jogi

fourth power of frequency.

Solid friction losses occur at the points of contact of the particles and according to work done by Hunter et al (1961), are characterised by a linear dependance on frequency. These losses depend on the shape, texture and size distribution of the individual grains and also the confining pressure.

Viscous losses are caused by the acoustic velocity differential between the solid particles and the fluid, and form the basis of the discussion by Biot in his papers (56a & 56b) previously mentioned.

2.4. Experimental studies in the laboratory

A number of methods have been used to investigate the acoustic properties of marine sediments in the laboratory in attempts to show the correlation between these and other physical properties.

Hamilton et al (1956) and Shumway (1960) made use of a resonant chamber method originally developed by Toulis (1956). The method makes use of a compliant walled cell (having dimensions of the same order as the transmitted wavelength) containing the sediment sample which is excited to resonate in several modes by a small transducer dipping into the surface of the medium. A second transducer is used to detect the resonances and from the centre frequencies, sharpness of resonance and cell dimensions both the velocity and attenuation of sound in the sample can be detected. The frequencies at which the sample will resonate are found from waveguide theory using boundary conditions of pressure-release surfaces. The walls of the chamber must

be very thin or very compliant to minimise acoustic losses as a result of rigidity in the walls (Fay 1952) if absolute measurements of velocity are to be obtained, corrections are necessary to account for the finite thickness of the cylindrical wall and one closed end. (figure 2.2)

The method has several advantages, one of the most important being that measurements of velocity and attenuation can be made at a number of frequencies corresponding to the different resonance modes without moving the sample or transducers.

In the low frequency region, below about 20KHz, acoustic transmission methods become impractical: wavelengths are longer and beam widths larger. This means that large sample volumes must be used to maintain reasonable pulse lengths and to prevent reflections from becoming a problem.

2.4.1. Acoustic transmission methods

The acoustic transmission methods that have been used to study marine sediments fall into two broad categories: the single path method which utilizes two transducers, one to transmit and the other to receive and the double path method which uses the same transducer to transmit and to receive, relying on a reflection usually from the bottom of the sediment column.

Yew and Jogi (1976) used a fairly simple single path apparatus to obtain velocity and attenuation measurements in porous rock samples. The fluid saturated porous specimen was sandwiched between a pair of resonant frequency piezoelectric discs. A train of oscillations either at a single frequency or in the form of a wide band pulse was transmitted

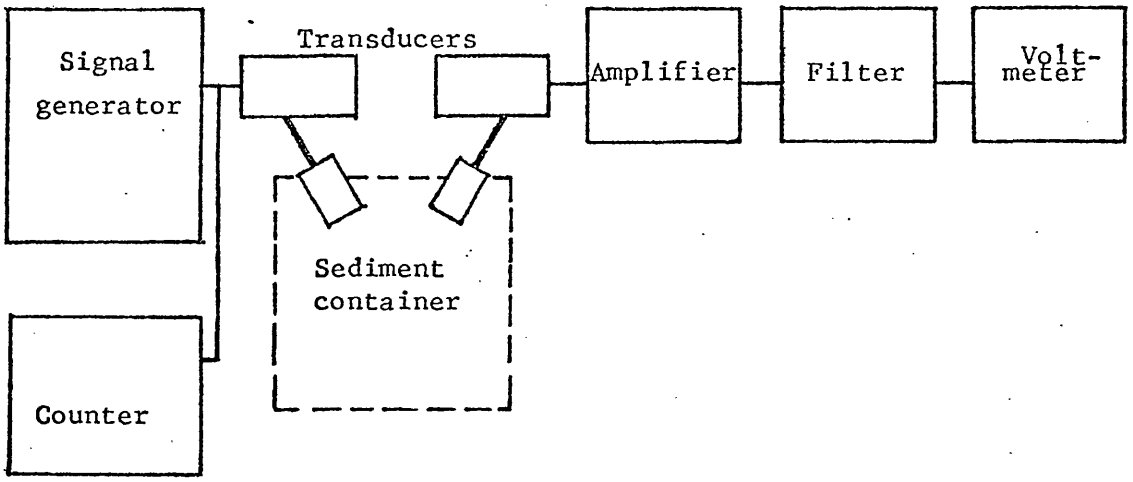

Figure 2.2 Schematic diagram of resonant chamber apparatus as used by Shumway (1956)

into the specimen and the signal propagating through it was monitored by the receiving disc.

The wave speed was determined by dividing the specimen thickness by the measured transit time and the attenuation found by assuming that the output voltage was directly proportional to the average displacement of the fluid and the solid portion of the specimen over the contact area of the disc.

i.e.

$$V_{out} = k_1 \, (u(x,t) + U(x,t)) \qquad 2.4$$

where k_1 = calibration constant

$u(x,t)$ = the displacement of solid skeleton

$U(x,t)$ = the displacement of the fluid

V_{out} = the output voltage

Rather than measure the transit time directly, some authors have constructed two identical cells, one containing the sample, the other containing distilled water, enabling results to be obtained by direct comparison of the two arrivals.

McCann (1972) again used a similar method to study core samples from the North Atlantic. In this case a water path was left between the transducers and the sediment sample and a more complicated arrangement was used to monitor the frequency of the sinusoidal oscillation in the pulse. Using this method the frequency of the sinusoidal oscillation in the pulse was determined by mixing the pulse with the output from a sinusoidal oscillator. The output from the mixer consisted of the two sinusoidal waveforms beating together within the pulse plus the r.f. from the continuous oscillator. The detector

isolates the low frequency beat signal which is displayed on the oscilloscope. When the condition of frequency coincidence is reached the pulse envelope contains only horizontal lines, the amplitude of which depends on the random phase differences between the pulsed sine wave and the continuous sine wave. (figure 2.3)

Most of the errors in such a system are caused by the container covers which must obviously form part of the acoustic path and give rise to internal reflections within the sample chamber. The effect of these covers on the pulse shape is negligible although the pulse amplitude is affected by both the cover thickness and the mismatch between the sediment and the water. Corrections can be made for this, however, as shown for example by Kinsler and Frey.

The double path method as used by Nolle (1953) depends on an echo from the bottom of the sediment column. (figure 2.4)

The velocity of sound in the sand-water mixture is calculated by multiplying the sound velocity in fresh water by the ratio of the travel time in water and water-filled sand paths of equal length. Experimentally the time of travel can be obtained by observing the time of arrival of an echo from the bottom of a water container with no sand and the times of arrival of echoes from the top and bottom of a few inches of sand.

Attenuation measurements can be made by observing the amplitude of the reflected signal from the bottom of the container as the depth of sand is increased.

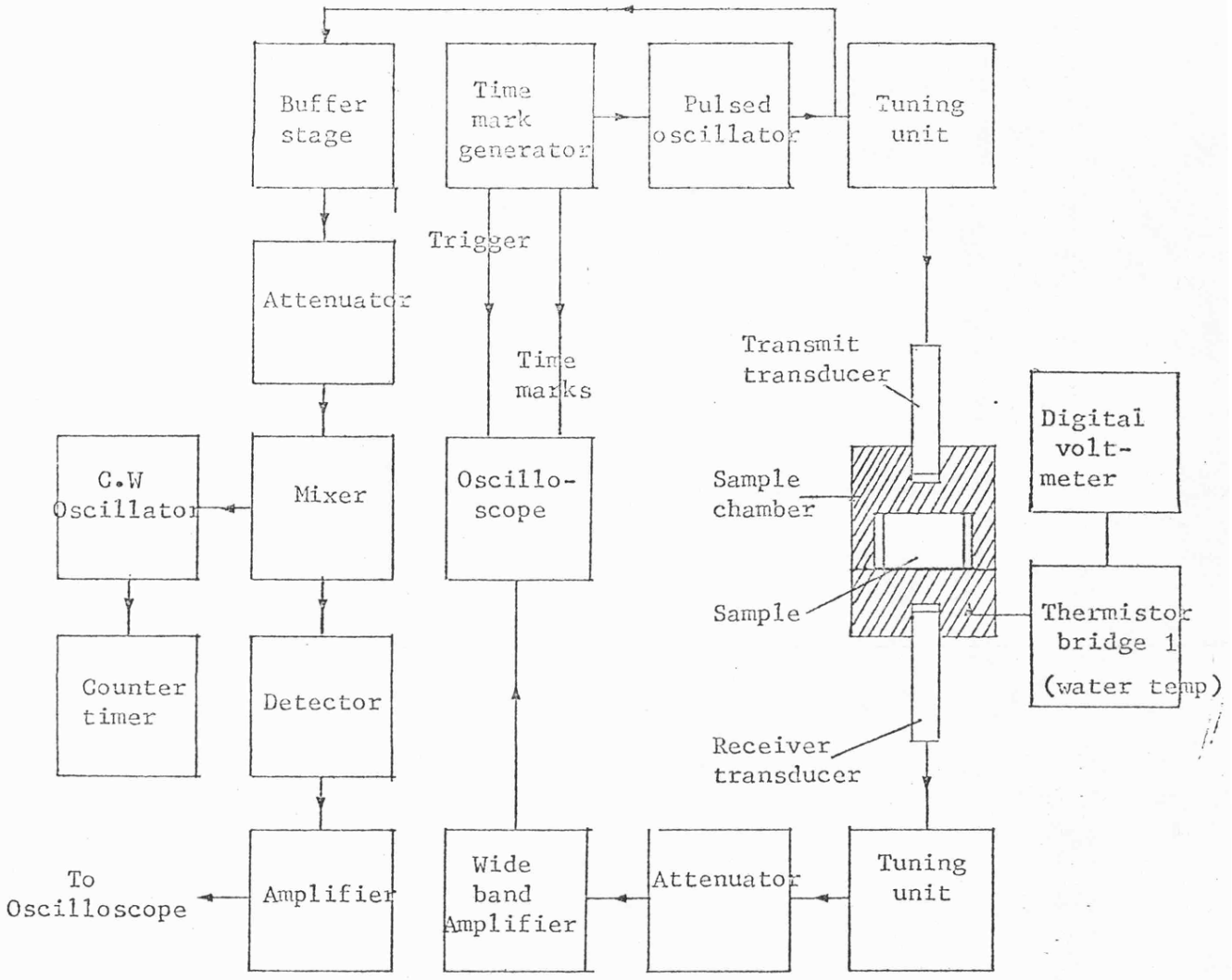

Figure 2.3 Schematic diagram of the accoustic apparatus used by Mc Cann (1972).

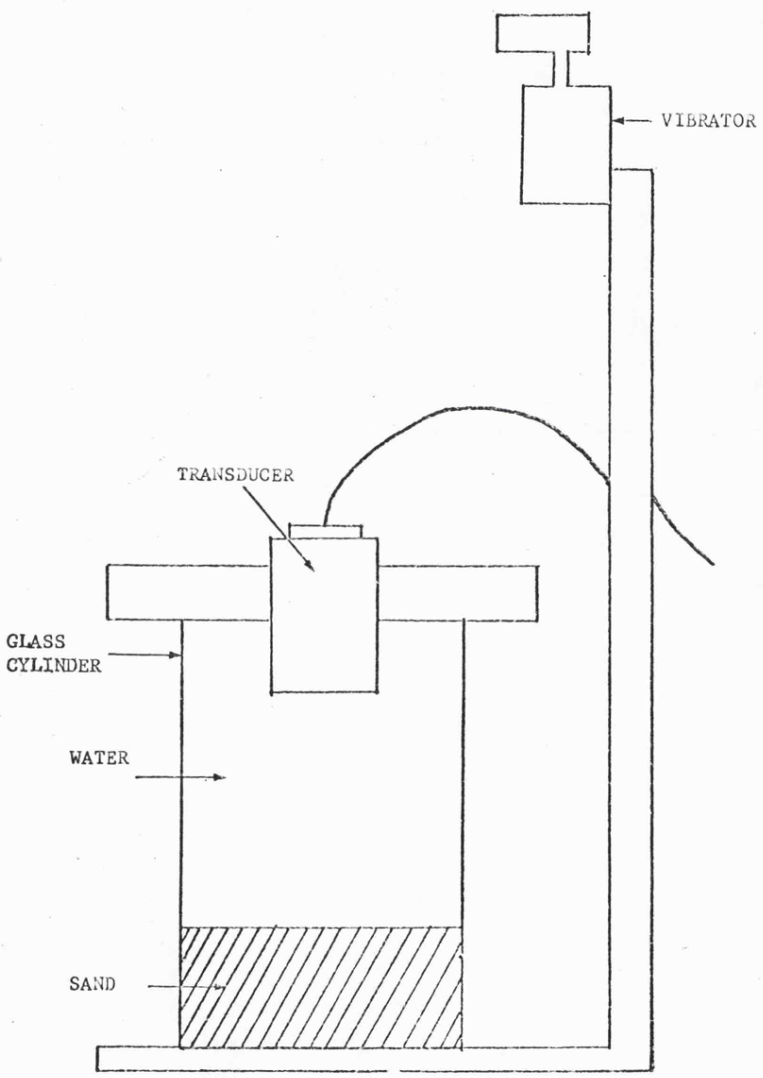

Figure 2.4 Double path apparatus as used by Nolle (1953).

Most laboratory methods used to study the acoustic properties of marine sediments are based on one of these three ideas. Variations on the theme include a method whereby a wedge shaped section of sand is moved between two transducers, one transmitter and one receiver, and measurements being made by observing the receiver voltage as a function of wedge thickness.

Another method based on the double path idea was again used by Nolle (1963) in which a box with a stepped bottom is used to contain the sediment and by comparison of the amplitudes of the echoes from the individual steps, the attenuation can be determined.

2.5. Experimental methods used for in situ measurements

There have been a number of reports in the literature of acoustical measurements on marine sediments in situ. Some of the methods that have been used are direct, for example, in refraction shooting, whilst some depend on measurements of reflection coefficients to give indirect results for velocities.

Weston and Wood (1964) used two probe transducers pushed into undisturbed mud in Emsworth harbour and by observation of pulses transmitted through the sediment were able to obtain velocity and attenuation measurements between 4 and 50 KHz with a range of between 1.25 and 180 feet. Hamilton (1956 & 1972) also used probes inserted by divers into the seafloor off San Diego and obtained velocity and attenuation data between 3.5 and 25 KHz.

Some authors, notably Ricker ('53), McDonald et al ('58) and Tallos

and Reid (1969) have made measurements on the attenuation of seismic energy as it propagates through the earth. After normalising with respect to the shot the spectra of many traces over a small interval of depth can be averaged to minimize reflection interference and to yield a frequency response function associated with a given depth.

Mackenzie (1959) obtained velocity and attenuation data for three different types of sea-bottoms using reflection results at 1 KHz for a range of grazing angles between 12^{o} and 90^{o} and at 1, 4, 7.5 and 16 KHz at normal incidence. Attenuation and velocity data were calculated using a modified Rayleigh theory modified by assuming a complex velocity for the bottom.

The study of the initial amplitude of reflection of explosive sound from the sea floor has shown many cases in which the amplitude decreases with increasing angle of incidence and becomes negative at angles of about 74^{o} to 80^{o}. Fry and Raitt (1961) showed that if the sediment can be treated as a fluid then the angle of phase change gives a measure of the sound velocity in sediments at the sea-floor.

2.6. Summary

In summary, most of the methods used for the laboratory studies utilise fairly small samples through which a short acoustic pulse is transmitted. The experiments can be more carefully controlled but are very dependant on the way in which the sample has been prepared. The in situ experiments have the advantage of virtually free field conditions but are less controllable, sample sizes are effectively much larger and the sediments undisturbed.

Chapter 3

EXPERIMENTAL PROCEDURES AND TECHNIQUES

3.1. Introduction

Most techniques aimed at investigating the acoustic properties of marine sediments have been restricted to a single frequency or, at best, a very narrow band of frequencies. This means that the variation of the acoustic properties with frequency cannot be obtained from a single experiment, making experimental inconsistencies a very likely source of error.

The impulse response technique that was used for this work has the advantage over single frequency pulse transmission methods that information can be obtained over a range of frequencies (from 80 to 320 KHz in this case) during a single experimental run. In addition to this, because the impulse response is obtained by correlation, which is an integration process, it has the advantage of having a higher signal to noise characteristic than methods utilising the transmission of single pulses.

This chapter sets out to describe the experimental arrangement and the techniques used for the acoustic investigation leaving the theoretical treatment of the method and the description of the equipment used for discussion in Chapter 4.

3.2. The impulse response method

The method used in this approach involved transmitting a continuous broad-band signal through different thicknesses of sample sediment and cross-correlating the transmitted signal with the signal received by a

second transducer buried within the sample. The transmitting transducer had a lower resonance frequency than that of the receiver giving the system a broader bandwidth. The broadband signal used was a pseudo-random binary sequence which is described in detail together with the rest of the electronic equipment in Chapter 4.

It can be shown (Appendix A) that if the transmitted signal is broad-band then cross-correlation of the transmitted and received signals gives the impulse response of the system.

The complete system can be visualised as being made up of a number of linear circuits each having its own characteristic impulse response.

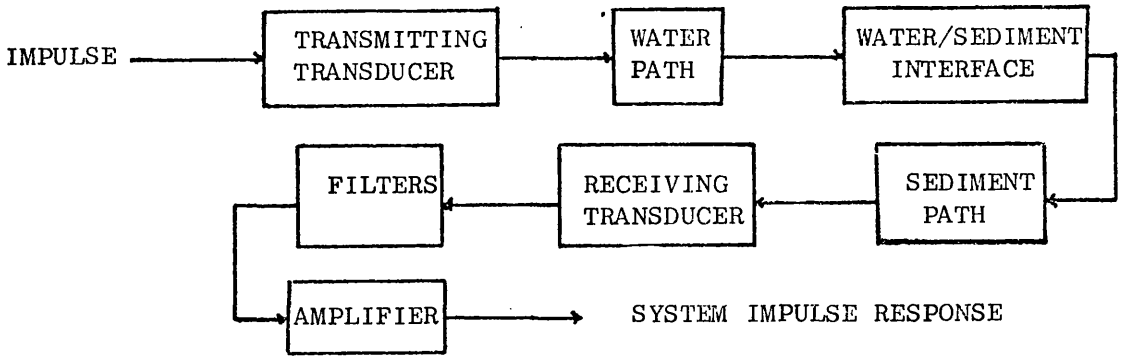

Figure 3.1 Linear network visualisation of measurement system

It is shown later that the responses of the two transducers, the filters and amplifier can be considered together in a single function.

The system impulse response is formed by a convolution, in the time domain, of each of these individual impulse responses. The total impulse response obtained here, therefore, contains information on these individual impulse responses which are best considered in two parts; the electrical response and the acoustic response. The electrical response encompasses the transmitted signal, transducers, filters and amplifier and effectively limits the bandwidth of the system. The acoustic response contains information about the water and sediment paths and is best considered in three parts:

(a) the water path

(b) the water sediment interface

(c) the sediment path.

The water path is by far the least significant of these, resulting in a simple time delay in the impulse response, the delay being dependant on the acoustic path length. It is, however, the second two parts which contain all the important information regarding the sediment, these can be separated to show the surface and volume effects independantly, an analysis of this is included in Chapter 6.

3.3. The tank assembly and sediment container

The acoustic experiments were all carried out in a laboratory tank constructed from glass reinforced plastic, having internal dimensions 2.40m x 1.22m x 1.07m. The structure was a sandwich of unsaturated glass fibre, approximately 9.5mm thick, laminated between two 3mm thick layers of saturated glass mat.

The sediment sample was held in a rigid PVC cylinder, inside

diameter 50cm. mounted on a perspex base on which the receiving transducer was mounted (figure 3.2).

Perspex windows were made in the side of the sample container and in the tank wall to allow observations of the packing structure and the depth of sediment within the column.

To ensure consistent packing of the sediment it was found necessary to shake down the sediments as they were added to the column. This meant that the container had to be isolated from the tank bottom in such a way that allowed small amplitude vibrations to be generated. The container was thus mounted in a framework suspended from the top of the tank and attached to an eccentrically loaded electric motor which provided a controllable vibration. The frequency of vibration was variable between 100 Hz and 1000 Hz.

The transmitting transducer was supported on a separate framework vertically above the receiver at a distance of 1.3m from it, the whole structure being held in a gantry system allowing accurate alignment of the transducer pair.

Diagrams and photographs of the tank structure and the sediment container are included in figures 3.3, 3.4 and 3.5.

3.4. Reflections

The apparatus was designed such that reflections from all the surfaces within the tank, including the sample container framework, were time-gated out from the final impulse response.

Figure 3.2 Sediment container and receiving transducer

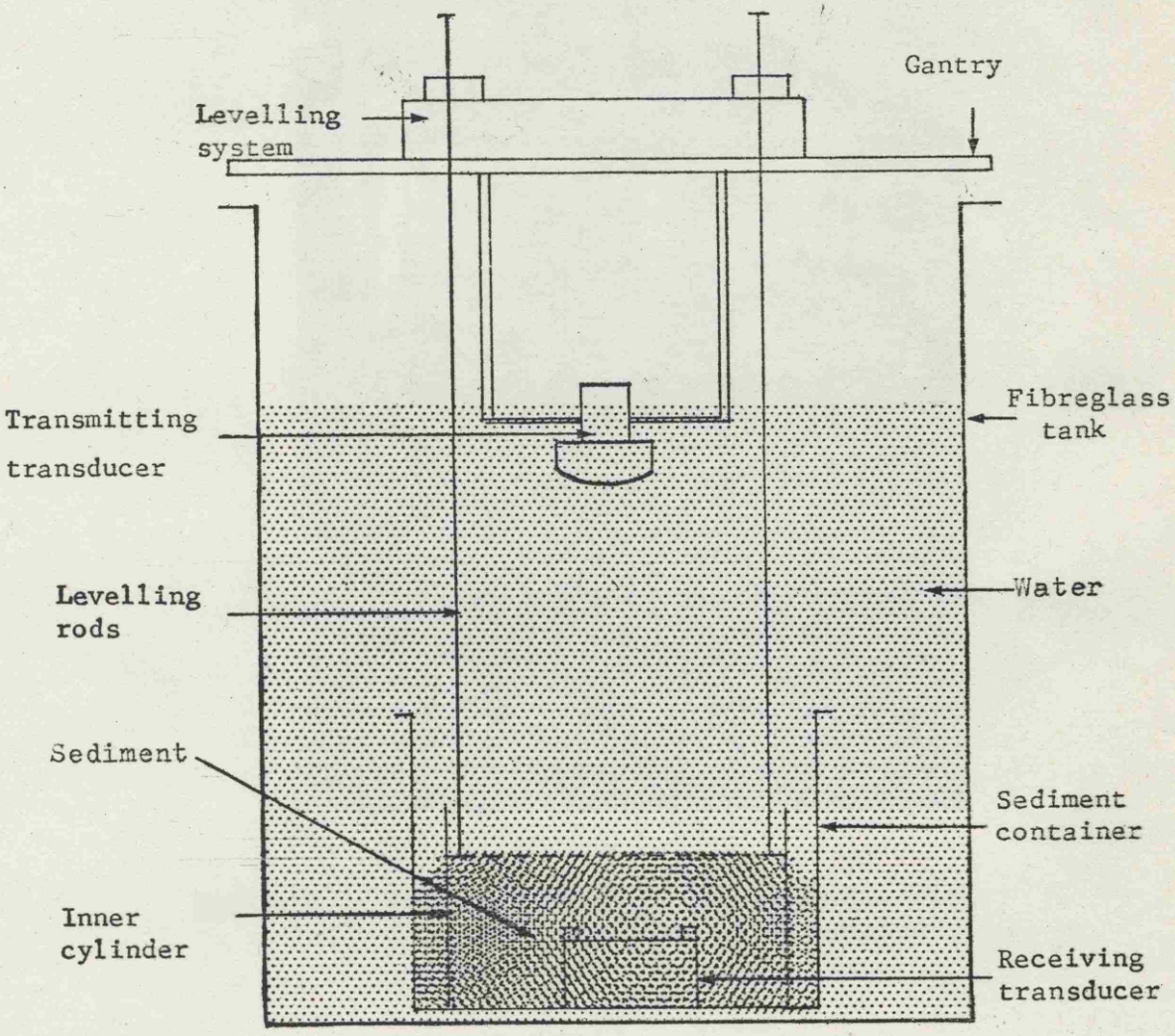

Figure 3.3 Diagram showing layout of equipment within the tank

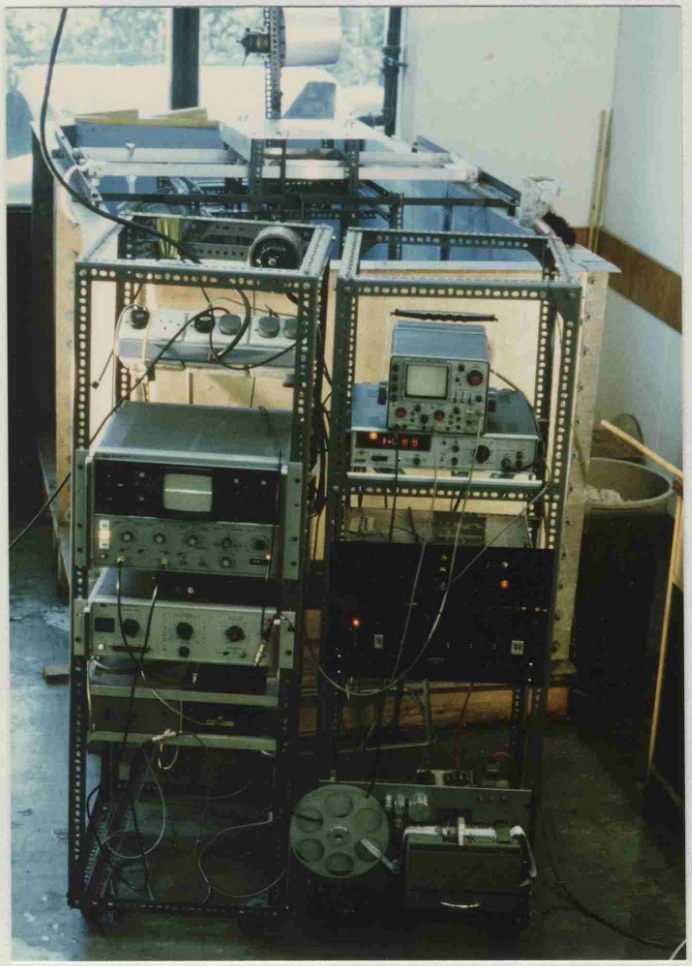

Figure 3.4 Tank structure and gantry system with electronic equipment in foreground

Figure 3.5 Sediment container within the tank assembly showing column of sand

The impulse response that was recorded in each case was 100μs in duration and therefore for a reflection to have any significance on the record it must have been as a result of a transmission having a path length of not more than 100μs greater than the direct path. If a maximum average velocity for a reflected path of $1700ms^{-1}$ is assumed then the minimum path length difference that could cause such a reflection is:-

Path difference = $1700 \times 100 \times 10^{-6}$m

= 0.17m

Therefore, provided there is no reflector within 0.17m of the direct path then theoretically there will be no second arrival within 100μs of the first arrival. Inside the tank there were no reflectors within 40cm. of the direct path apart from the container walls which were 25cm. away allowing about 270μs of undisturbed impulse response.

It should be noted, however, that a multiple reflection from the sediment surface will be observed if the sediment depth is less than 9cm. This is a feature of the system which can be made use of and is considered in Chapter 6.

3.5. Building up the sediment column

The acoustic transmission properties of the sediments under investigation were evaluated by observation of the change in the impulse response as the acoustic path length through the sample was varied. For the acoustic measurements to be meaningful it is essential that the only change in the system between the acquisition of consecutive impulse responses is the increase in path length. That means

that the structure within the sediment mass must be reproducable, there must be no 'layering' effect due to the way in which the sediment bulk is built up and the effect of the surface on the acoustic signal should be constant.

The column was built up slowly by adding only small quantities of sediment at a time and agitating the whole container until minimum porosity (see figure 3.11) was attained. In this way reproducible columns of sediments were produced having no detectable layering, as observed through the perspex side window.

3.6. Depth measurement and surface preparation

If accurate measurements of velocity and attenuation are to be achieved it is essential that the surface of the sediment is at a known position so that the path length can be determined and is also regular so that there are negligible direct-path length variations over the insonified area. The surface must therefore be smooth and level.

Initially a fibre optic link was constructed using 3 metre lengths of continuous light guide (0.25mm in diameter) mounted at each end in the line array, the fibres being mounted in the same order at both ends into two perspex blocks. The fibre optic 'read head' was then mounted in a vertically moving slide on one side of the sediment container opposite a light source (figure 3.6).

This could then be moved in a vertical plane and by observing the 'write' head the cut off point could be set to a predetermined position. This meant that the fibre optic read head could be positioned accurately with respect to the sediment and as its movement was controlled via a

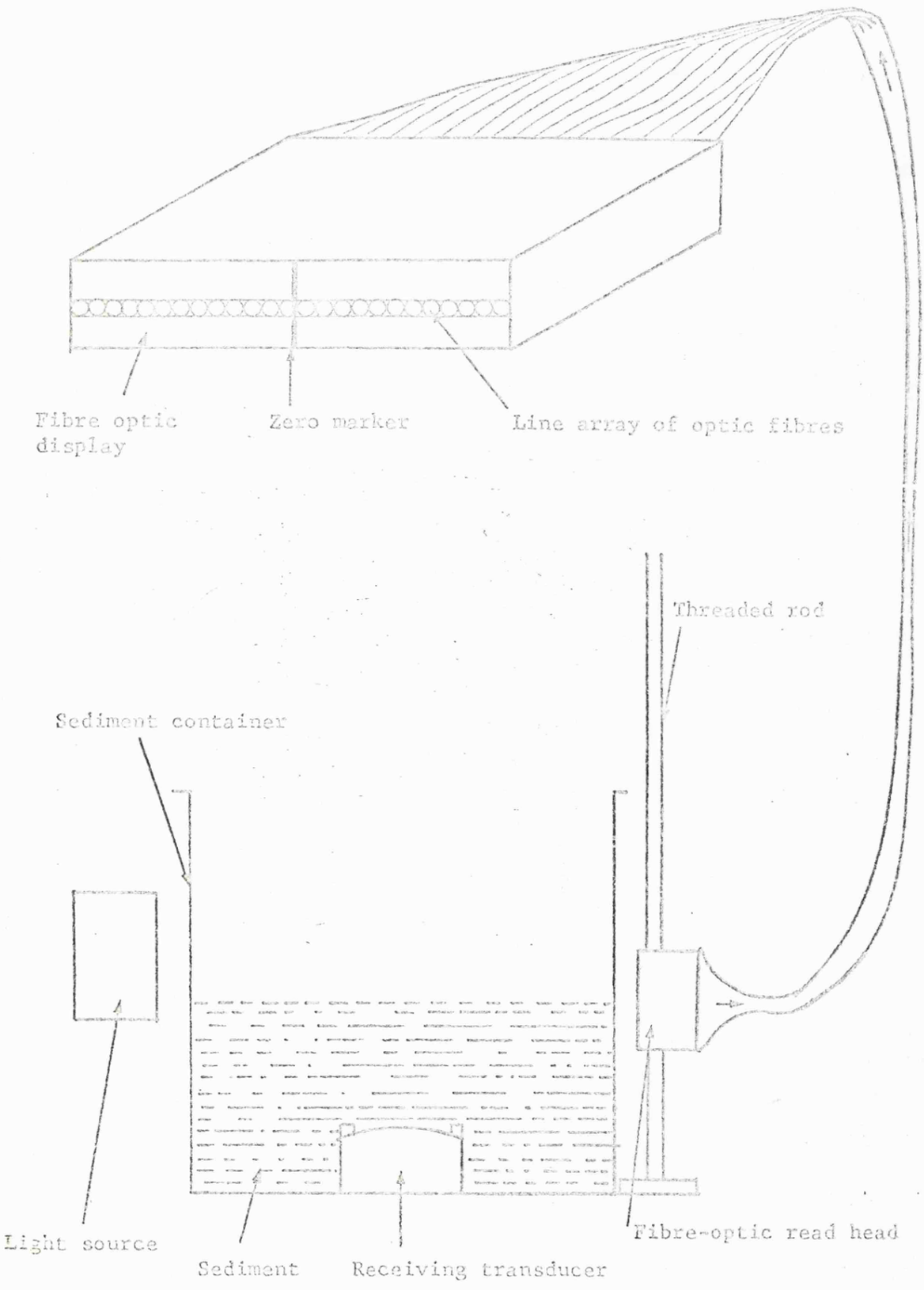

Figure 3.6 Diagram showing fibre-optic height measuring system.

threaded rod from the surface, depth measurements could be made.

Although this technique worked effectively with the sand samples provided the surface was level it was not so successful with the more transparent Ballotini. The accuracy also suffered when the surface was anything other than smooth because of diffraction effects, the result being a less clearly defined cut-off and hence a lack of definition in height estimation.

The second method was designed to level the sediment in the container to a predetermined position. This was done by lowering a second cylinder, open at both ends and 5cm. smaller in diameter, inside the first. The inside cylinder was then overfilled with sediment and the surplus removed down to the level of the top of the inner cylinder using a specially designed scraper, operated from above the tank. (Figures 3.7 and 3.8).

The scraper had four milled slots cut into it as shown so that when rotated in the appropriate direction the excess sediment flowed along the grooves radially until the whole scraper rested on the inner cylinder leaving a smooth and level surface of sediment. The scraper was designed so that it could be removed before acoustic measurements were made. It was constructed from a lcm. thick disc of perspex, allowing observation of the sediment surface during levelling.

The inner cylinder which controlled the height of the sediment

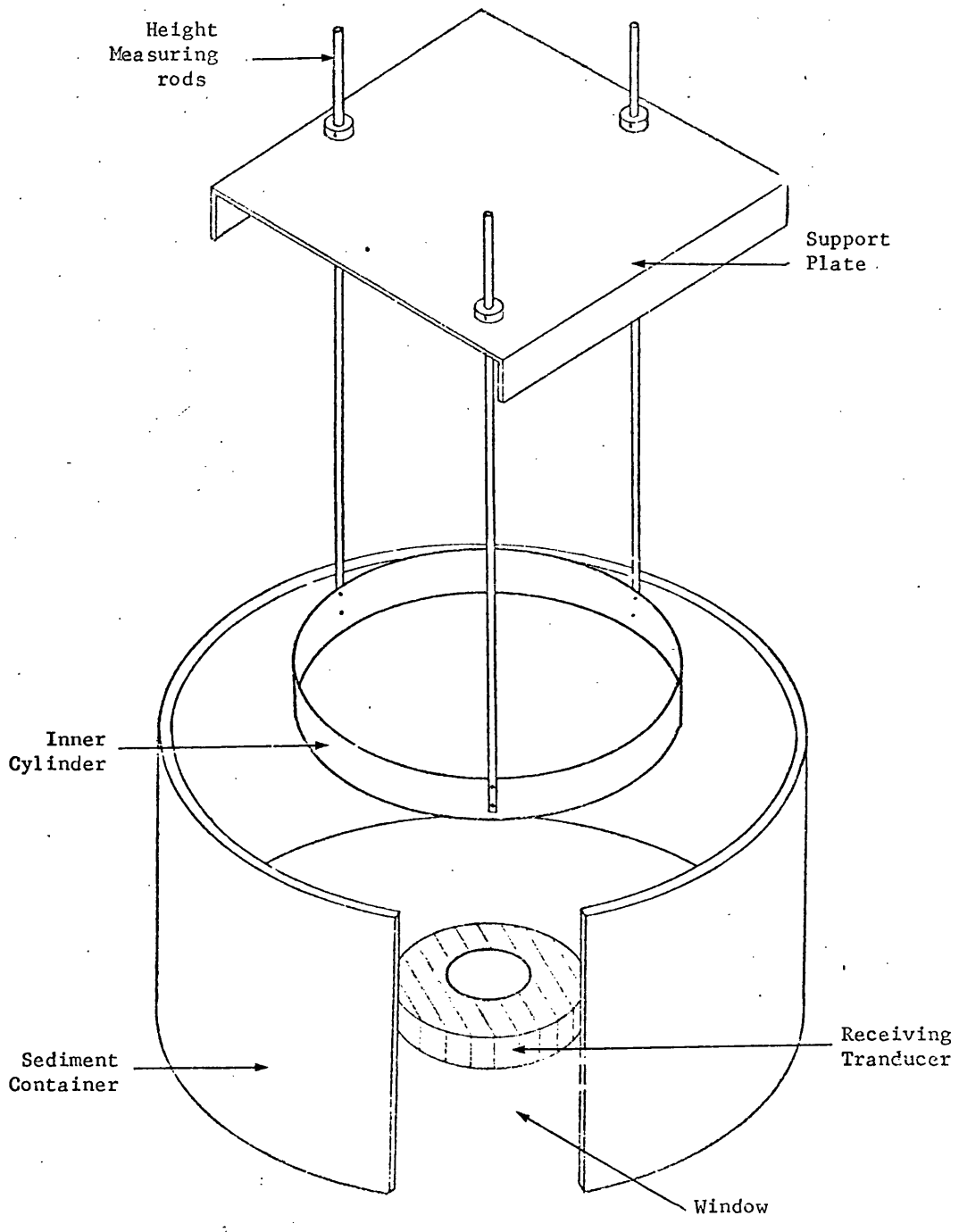

Figure 3.7 Diagram of levelling system

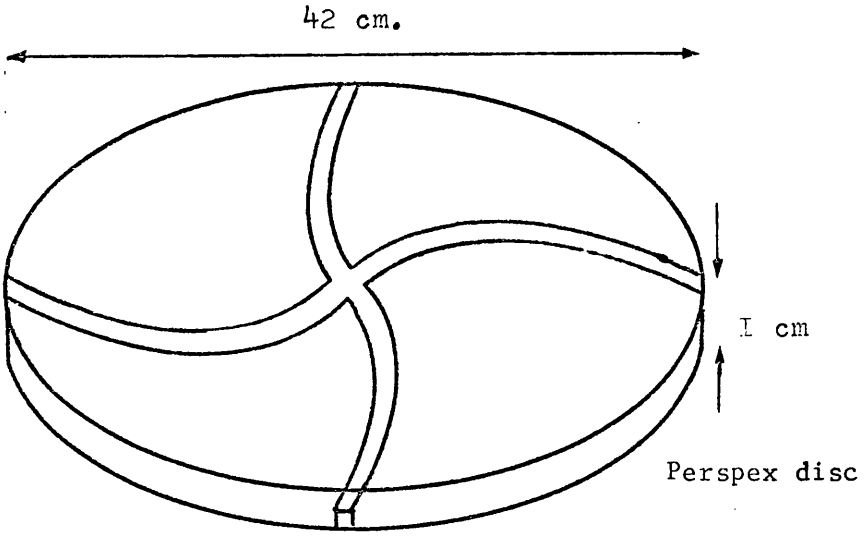

Isometric view,

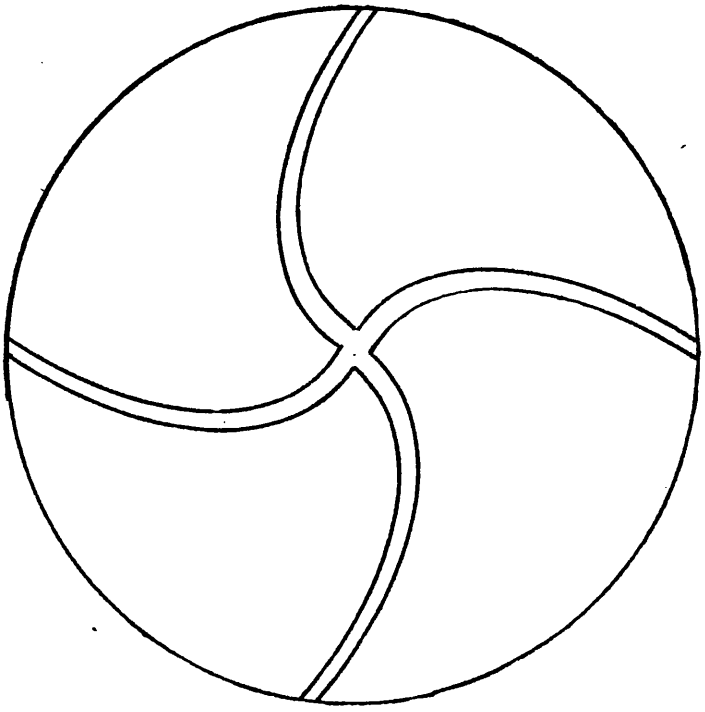

Plan.

Figure 3.8 Perspex scraping disc.

was held by three tubes which passed through a drilled levelled plate above the gantry system on the tank. Three lockable collars were used to lock the individual tubes enabling the cylinder to be accurately positioned and levelled.

3.7. Sediment preparation

3.7.1. Air Bubbles

Air trapped between the sediment grains causes inconsistent and high values of attenuation. Although it is possible to remove a great deal of the air by pouring the aggregate between containers underwater and by agitation, it is difficult to remove the last few percent in this manner and in fact if such a sample is observed under reduced pressure in a dessicator, considerable quantities of air can be seen to be displaced.

The apparatus shown in figure 3.9 was designed to give an idea of the quantity of air that might be trapped within the sand that had been poured through a column of water, that is the total volume of the small bubbles that attached themselves to individual grains.

The apparatus consisted of a graduated glass cylinder with a freely moving piston have a O-ring seal, a small quantity of water-saturated sediment was introduced to the container, the piston replaced and the excess air removed via the bleed screw. The whole cylinder was then placed inside a dessicator and the pressure reduced to about 15 torr, the air displaced from the sand being collected below the piston. On returning the apparatus to atmospheric pressure the volume of air displaced and the volume of sediment were measured

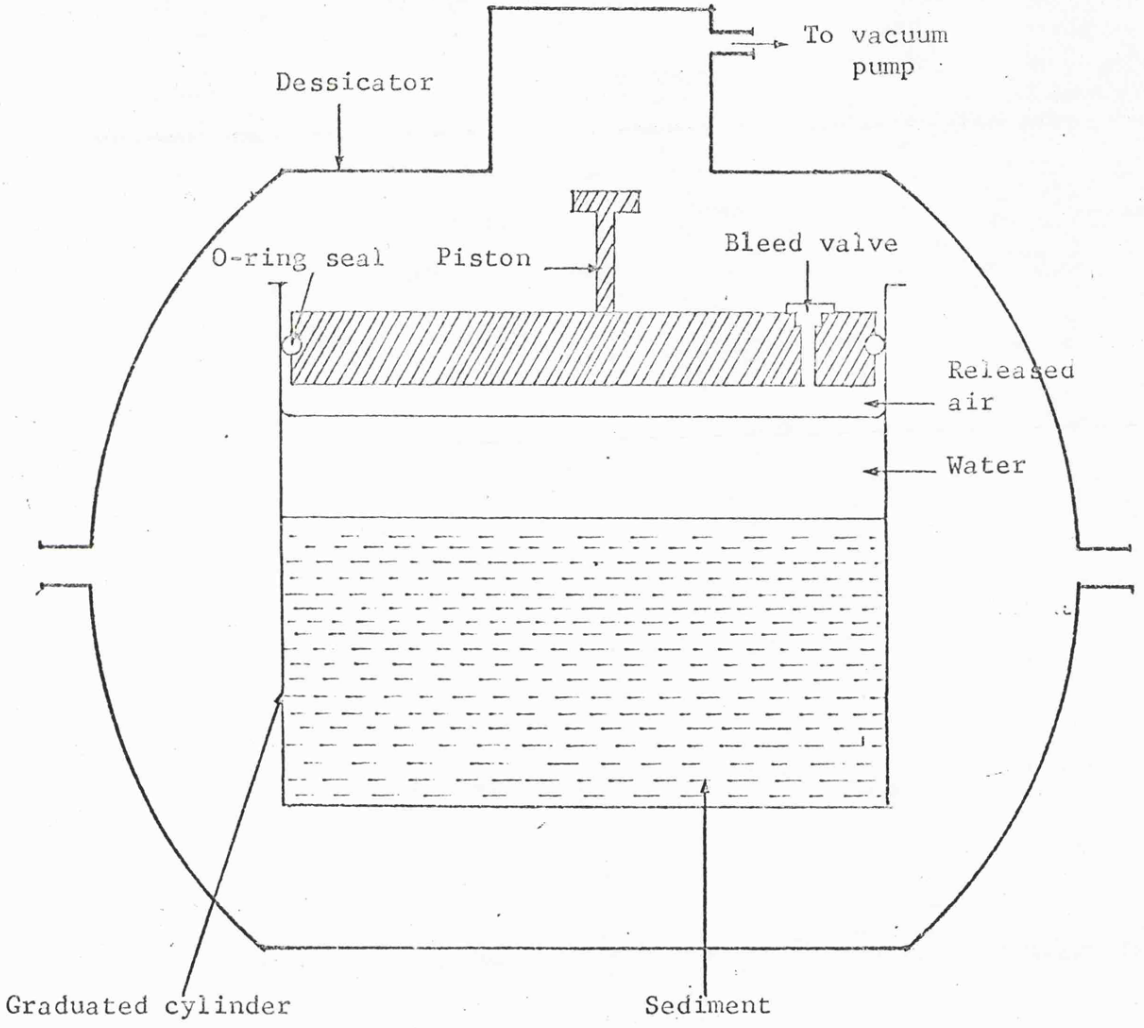

Figure 3.9 Apparatus used to measure the volume of air trapped within the sediment samples.

hence the percentage by volume of air in the original sample was estimated. The results of these tests are shown in Table 3.1.

The volume of air in the Ballotini samples was always lower than that in the sand but the variation with grain size does not seem significant.

Sediment		Percentage by volume of air trapped
Ballotini	1	1.3
	2	1.3
	3	1.2
	4	1.3
	5	1.1
Sand	1	1.6
	2	1.8
	3	1.5
	4	1.5
	5	1.9

Table 3.1. Volume of air trapped within sediment samples

The greater volumes of air associated with the sand grains is probably because of the greater angularity.

It should be noted that these figures represent the amount of air that is removed on evacuation to 15 torr and does not infer that this is all the air that is trapped which may be slightly higher.

Although the volume of air likely to be contained in non-evacuated sediment samples was fairly small it had a dramatic effect on the attenuation of sound waves passing through it. Because of this it was decided to evacuate all sediment samples before any acoustic measurements were made, using the apparatus shown in figure 3.10.

Fifty kilogrammes at a time of dry sediment was introduced into the evacuation barrel, the lid sealed and the pressure reduced to 15 torr using the rotary vacuum pump. Water was then bled into the system until the sample was totally saturated. The pressure was then reduced a second time and held at 15 torr for about two hours to remove the last few traces of gas.

The evacuated sample was always transferred to the sediment cylinder inside the main tank under water to prevent the reintroduction of air.

3.7.2. Packing

Although it was not possible to pack the sample into some regular

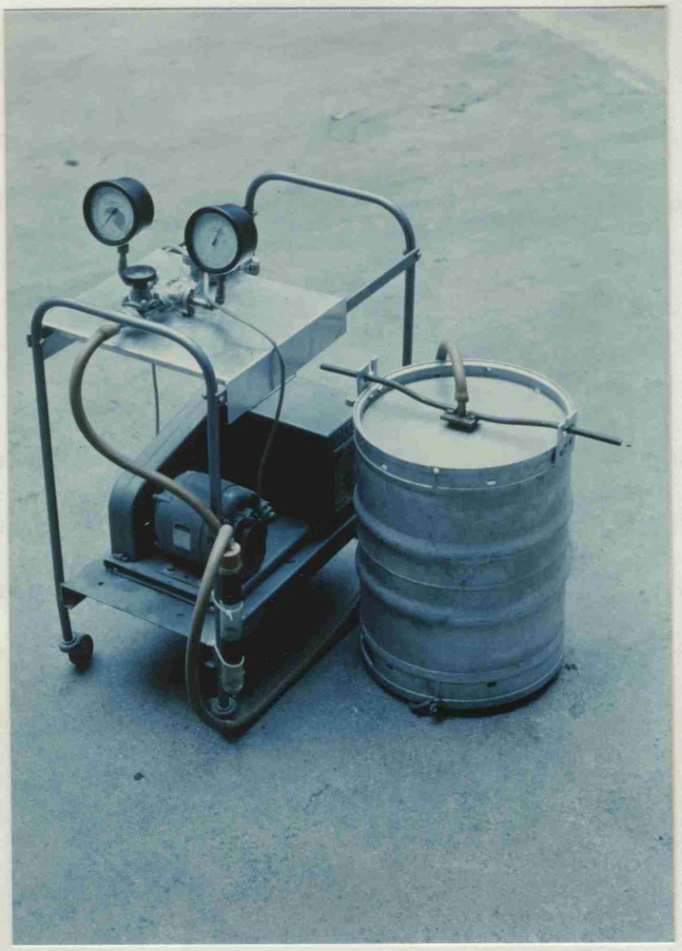

Figure 3.10 System used to evacuate sediment samples

predetermined arrangement, it was found that provided the column was always built up in the same manner and was agitated for a period of more than 200 seconds its porosity and measured acoustic properties were consistent and stable. Porosity values for sand and Ballotini samples are shown as a function of agitation time in figure 3.11.

Sediment was always added to the column in the same quantities by pouring it through about 20cm. of water. The sample was then shaken and finally the surface levelled before acoustic measurements were made.

3.8. Summary

The transmission impulse response of the system consisting of transducers and sediment column was obtained by cross-correlation using a continuous broad-band signal. The sediment column was built up systematically using outgassed samples poured through the water into the sample container, agitated and levelled.

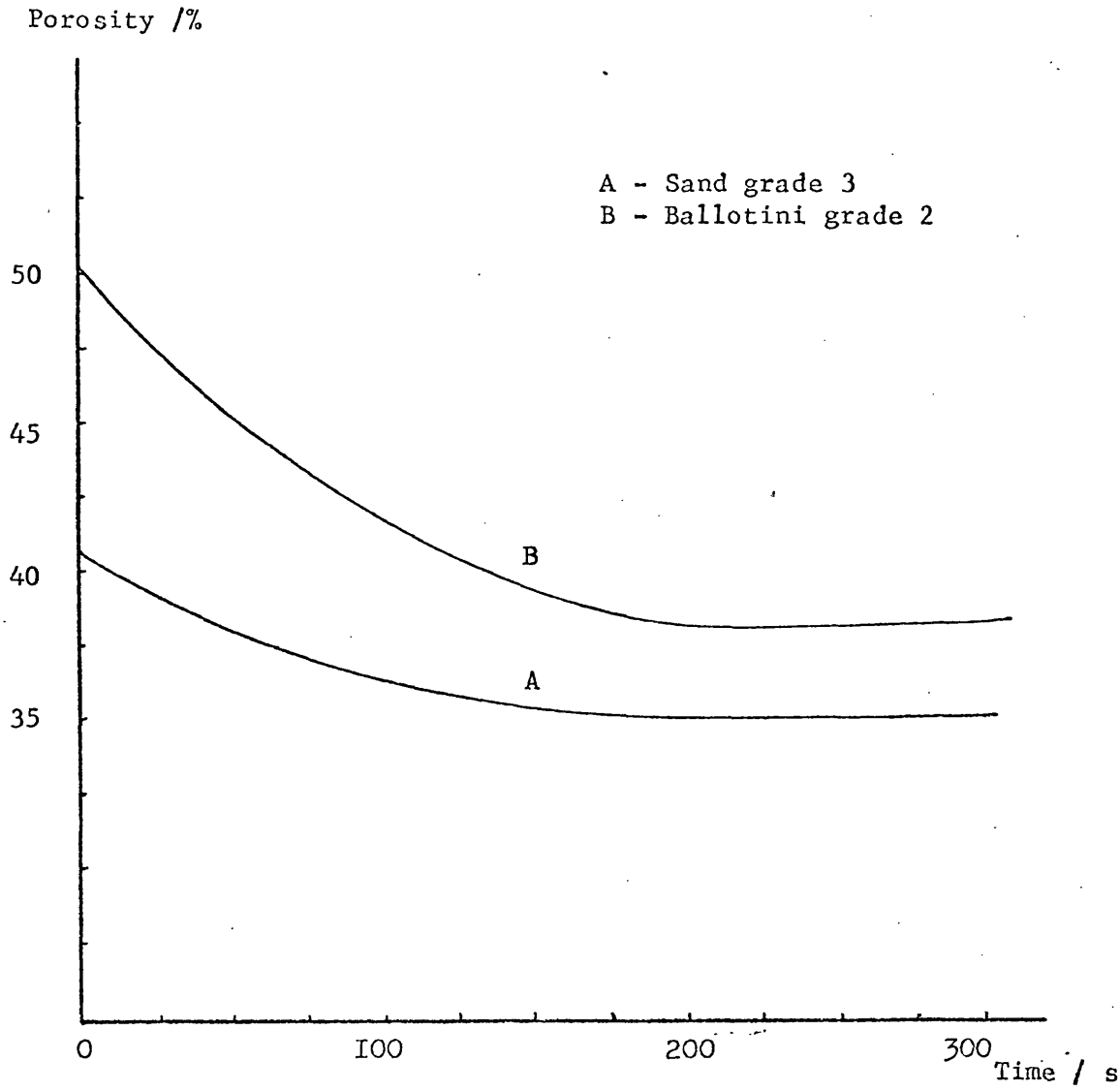

Figure 3.11 Porosity as a function of agitation time.

Chapter 4

THE CORRELATION TECHNIQUE AND EQUIPMENT USED

4.1. Introduction

Although correlation techniques have been extensively used in many branches of science , apart from the work done by Pace (1975) on sediment identification using reflection data, there are no references in the literature to the use of such methods applied to the analysis of the acoustic properties of marine sediments. It is therefore worth devoting a chapter to some of the theory behind the technique, and to the individual components making up the analysis system.

4.2. The experimental arrangement

It is shown in Appendix A that if a broadband signal is input to a linear system, the cross-correlation function obtained from the input and output sequences is the impulse response of the system. The experimental arrangements of the appratus is shown in figure 4.1. A pseudo-random binary sequence was fed to the transmitting transducer and to one input of the Hewlett Packard correlator. The signal detected by the receiving transducer was input to a low noise amplifier (Brookdeal model 451) having two filters, one active and the other passive, between stages. The output of the amplifier was then the second input to the correlator. In this arrangement the signal that was fed to the transmitting transducer and the amplified, filtered signal present at the receiving transducerwere cross-correlated resulting in the impulse response of the complete system. This impulse response was

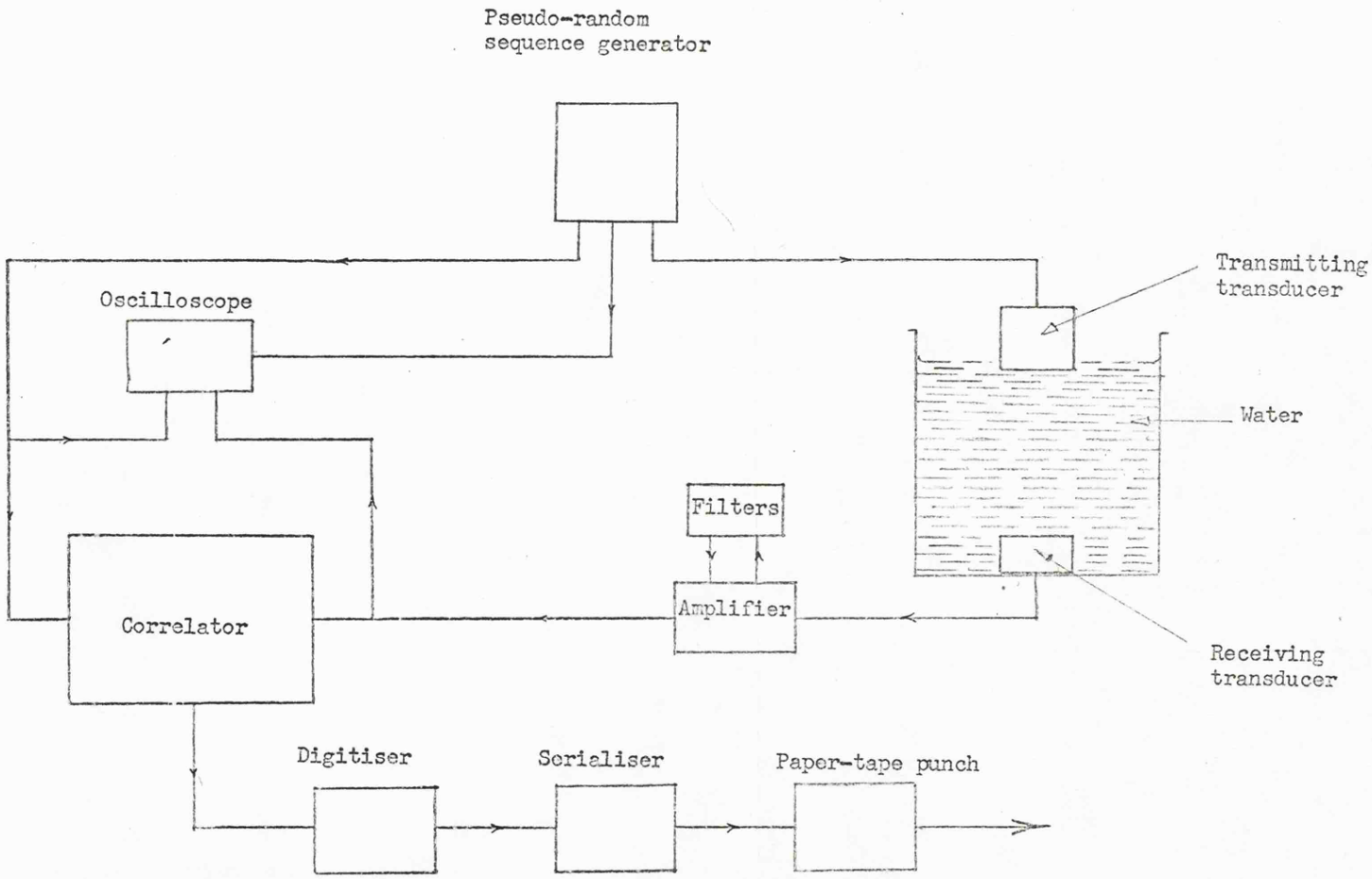

Figure 4.1 Block diagram showing arrangement of apparatus used for acoustic measurements

then digitised and recorded on punched paper tape for subsequent computer processing. The impulse response was 100 μs in length represented as successive amplitude values at 1μs. intervals of time delay.

4.3. Correlation

Correlation is a measurement of the similarity between two waveforms, in this case the signal applied to the transmitting transducer and the signal detected across the receiving transducer.

Consider two waveforms x(t) and y(t) (figure 4.2).

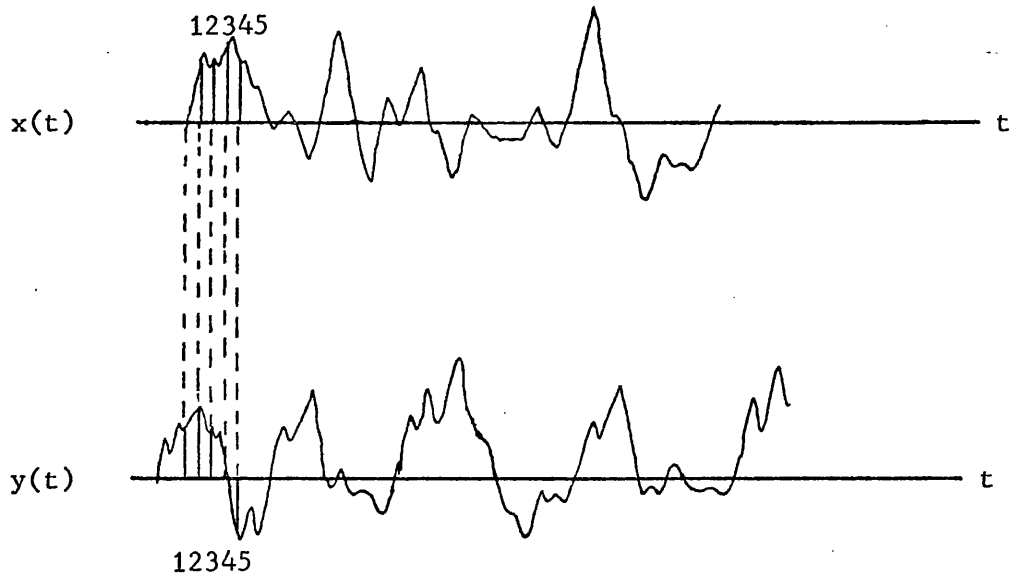

Figure 4.2 Correlation of two waveforms.

The cross-correlation factor is computed by multiplying the waveforms, ordinate by ordinate, and finding the average product, that is:

$$Rxy(o) = \frac{1}{N} \sum_{n=1}^{N} x_n y_n \qquad 4.1$$

Where N is the total number of terms in x(t) and y(t)
This corresponds to the cross-correlation factor at zero lag.

If one waveform is now shifted with respect to the other by an amount equal to one ordinate spacing then the cross-correlation factor corresponding to a lag of one is computed:

$$Rxy(1) = \frac{1}{N} \sum_{n=1}^{N} x_n y_n + 1 \qquad 4.2$$

This can obviously be done for any number of lags, provided the waveforms are infinite, the value of the individual cross-correlation factor indicating the similarity between the waves after having imposed the particular time shift.

The cross-correlation function is now the cross-correlation factor, plotted as a function of lag.
that is:-

$$Rxy(\Gamma) = \frac{1}{N} \sum_{k=1}^{N} x(k\Delta t - \Gamma) y(k\Delta t) \qquad 4.3$$

In actual fact the cross-correlation function should be defined as

$$Rxy(\Gamma) = \underset{T \to \infty}{\text{Limit}} \frac{1}{T} \int_0^T x(t - \Gamma) y(t) dt \qquad 4.4$$

but, in a digital system it is more convenient to approximate this average by sampling the signal every Δt seconds and then summing a finite number, N, of the sampled products, resulting in equation 4.3.

In summary, correlation provides a measure of the similarity between two waveforms. Its role in this study was to measure the time delay and distortion incurred during acoustic transmissions through different sediment layers.

4.4. Pseudo-Random Binary Sequence

The input constant spectral density signal used in this work was a pseudo-random binary sequence, output from a Hewlett-Packard HO1-3722A.

Operated in the pseudo-random mode the Hewlett-Packard noise generator produces repeated sequences or patterns of binary ones or zeros ($\pm$ IOV). The form and length of the sequence being controlled by the 'clock period' and sequence length. See figures 4.3 and 4.4.

The sequences are described in terms of the clock period and the number of clock periods or bits they contain. The number of bits, N, is always of the form

$$N = 2^n - 1 \qquad 4.5$$

The period of the sequence is equal to the product of N, the number of bits, and ΔT, the clock period.

$$T = N.\Delta T \qquad 4.6$$

4.5. Spectrum of Binary output

A pseudo-random binary sequence has a line power spectrum (figure 4.5), the envelope of which is of the mathematically defined $\left[\frac{\sin(x)}{x}\right]2$ form. The fundamental frequency (i.e. lowest frequency component in the spectrum) is

$$f_L = \frac{1}{T} = \frac{1}{N\Delta T} = \frac{f_c}{N} \qquad 4.7$$

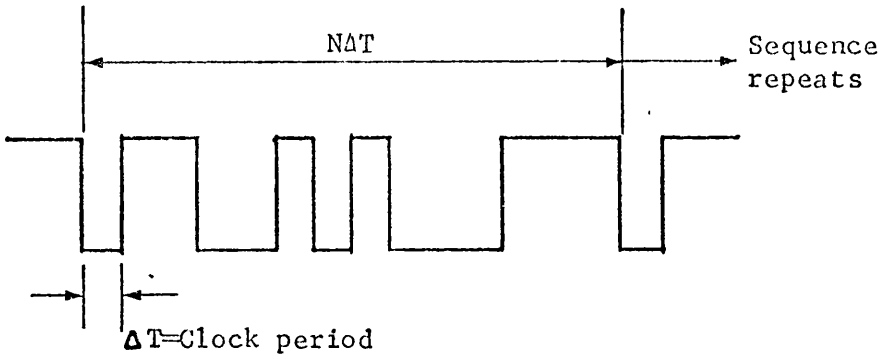

Figure 4.3 Pseudo-random binary sequence.

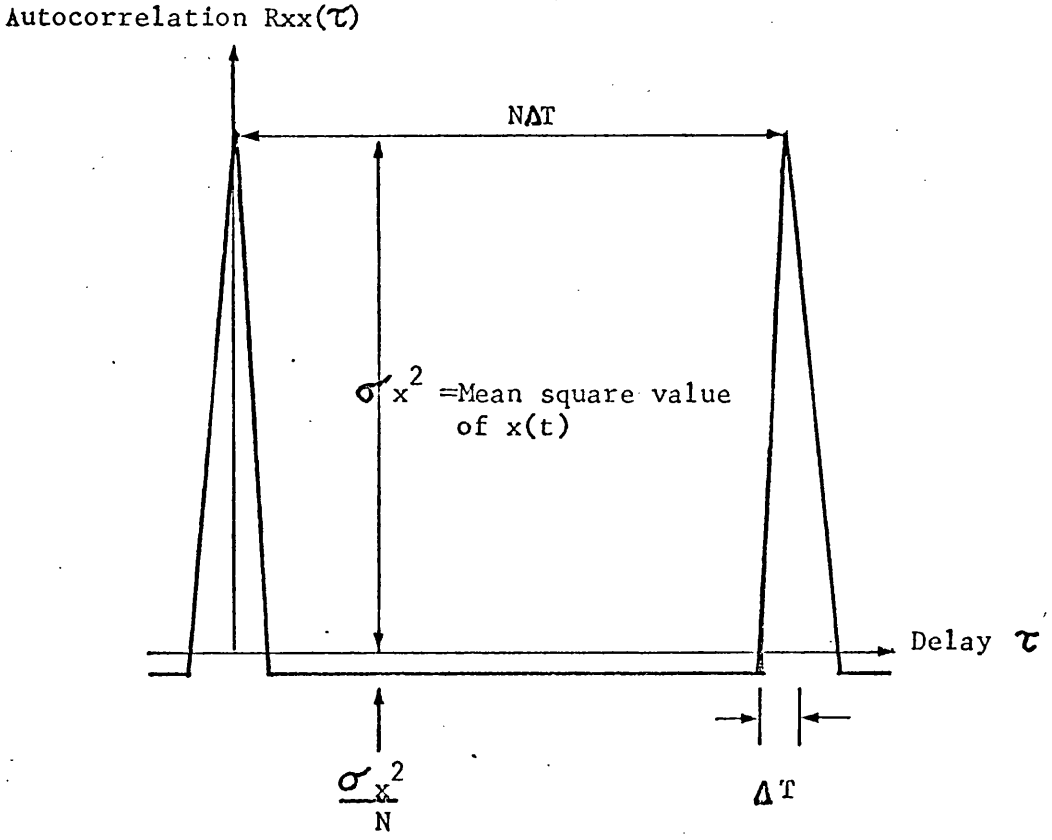

Figure 4.4 Autocorrelation of above pseudo-random binary sequence.

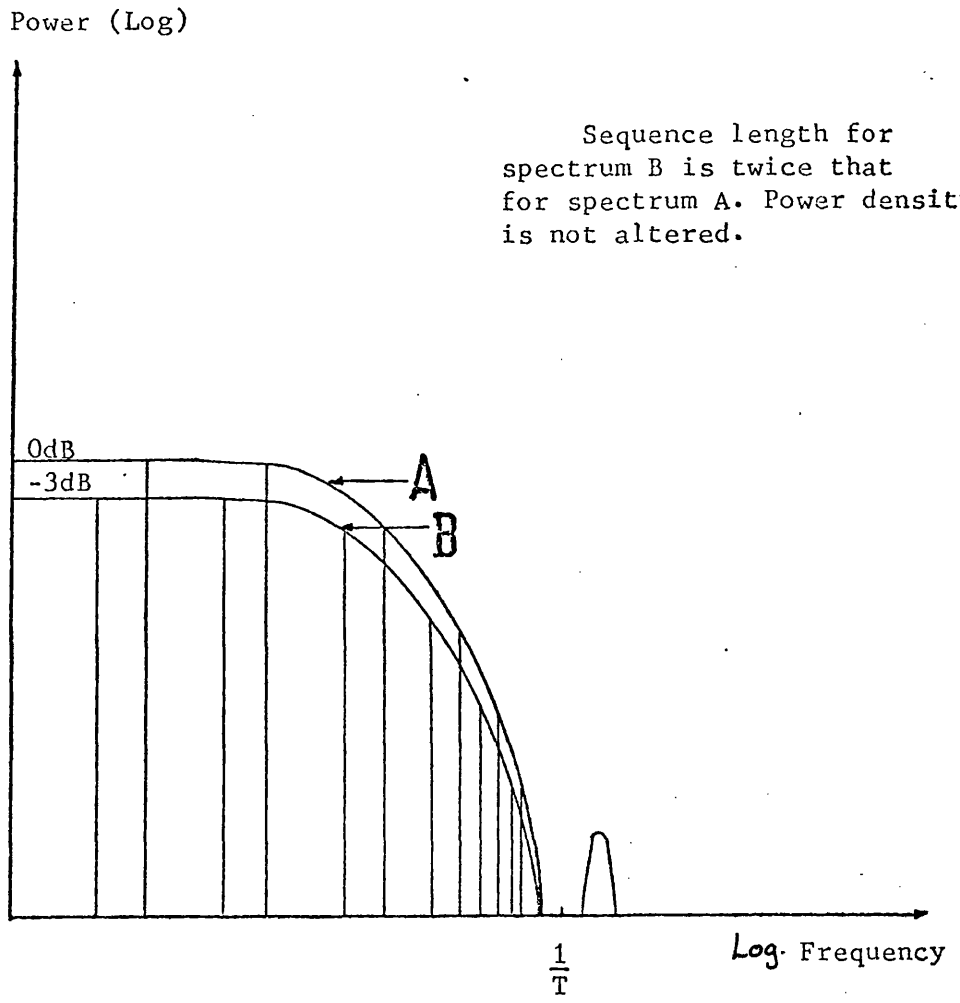

Figure 4.5 Spectrum of Pseudo-random binary sequence

where T is the period of the pseudo random binary sequence.

All other components in the spectrum are harmonics of $\frac{1}{T}$.

If with constant ΔT, N is increased, the frequency of the fundamental and also the spacing of the harmonics are reduced, causing the number of harmonic components per spectrum lobe to increase.

Since the total power of the binary output remains the same (the waveform still switches between the same amplitude levels) the magnitude of the harmonics is proportionately reduced. For example, if N is doubled, the number of components in the spectrum will double and the power contribuiton of each component will be halved.

The envelope of the pseudo-random binary sequence line spectrum is given by the expression:

$$G(fk) = 2a^2 \left(\frac{N+1}{N^2}\right)\left(\frac{\sin\frac{\pi k}{N}}{\frac{\pi k}{N}}\right)^2 \qquad 4.8$$

where

G (fk) is the power in $(\text{volts})^2$ contributed by the K th harmonic.

'a' is the rms amplitude of the binary signal

N is the sequence length

4.6. Transducers

In order to obtain a 'sharp' impulse response with very little ringing after the main peak it is desirable to have a transmission

system with as wide a bandwidth as possible. With this in mind it was decided to use transmitting and receiving transducers having staggered resonance peaks.

The response of a ceramic transducer in the normal transmission mode is of the form of a bell-shaped resonance curve roughly symmetrical about the resonance frequency of the transducer. On reception, however, the response in the low frequency range is fairly 'flat' from just above DC to a little below the resonance frequency after which it follows the transmission shape.

The resonance frequencies of the transmitter and receiver used for this work were 167 KHz and 258 KHz respectively.

4.6.1. Transmitting transducer

The transmitting transducer used for this study was on loan from the Admiralty Underwater Weapons Establishment at Portland. A picture of this together with the beam pattern and projector sensitivity curves are shown in figures 4.6, 4.7 and 4.8.

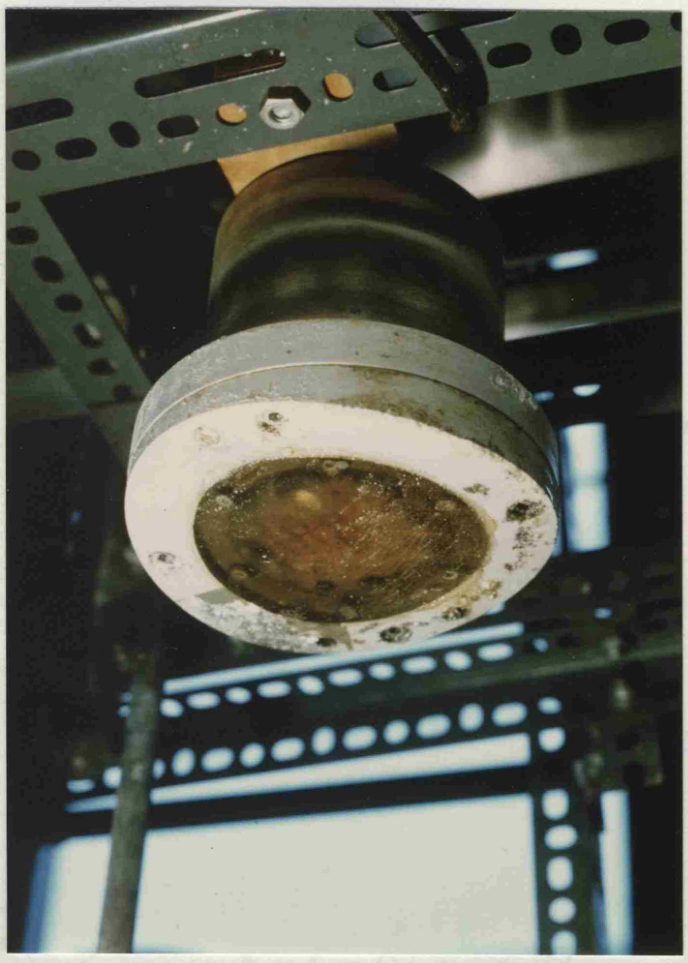

Figure 4.6 Transmitting transducer

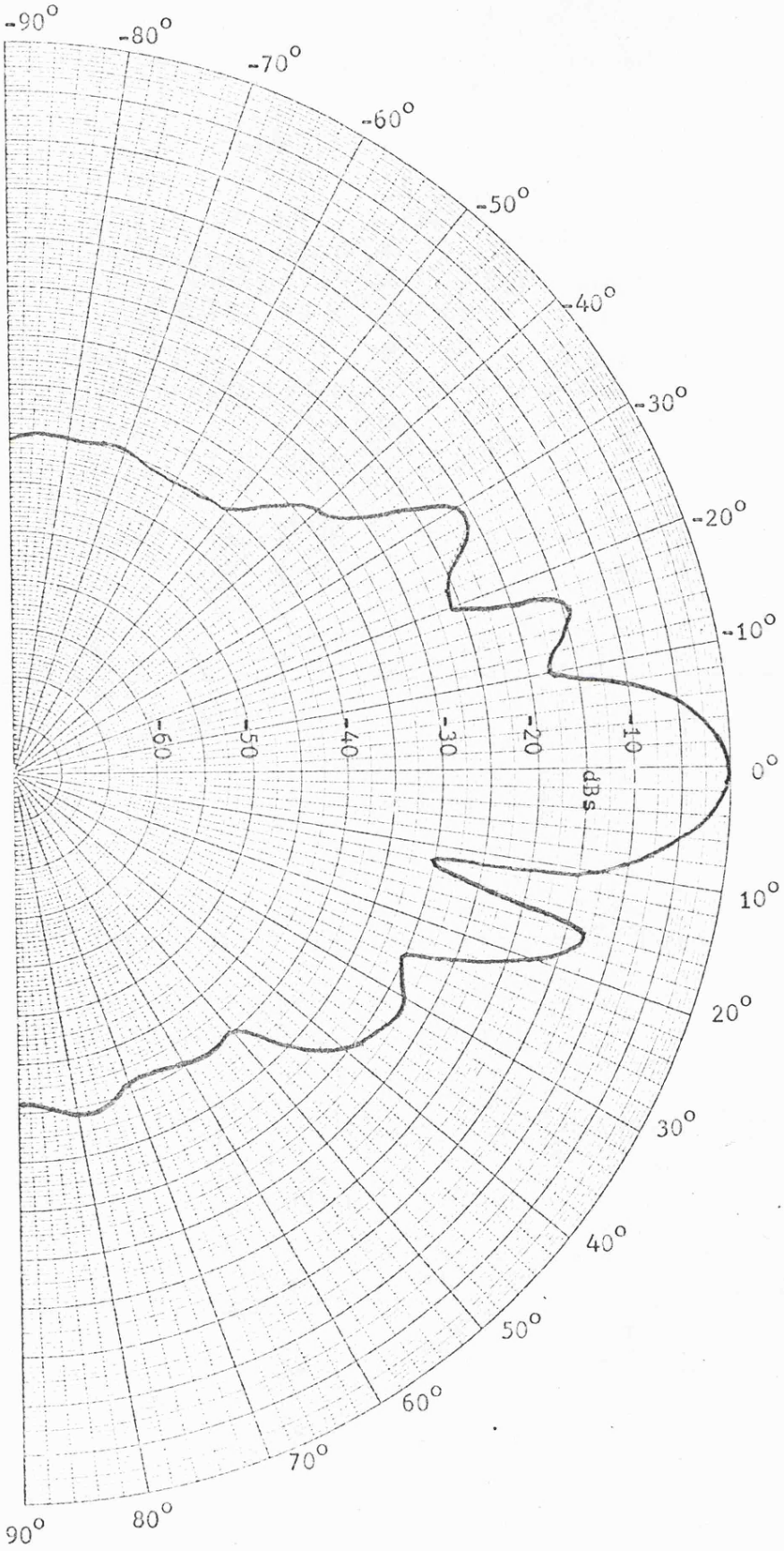

Figure 4.7 Beam pattern of transmitting transducer about normal axis at resonance.

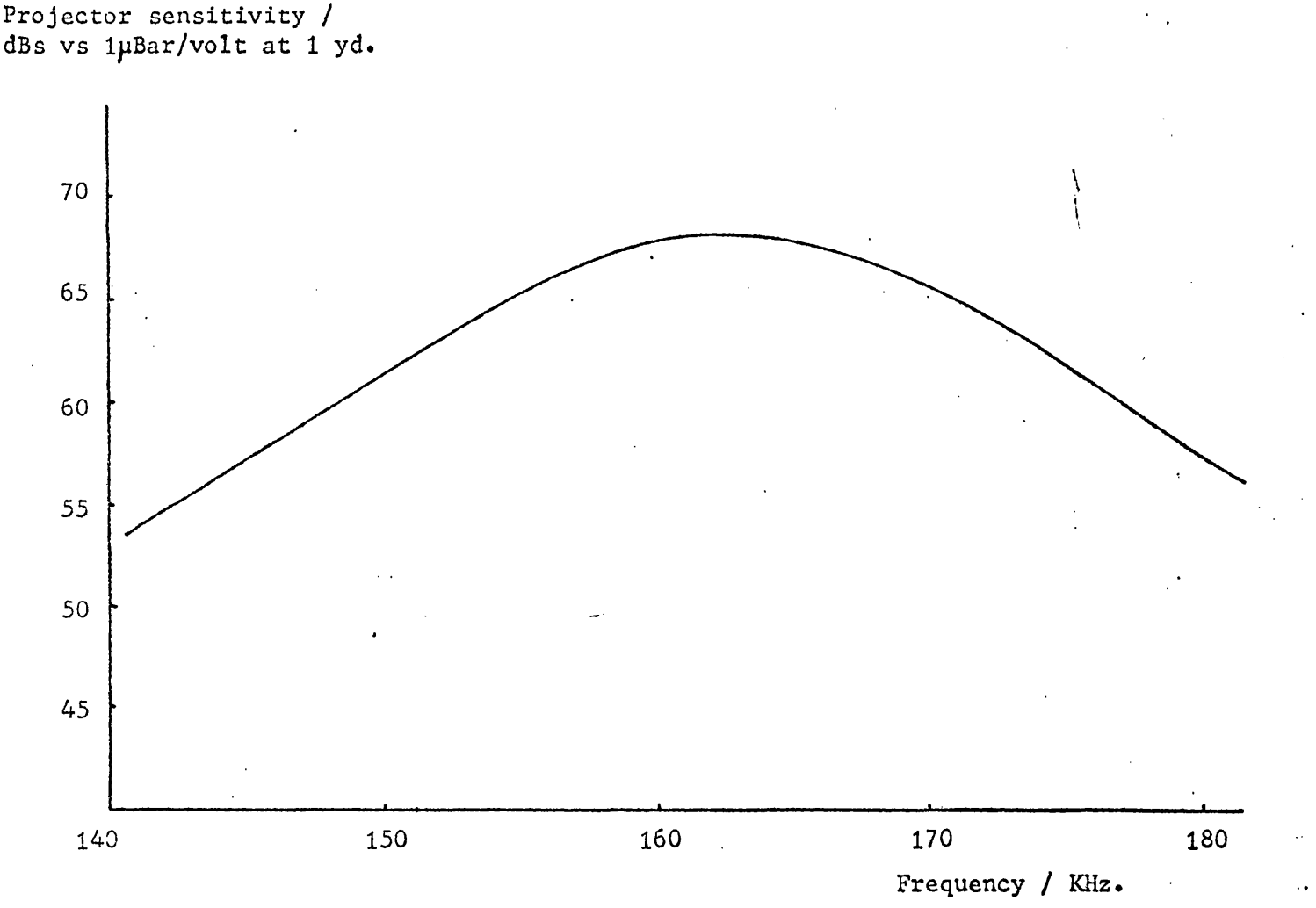

Figure 4.8 Transmitter sensitivity.

4.6.2. Receiving transducer

The receiving transducer was the unit used by Salkield (1975). This is an 88 element array arranged as a square matrix having element spacings of 3mm., the indivudal P.Z.T. ceramics having average dimensions 4.1mm x 4.1mm x 6mm thickness.

The elements are stuck individually to 1.5mm thick strips of cork, to reduce the inter-element coupling, using Araldite (AY100/HY100). The strips are cemented together and mounted on 4mm. thick closed cell neoprene, which is attached to a 1.5mm thick aluminium sheet.

The complete array is mounted in a 30mm radius cylinder with a thin rubber diaphragm over the front and filled with filtered, de-aerated castor oil.

The construction of the array is shown in figure 4.9 and its admittance loop and beam pattern are shown in figures 4.10 and 4.11. The admittance loop was measured using a Wayne Kerr R.F. Bridge, Type B601.

4.7. Filters

Having mounted the transducers in their appropriate positions in the tank it was possible to obtain the impulse response of the system by performing a cross-correlation with a water path only. This impulse response contains all the information about the transducers and the rest of the electronic system including the amplifiers.

This was done initially using the arrangement shown in figure (4.1) but without the filters, producing the impulse response shown in figure

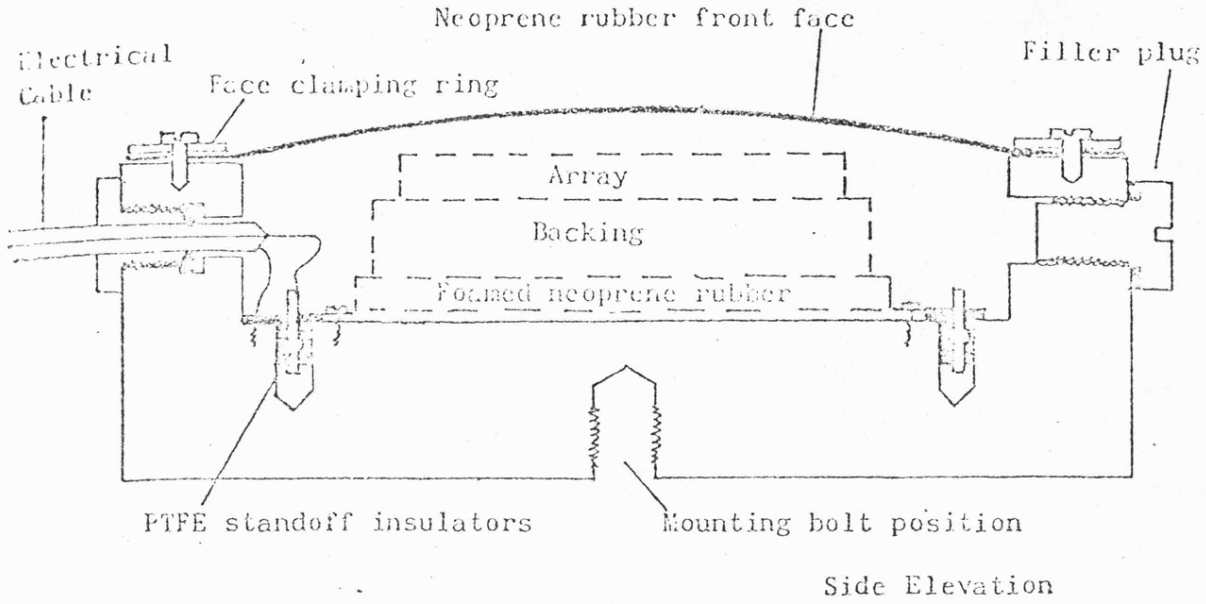

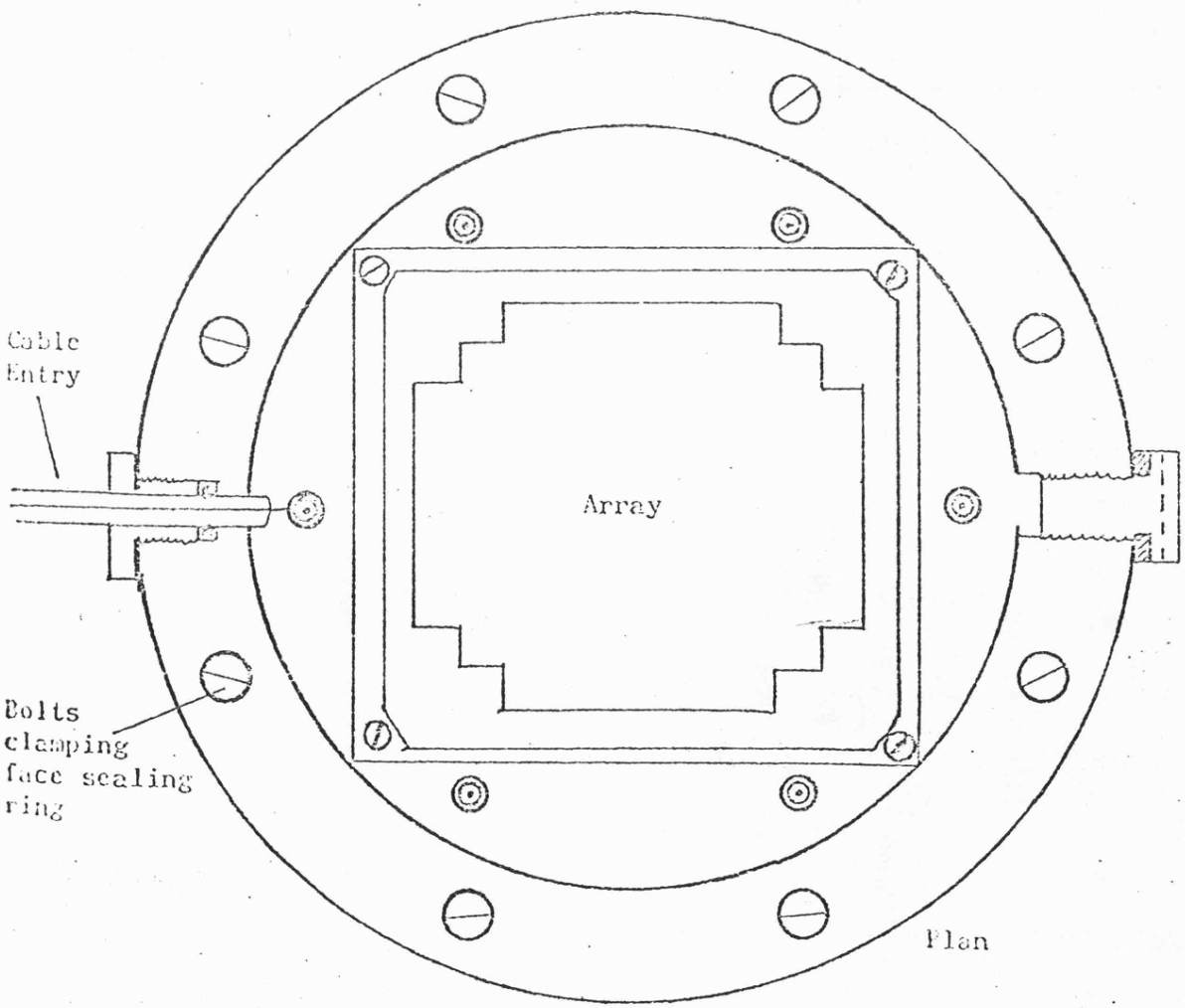

Figure 4.9 Construction of receiving transducer. (after Salkield 1975).

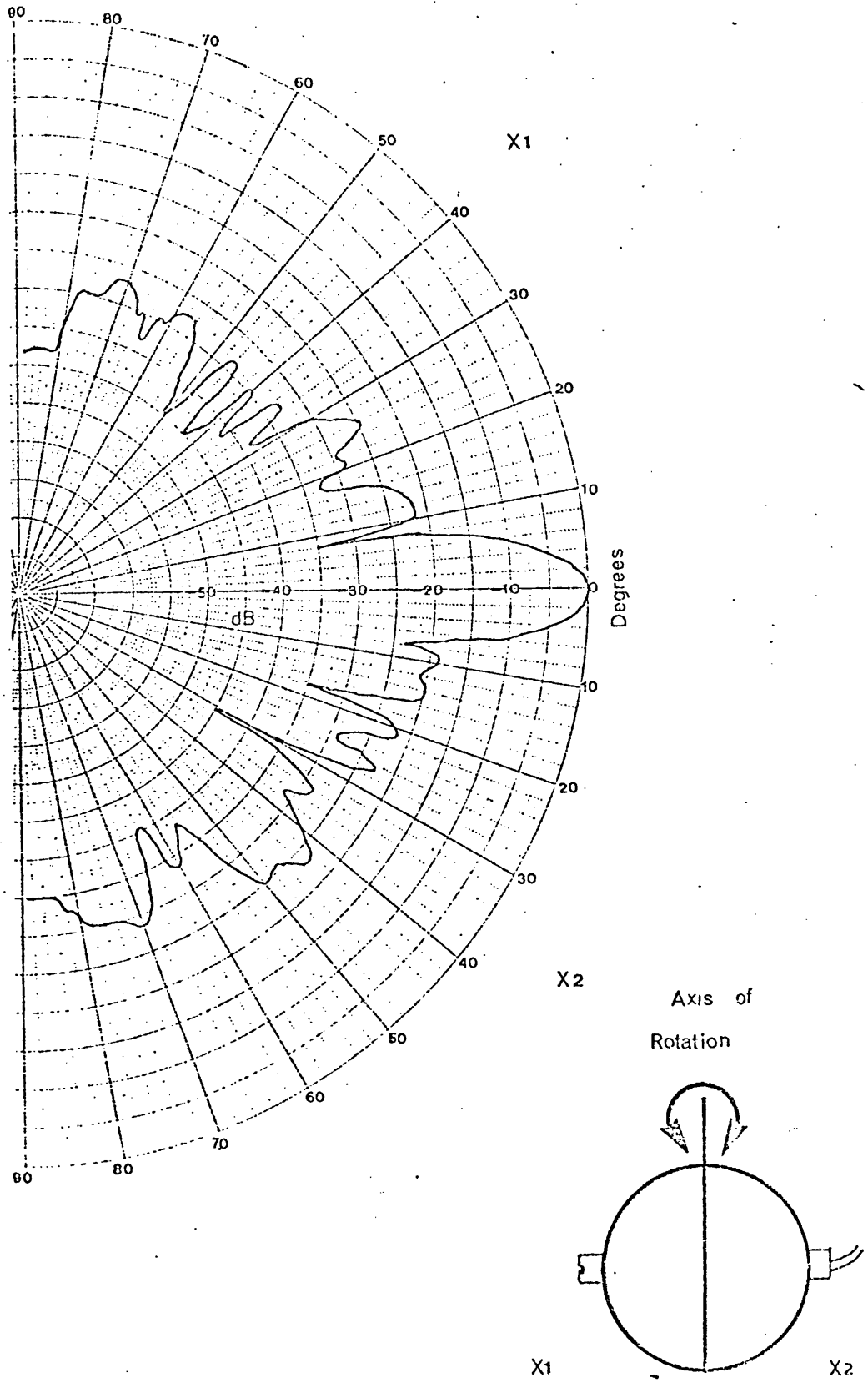

Figure 4.10 Beam pattern of receiving transducer at resonance.

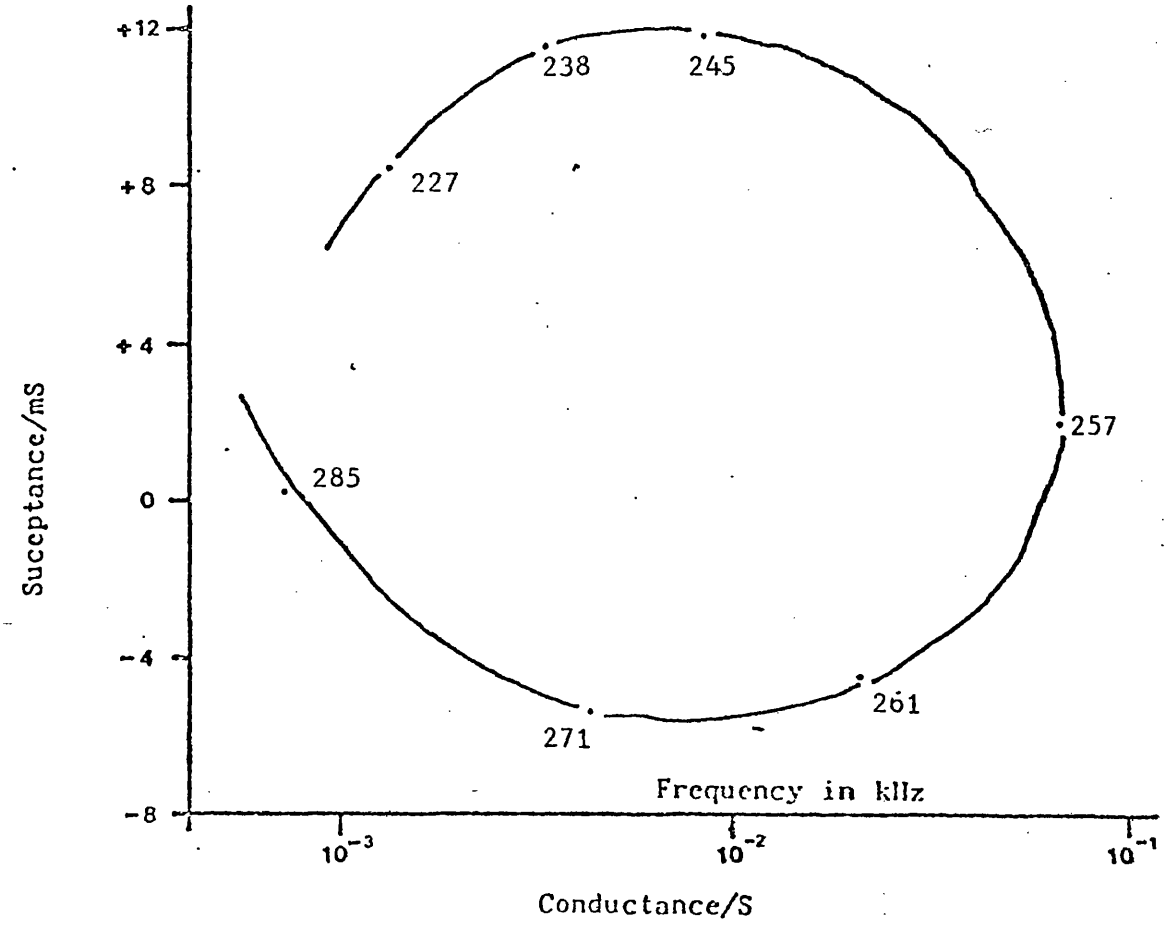

Figure 4.II Circle diagram of receiving transducer.

4.13 the power spectrum of which is shown in figure 4.14.

The important points to be noted are, the 'ringing' after the main peak of the impulse response and the transducer resonance peaks in the power distribution function. The ringing is caused by the predominance of energy at 167 KHz of the spectrum and could be reduced if the overall transfer response of the system could be flattened.

To achieve this, an analogue filter was designed having band cut regions centred around the two transducer resonances. The filter was considered in two matched sections, the first tuned to the lower frequency resonance and the second to the higher frequency.

The basic design of the circuits was of the form shown in figure 4.12.

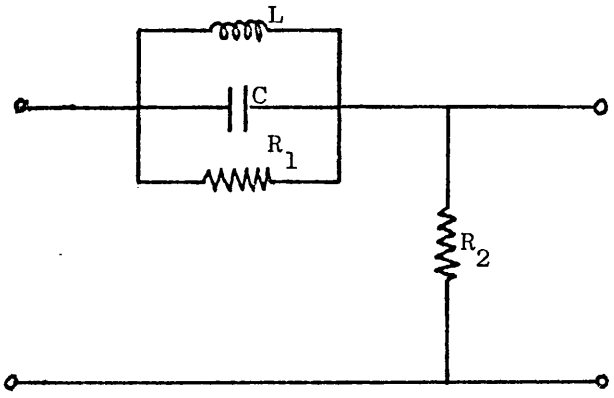

Figure 4.12 Basic design of resonance compensating filter.

The component values were calculated by consideration of the attenuation required at resonance, the resonant frequency and the Q factor of the resonance required; this must obviously match up with

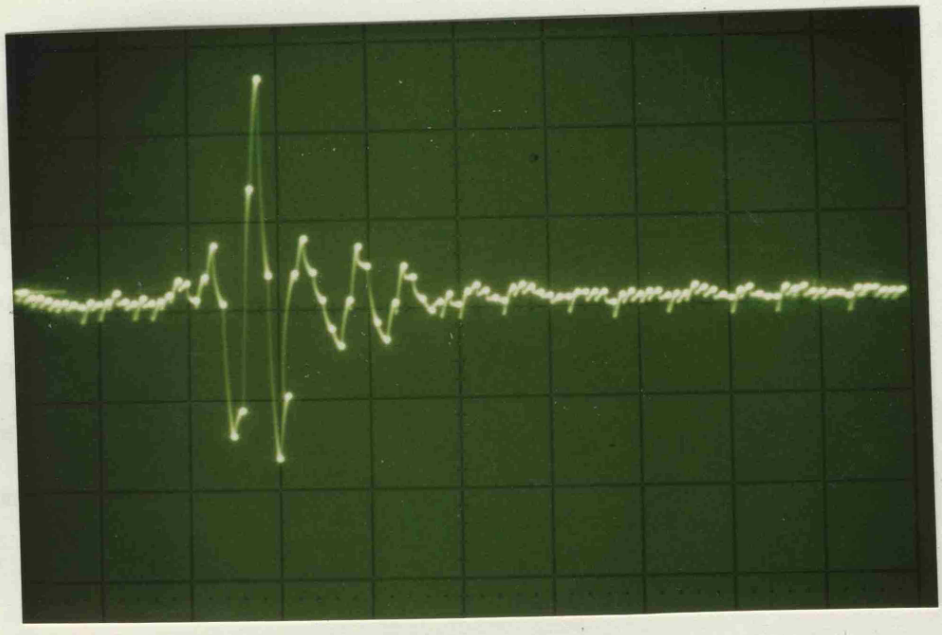

Figure 4.I3 Unfiltered impulse response.
Horizontal scale 10 μs. cm.$^{-1}$

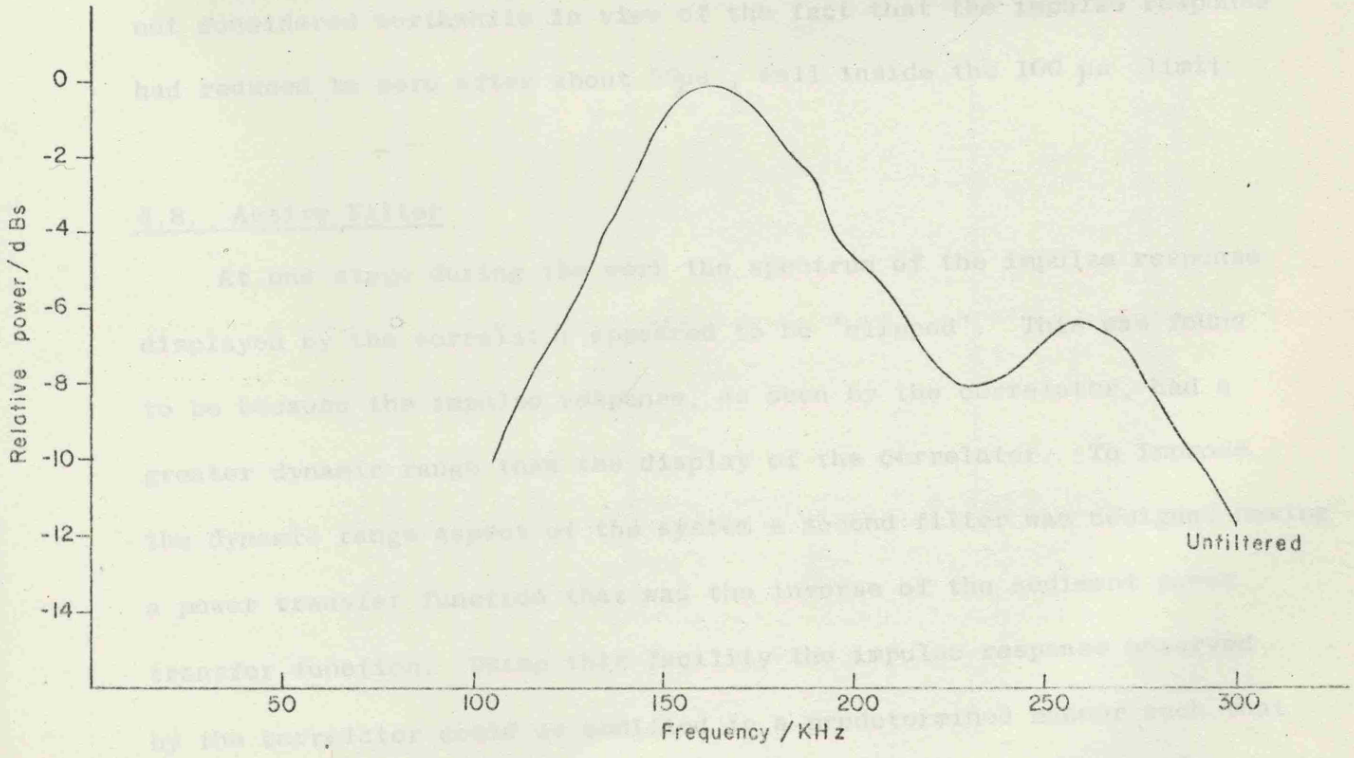

Figure 4.I4 Power spectrum of unfiltered impulse response.
(Water path only)

the power distribution peaks.

The final filter design used was as shown in figure 4.15. There was a small amount of trim available on each of the inductors to allow for fine tuning of the centre frequencies.

Figure 4.16 shows the impulse response as recorded with the analogue filter in circuit, the ringing after the main peak has now been considerably reduced and the power distribution of this new response (figure 4.17) demonstrates the way in which the overall spectrum has been smoothed and broadened at the 3.dB points. A direct comparison of the responses is shown in figure 4.18.

It was not possible to produce a completely flat spectrum using just a two element filter because of the complicated nature of the initial response. Better results could be obtained by using more elements but the slight improvement that would have been achieved was not considered worthwhile in view of the fact that the impulse response had reduced to zero after about 50μs , well inside the 100 μs limit.

4.8. Active Filter

At one stage during the work the spectrum of the impulse response displayed by the correlator appeared to be 'clipped'. This was found to be because the impulse response, as seen by the correlator, had a greater dynamic range than the display of the correlator. To improve the dynamic range aspect of the system a second filter was designed having a power transfer function that was the inverse of the sediment power transfer function. Using this facility the impulse response observed by the correlator could be modified in a predetermined manner such that its dynamic range was within the limits of the display.

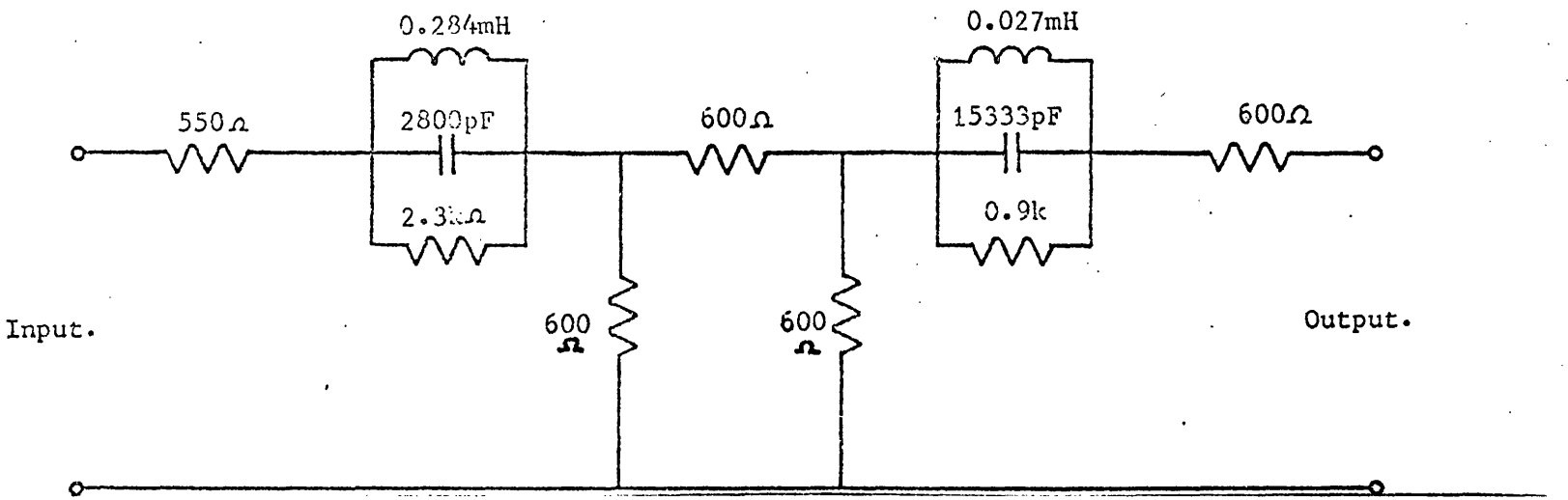

Figure 4.15 Circuit diagram of analogue filter used to compensate for transducer resonances.

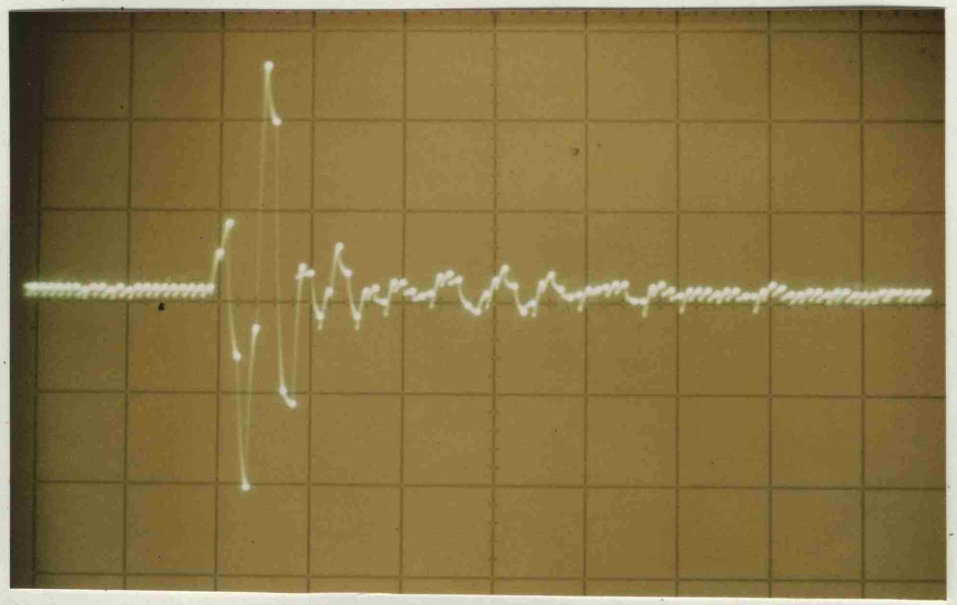

Figure 4.I6 Filtered impulse response.
Horizontal scale 10 μs. cm.$^{-1}$

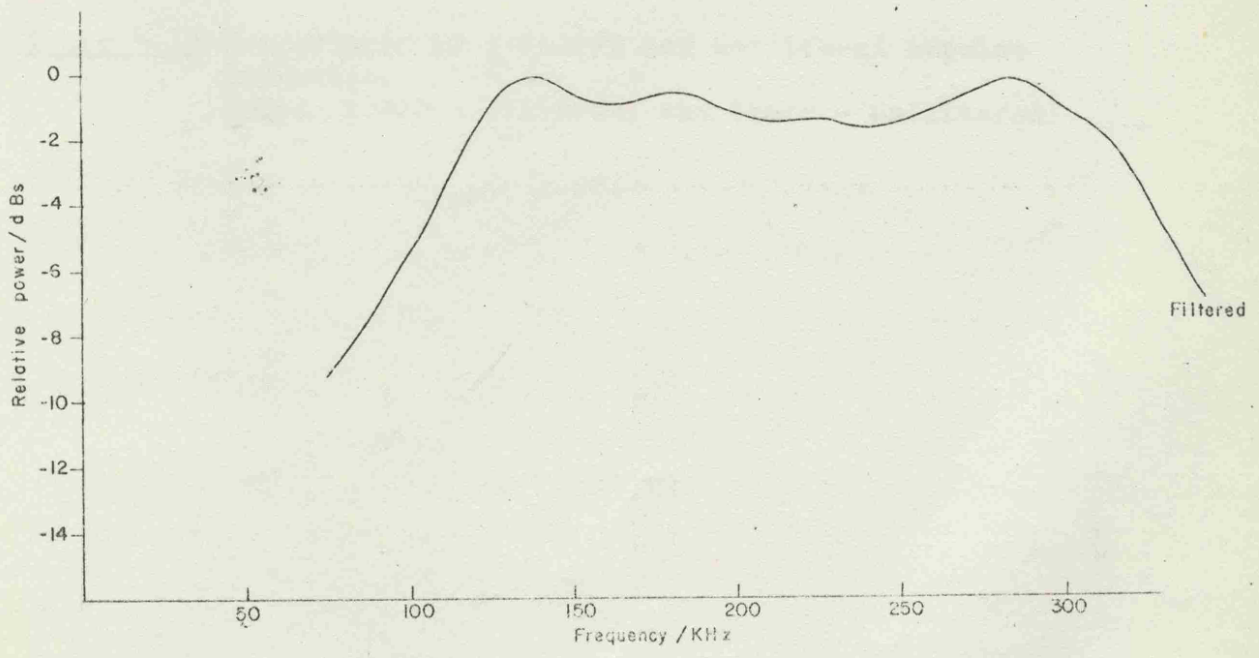

Figure 4.I7 Power spectrum of filtered impulse response.

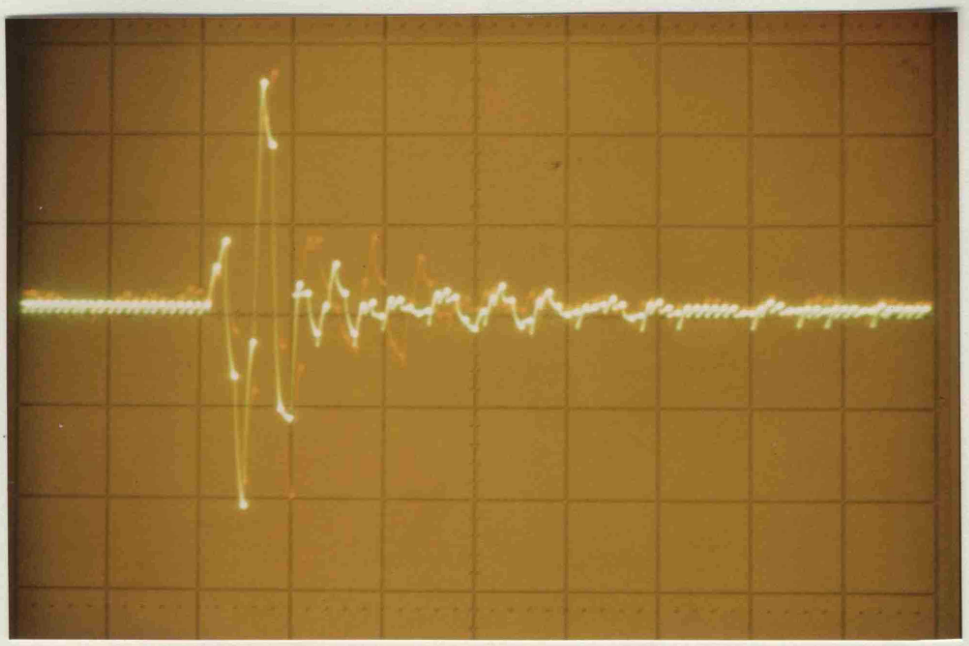

Figure 4.18 Comparision of filtered and unfiltered impulse responses.
(green trace - filtered, red trace - unfiltered)

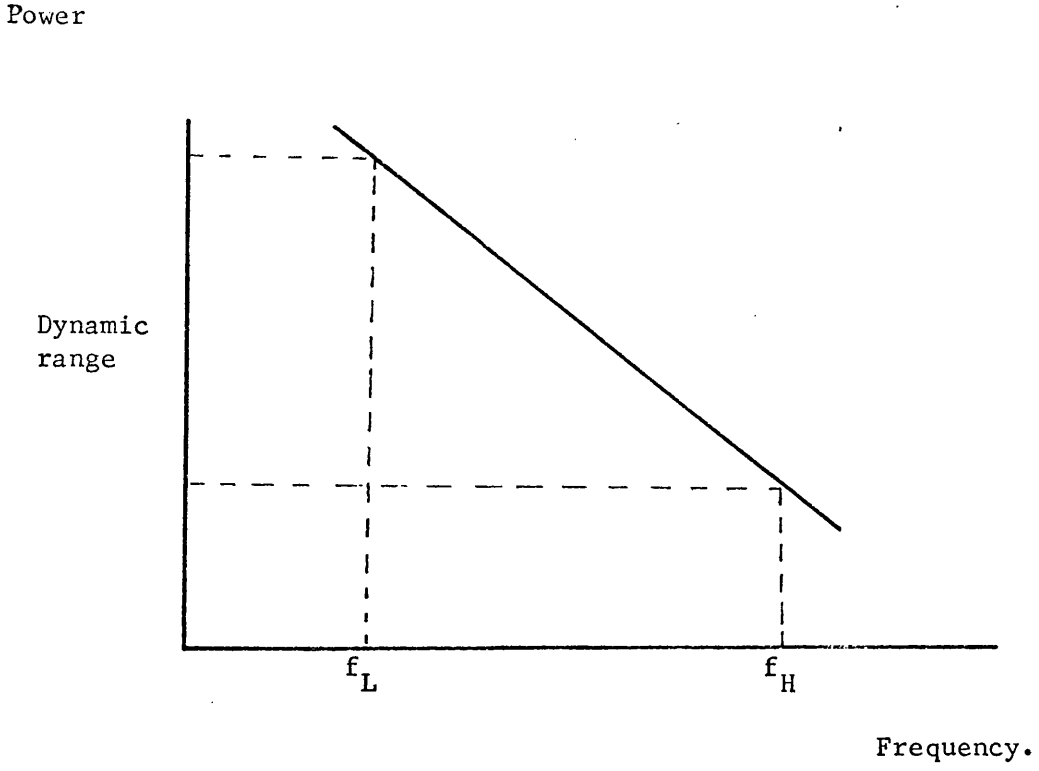

Figure 4.19 Dynamic range limitation.

If a particular sediment sample has an associated power transfer function having a near predictable frequency dependence (eg af^k) then the impulse response associated with this sediment will have a dynamic range of

$$D_R = af_H^k - af_L^k \qquad 4.9$$

where

f_H is the highest frequency of interest

f_L is the lowest frequency of interest

a and k are constants.

This dynamic range could be greater than the limits of the correlator display.

If, however, the signal was passed through a filter having a power transfer function of the form bf^{-k}, (where b is a constant less than a), then the dynamic range of the signal could be reduced to an acceptable level by suitable choice of the constant b.

The choice of b is limited by the fact that its own transfer function must have a dynamic range that lies within the limits of the correlator so that its effect can be assessed and subsequently corrected for.

Hence the dynamic range of the correlator

$$D > bf_H^k - bf_L^k \qquad 4.10$$

It is clear that by introducing such a filter the dynamic range of the system can be doubled.

An active filter circuit, designed to improve the dynamic range of the system was built and used between the stages of the Brookdeal amplifier. The circuit made use of three operational amplifiers and is shown in figure 4.20.

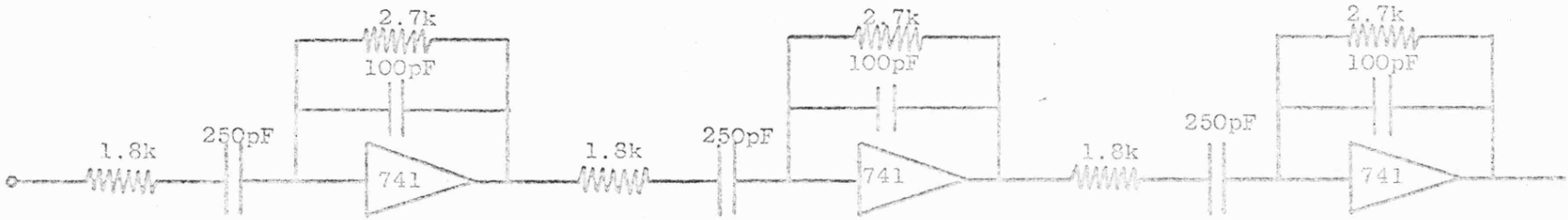

Figure 4.20 Circuit diagram of active filter system

4.9. Amplifier

The amplifier used for this work was a Brookdeal Model 451 systems amplifier having a frequency range of 1Hz to 1MHz. The amplifier had five calibrated gain options together with a variable gain facility.

4.10. Correlator

The correlator used for this work was a Hewlett Packard model HP 3721A. Averaging was always done in the summation mode using 128 x 1024 updatings to give each impulse response. The time scale was set to 1μs per horizontal division giving maximum resolution and an impulse response of 100μs in length. The correlator has an offset delay facility meaning that if the event of interest occurs, for example, after 620μs of impulse response, it is possible to set the delay offset to 600μs and just look at the 100 μs of interest. It also means that by using this facility it is possible to record impulse responses greater than 100μs in length in stages of 100μs at a time.

The resolution of the correlator is dependant on display sensitivity but is always better than 25 levels/cm giving a dynamic range of 70dB at the sensitivities being used.

4.11. Pseudo-Random Binary Sequence Generator

The particular generator used had a delayed output facility. This enabled a second output to be used that was identical to the primary output but delayed with respect to it by an integral number of clock periods selected by thumbwheels on the front of the unit. When looking at the cross-correlation function between the signal transmitted into the water and the signal received after transmission, the delay facility was used to remove the uninteresting 'water path' sections of the impulse response.

4.12. Sequence parameters

The sequence parameters used for all of this work were:

clock period 1μs giving fc = 1MHz

sequence length 2047 giving fL = 488Hz

(see section 4.5)

4.13. Paper Tape

The impulse response data was transferred to a digital computer in the form of punched paper tape, output from a Datek paper tape punch. The data in normal ASCII was stored in the form of one hundred five digit numbers, separated into blocks of ten numbers by control characters. Each block of one hundred numbers represented one impulse response of 100μs sampled at 1 MHz and was preceded by five manually entered identification numbers.

Chapter 5

PHYSICAL PROPERTIES OF THE SEDIMENTS USED

5.1. Introduction

The objectives of this work were to obtain velocity and attenuation measurements for a range of marine sediments and to assess how these properties varied with frequency and with sediment parameters.

Although, in particular areas, the properties of some sea-floor sediments may be fairly consistent, by their nature they are generally highly irregular in size, shape, packing structure and porosity. If then, one tries to relate the acoustic properties of such a material to some of its physical properties it is an advantage to be able to control at least some of these parameters to reduce the number of variables involved. In general, a marine sediment will be composed of a number of different types of materials (for example, the main constituent may be quartz but there may also be a reasonable amount of calcareous material together with some organic material) each having different densities and probably each having a characteristic shape.

For these reasons it was decided that the initial work should be directed at artificial sediments where greater control was possible over some of the important parameters and the later work at real sediments using different ranges of sand sizes.

In the real situation there is a considerable variety of sizes of granular material found on the sea-floor although a large proportion of sediments found on continental shelf areas can be grouped into the

'sand' size range. For this reason it was decided to study granular material in the range 50 to 1200μm diameter with an extension to 4mm and 8mm in the case of the artificial sediment to look at the region where the wave-length of the acoustic signal was of the same order as the diameter of the particles.

This enabled data to be collected on a range of non-cohesive materials and allowed evaluation of the importance of individual sediment parameters in relation to the acoustic properties.

5.2. The Sediment

5.2.1. Artificial Sediment

The artificial sediment used for the study was a type of small, solid soda glass sphere called Ballotini, obtained from Englass Ltd.

These small beads are manufactured by a variety of processes, most of which depend on the property of an irregular glass particle to contract into a sphere when molten. The final sorting of the particles is done by sieving. The Ballotini are well sorted, well rounded and exhibit reasonable sphericity.

The mean grain sizes of the Ballotini used were, 250μm, 490μm, 1200μm, 4mm and 8mm.

5.2.2. Sand Samples

Sand samples were obtained from British Industrial Sands Ltd. at Redhill in four ranges, having mean grain sizes of: 330μm, 250μm, 130μm and 50μm and also from the Institute of Oceanographic Sciences

at Taunton, having a mean grain size of 480μm.

Photographs of the Ballotini and sand samples were obtained using a scanning electron microscope as shown in figures 5.1 and 5.2 respectively. The pictures demonstrate clearly the greater angularity of the sand samples together with their wider size distribution. The sand grains are mostly quartz and are highly irregular in shape. In contrast the Ballotini are well-rounded and have good sphericity. The individual particles can be seen to be slightly pitted or chipped and there are a small percentage of elongated grains noticeable on the photograph of the 250μm sample.

5.3. Properties of interest

The physical properties which are perhaps of most relevance to the acoustic properties are concerned with the way in which fluid flows through, or oscillates within the granular mass. Under this category come a number of parameters, for example, the size and shape of individual pores, the texture of the grains and the distribution of pores. It should also be noted that some of the pores are 'closed' to the system, that is, they are cut off from the other pores and the pockets of fluid within them are virtually stagnant. The proportion of open and closed holes is therefore also an important parameter.

These are the most fundamental properties of interest as they dictate the resistance to fluid flow through the sediment. They are, however, almost impossible to measure directly and cannot be assessed without disturbing the sediment and hence causing some degree of physical change.

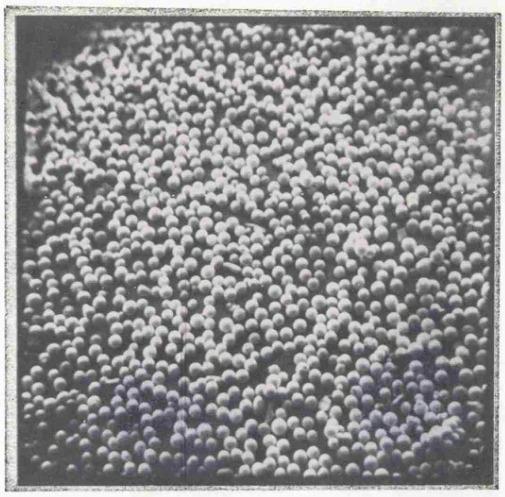

250 μm. diameter.
Magnification x 8.1

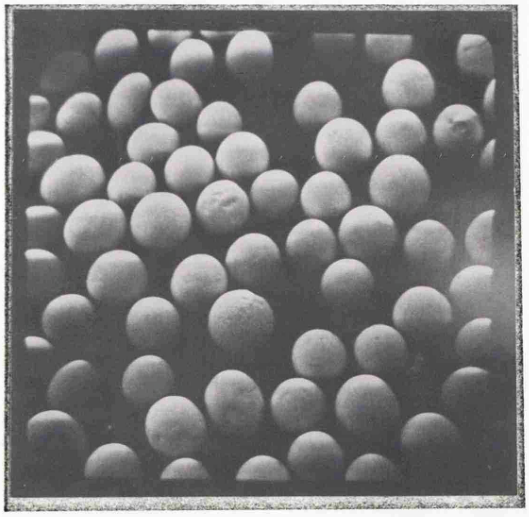

490 μm. diameter
Magnification x 16,2

Figure 5.1 Scanning electron microscope pictures of Ballotini samples.

SAND

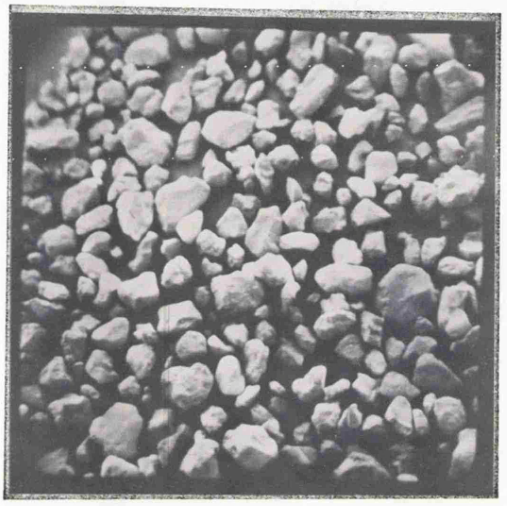

250μm. diameter.

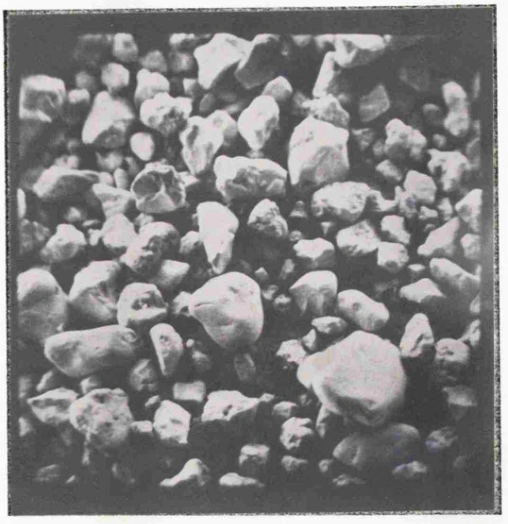

330μm. diameter.

Figure 5.2 Scanning electron microscope pictures of sand samples.

Magnification - x 23.

For this reason it is necessary to look at the less fundamental properties and concentrate on those that have more direct relevance to the acoustic properties and can be measured directly without disturbing the sample.

The physical parameters selected for analysis were:-

(1) The size and size distribution of the grains

These indirectly determine the size and to an extent the shape of the pores and are hence of prime importance.

(2) The porosity

This is determined by the number and size of the voids within the matrix.

(3) The permeability

This is determined by a large number of fundamental parameters including the ratio of open to closed pores and the d.c. flow resistance.

(4) The specific gravity

This is important because of its relevance to the wave equations for the propagation of elastic waves, and its effect on the inertia of the system.

5.4. Particle size analysis

For the analysis of size distributions within this range mechanical seiving was considered to be the most suitable and convenient method of analysis.

Dry samples of each sediment weighing approximately 200 gm. were dry seived using an Endicott Model E.F.1. Shaker and B.S. 450-1962 seives for 20 minutes. A table of B.S. seive aperture widths and phi scales

is given in Appendix B. Details of the actual technique are not included here as this is a well established geotechnical measurement that is adequately described in standard texts, (e.g. Akroyd 1964).

The particle sizes and size distribution are described by the graphic mean diameter (M_ϕ) and the phi deviation (σ_ϕ).

These have been calculated using the formulae defined by Inman (1952) who showed

Mean graphic diameter:

$$M_\phi = \frac{1}{3}(\phi_{16} + \phi_{50} + \phi_{84}) \qquad 5.1$$

and phi deviation

$$\sigma_\phi = \tfrac{1}{2}(\phi_{84} - \phi_{16}) \qquad 5.2$$

where ϕ subscript is the phi value corresponding to the cumulative percentage weight given by the subscript.

The quantities are all evaluated in phi-units where the phi diameter is given by

$$\sigma_\phi = -\log_2 d \qquad 5.3$$

Where d is the particle diameter

The cumulative size distribution curves for the sediments used are shown in figures 5.3a and 5.3b and the size parameters taken from these are reproduced in Table 5.1.

5.5. Discussion of size analysis

It should be expected that the size analyses for the Ballotini

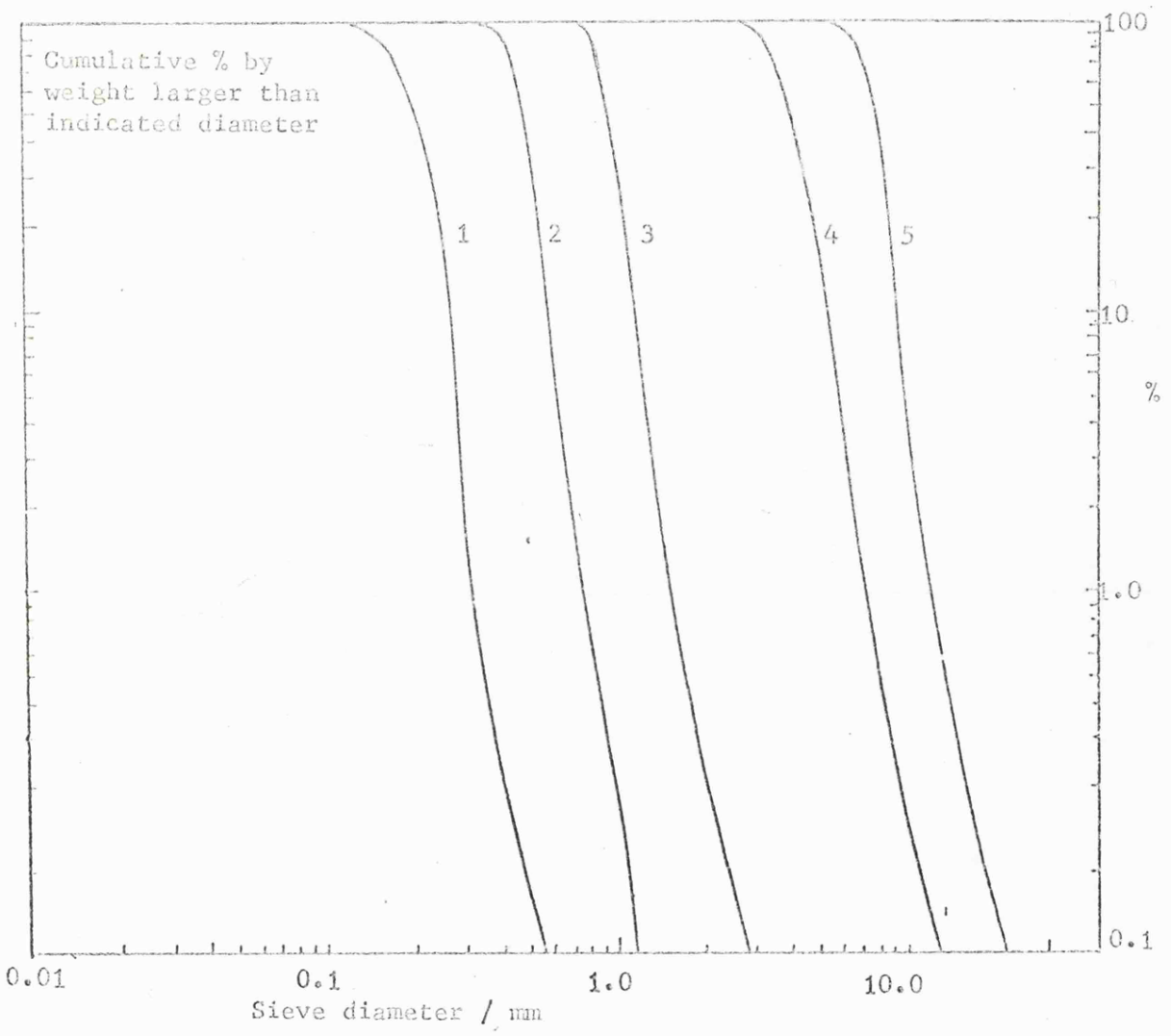

Figure 5.3 a Cumulative size curves for Ballotini

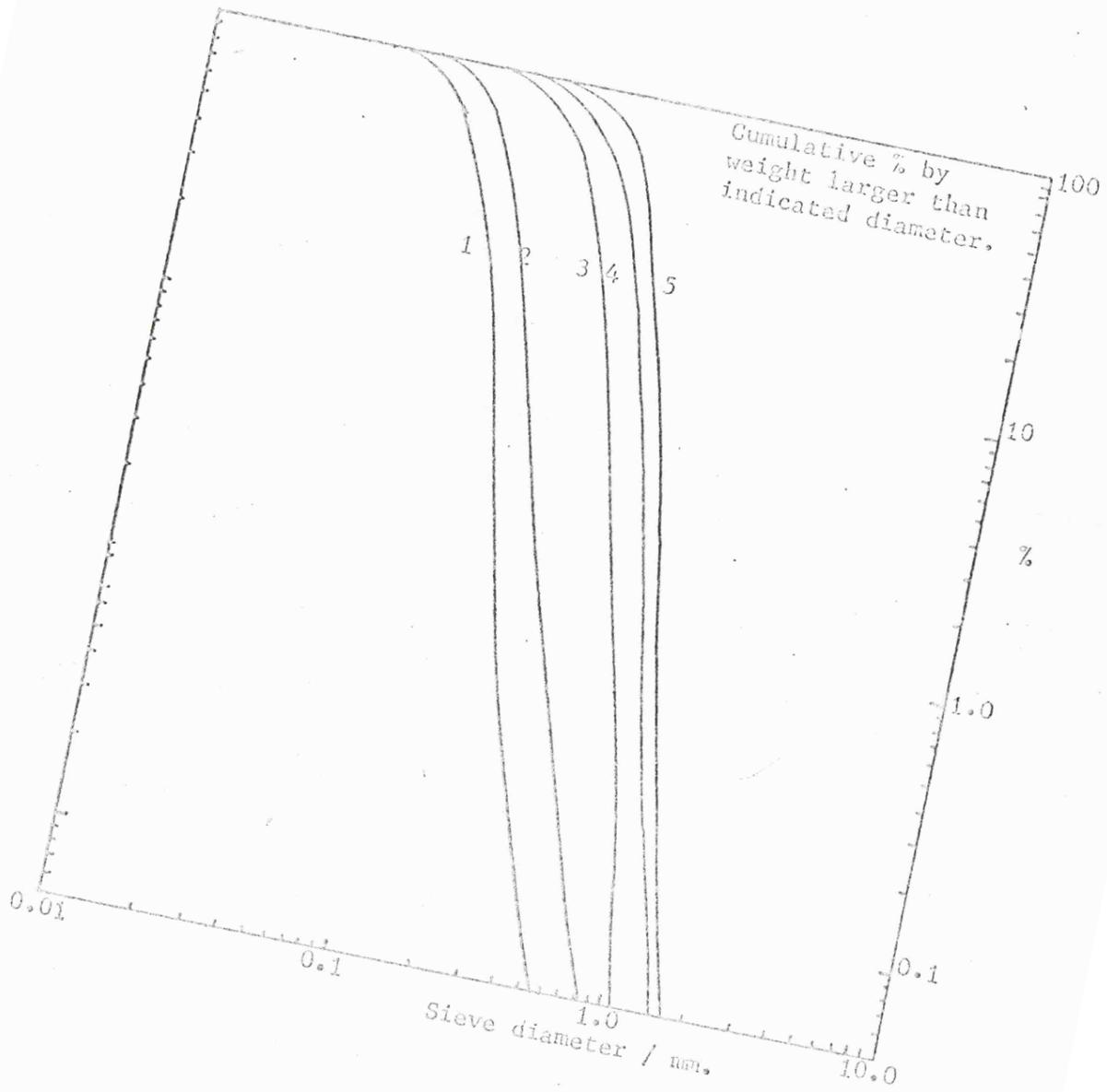

Figure 5.3 b

Cumulative size curves for sand samples.

Sediment	Mean Diameter μm	Mø	Phi Deviation σ_ϕ
Sand No. 1.	50	4.32	0.85
Sand No. 2.	130	2.94	0.79
Sand No. 3.	250	2.00	0.50
Sand No. 4.	330	1.60	0.52
Sand No. 5.	480	1.06	0.49
Ballotini No. 1.	250	2.00	0.16
Ballotini No. 2.	490	1.03	0.20
Ballotini No. 3.	1200	-0.26	0.15
Ballotini No. 4.	4000	-2.00	0.15
Ballotini No. 5.	8000	-3.00	0.08

Table 5.1. Mean grain sizes and phi deviation values

samples should be more acceptable than those for the sand sediment. This is because mechanical sieving as an analysis technique has the tendency to give the smallest individual particle dimensions rather than the mean. For almost spherical particles there is very small variation in the dimensions of individual grains and hence sieving will give a much more accurate result. The sphericity of the Ballotini is much higher than that of the more angular, naturally occuring sand samples and hence the size analysis has more physical significance.

The Ballotini had smaller phi deviations than those of the sand samples as can be seen from figures 5.3a and 5.3b although all the distributions were fairly narrow. The relationship between phi deviation and mean grain diameter for the sands used in this study (figure 5.3c) is typical of marine sediments in general (e.g. Inman and Chamberlain 1955) the sediments showing the best sorting being those having the largest mean diameters. For the Ballotini however, this trend does not apply and there is no significant correlation between phi deviation and mean grain size.

5.6. Porosity

The porosity of a granular mass is dependant on the size and the size distribution of the individual grains and also on the way in which they are packed. The problem of packing is a complex one due to irregularities of the sediment. Some indication of the packing can be obtained from porosity measurements. The main problem, however, will be discussed later in section 5.10.

5.7. Measurement of Porosity

Porosity is defined as the fractional percentage of void space to the total volume.

$$= \frac{V_o}{V + V_o} \times 100 \text{ percent} \qquad 5.4$$

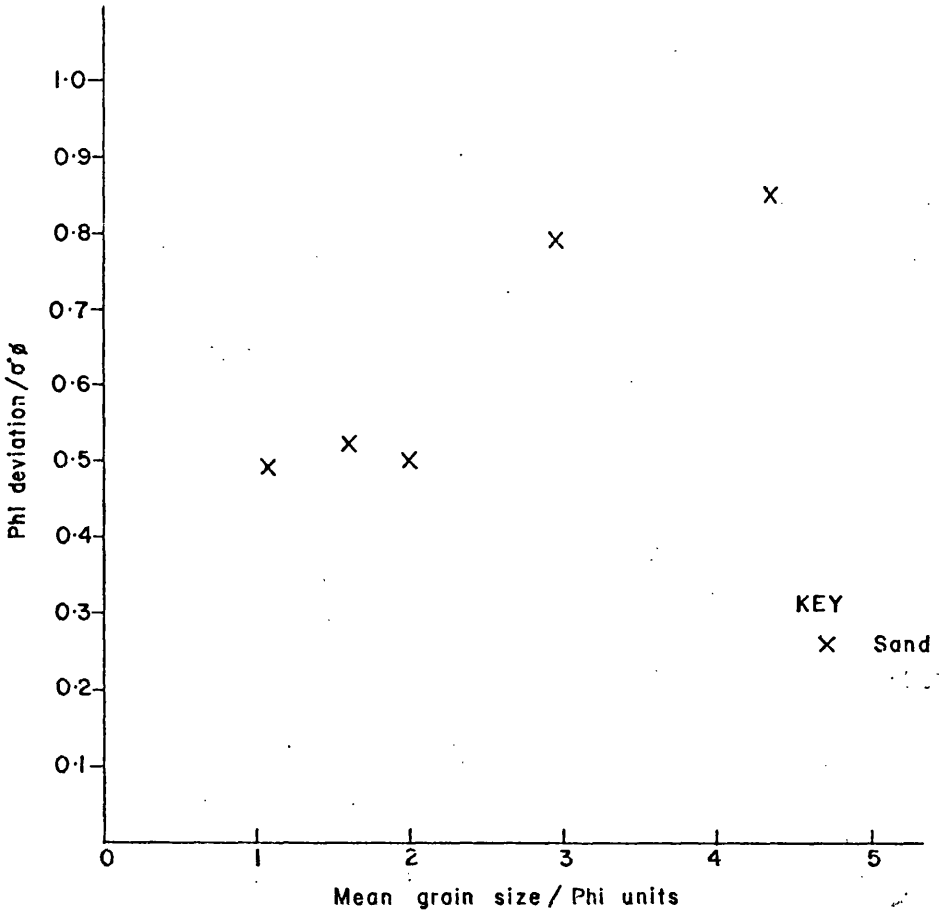

Figure 5.3c Relationship between phi deviation and mean grain size

where

V_o = volume of voids

V = volume of solids

There are many ways of measuring porosity, some depend on measuring the density of the granular material and some on measuring the weight and volume of saturated and unsaturated samples. The particular method used here was chosen as being the one most likely to reveal the characteristics of the individual sample being used for the acoustic analysis without causing any disturbance. Ideally one should choose to perform the physical and acoustical analyses on exactly the same sample without moving or disturbing it in any way. However, the extra complications that this would have meant to the experimental arrangement within the tank were not deemed worthwhile and so the analyses were carried out on samples prepared in exactly the same way as those used for the acoustic experiments.

The technique used involved the measurement of the weight of the water saturated sample, contained in a cell of known weight and volume. A circular cell was chosen for this, to imitate the conditions in the actual sample container. Other experimenters (e.g. Evans and Millman 1964) having previously shown that the shape of the cell affects the porosity of the enclosed mass. The material was then carefully dried and re-weighed.

If it is assumed that the density of the interstitial water is unity then the porosity is given by:

$$\eta = \frac{W_w - W_d}{V} \times 100 \text{ percent} \qquad 5.5$$

where

W_w = weight of water saturated sample

W_d = weight of dried sediment

V = volume of water saturated sample

The actual measurements were made in a graduated cylindrical cell of radius 3cm and height 10 cm. This was positioned in the sediment container under water and the evacuated sediment added in exactly the same way as it was for the acoustic analysis. The porosity cylinder was then carefully removed from the tank, dried and the above measurements noted. In this manner it was hoped to produce cells that were packed in as near identical conditions as possible to those occurring during the preparation of the bulk volume used for the acoustic analyses. The porosity results are shown in graphical and in tabular form in figure 5.4 and Table 5.2 respectively.

The porosity values obtained for a particular sediment varied depending upon the way in which the samples were prepared. The critical factors were the time that the sediment was shaken for, this was more significant for the sands than the Ballotini; and the way in which the sediment had been outgassed.

For consistency of results and in an attempt to simulate as closely as possible the real situation, it was decided that the sediment should be evacuated and agitated until the porosity remained constant. The agitation process took about 200 seconds to achieve stable results but was always allowed to run for 400. Figure 3.11 shows the way in which the porosity varied with agitation time for two of the sediments,

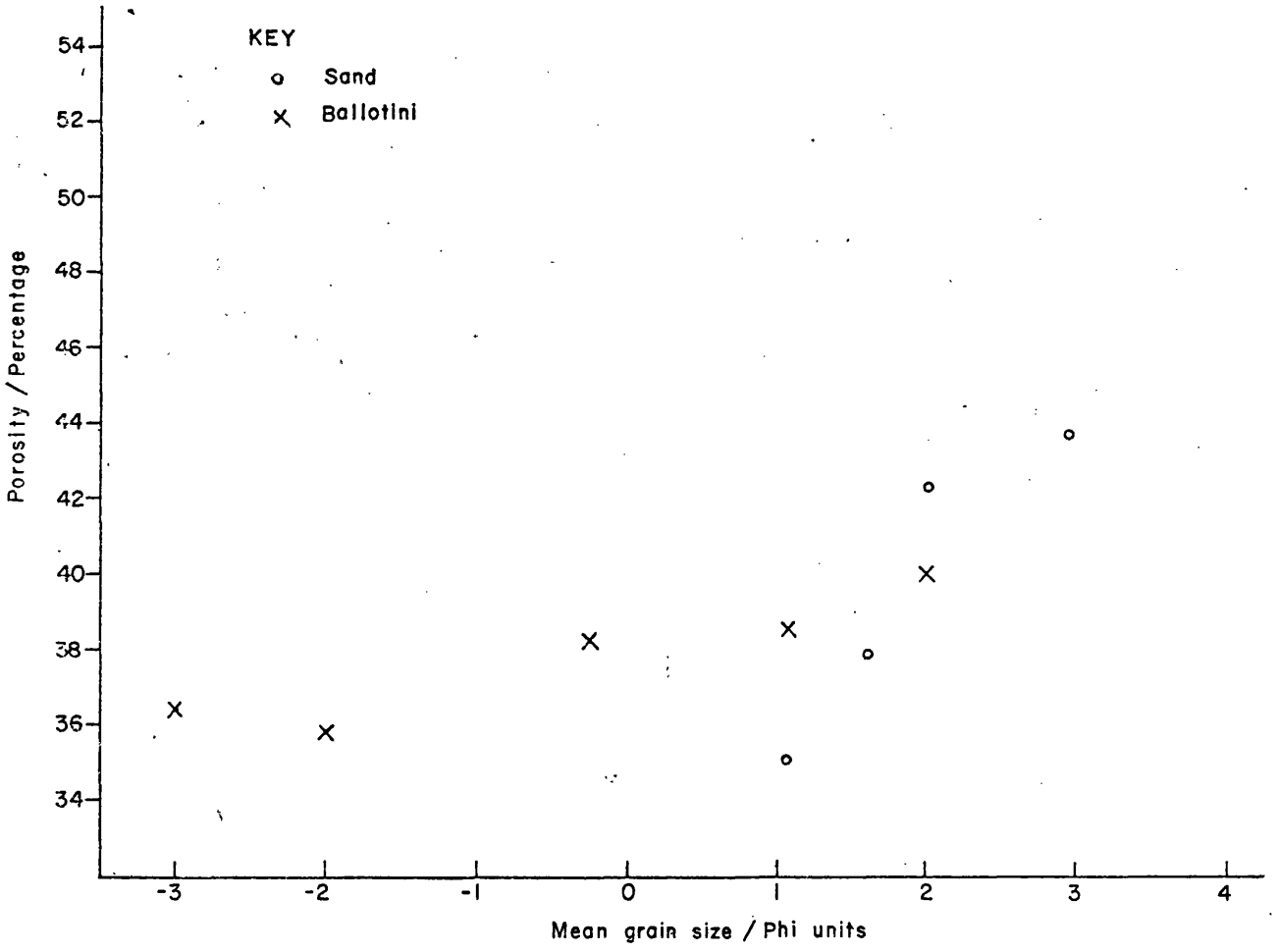

Figure 5.4 Relationship between porosity and mean grain size

Sediment	Mean Diameter (μm)	Porosity %
Ballotini Grade 1	250	40.0
" " 2	490	38.3
" " 3	1200	38.2
" " 4	4000	35.8
" " 5	8000	36.3
Sand Grade 1	50	55.0
" " 2	130	43.7
" " 3	250	42.3
" " 4	330	37.9
" " 5	480	35.0

Table 5.2 Porosity values for sediment samples.

indicating the manner in which stability of packing is reached. The evacuation process was carried out in a cylindrical drum and is described in section 3.7.

It can be seen from figure 5.4. that the dependence of porosity on mean grain size is more significant for the sand samples than for the more rounded Ballotini. The linear regression lines for the two sets of results indicate gradients of 5.85 and 0.77 for the sand and Ballotini samples respectively. This result is not surprising since porosity tends to be less dependent on grain size for matrices of packed spherical particles.

5.8. Permeability

One of the mechanisms by which acoustic energy can be lost from a fluid saturated porous granular medium is as a result of relative movement between the fluid and solid portions. If this is an important loss mechanism then it is reasonable to assume that attenuation is strongly related to permeability. Permeability also provides additional information on the packed sediment structure with particular emphasis on the shape of the grains.

Darcy (1856) showed that the rate of flow of a liquid through a porous medium was proportional to the hydraulic gradient; that is to the hydraulic head per unit length. The quantity of liquid passing through a porous medium also depends upon the viscosity and the density of the liquid, that is:-

$$q = \frac{A.i\ k\ \rho}{\eta} \qquad 5.6$$

where

q = quantity of liquid per unit time

A = cross sectional area

i = hydraulic gradient

k = coefficient of permeability

ρ = density of the fluid

η = coefficient of viscosity

The coefficient of permeability given above is a generalised one although for most soil mechanic and civil engineering problems the fluid is water at a temperature of about 10^{o}C. The density of water does not vary significantly with temperature and the small variations of viscosity can be considered negligible without introducing much error.

It is therefore convenient to combine these two factors together with the generalised coefficient of permeability and obtain what is ususally termed the Darcy coefficient of permeability

$$k = \frac{k\rho}{\eta} \qquad 5.7$$

The quantity of water flowing then becomes

$$q = Ak.i = \frac{Akh}{l} \qquad 5.8$$

where

h = hydraulic head

l = path length

If the hydraulic head is maintained constant and the dimensions of

the sample container do not change then the value of the coefficient of permeability is proportional to the quantity of water flowing per unit time. This is the basis of the constant head permeameter.

Permeability measurements were made on each of the sediments using a constant head permeameter constructed on the basis of a cylindrical cell having a cross-sectional area of approximately 30 sq. cm. (as shown in figure 5.5).

The end plates were constructed with 300 gauge stainless steel containing screens. Measurements of pressure were made using manometers at either end of the column enabling the hydraulic gradient to be estimated.

In each case the cell was packed under the same conditions as the porosity cell and the in-tank container were, for correlation of results.

The results of the permeability measurements are shown in figure 5.6. The slopes of the plots being 2.15 and 1.92 for the Ballotini and sand respectively, indicating an approximate square law relationship. The values for the Ballotini samples are higher due to the reduced angularity of the grains.

5.9. Specific gravity

The specific gravity of the sediment effects the inertia of the system and is hence a parameter worth measuring.

The specific gravity of each of the sand samples was measured using a 50 ml. specific gravity bottle. Measurements were also made on two of the Ballotini samples and were taken to be representative of the material used for all the Ballotini. This is a reasonable assumption bearing in mind that the Ballotini are all made from the same glass

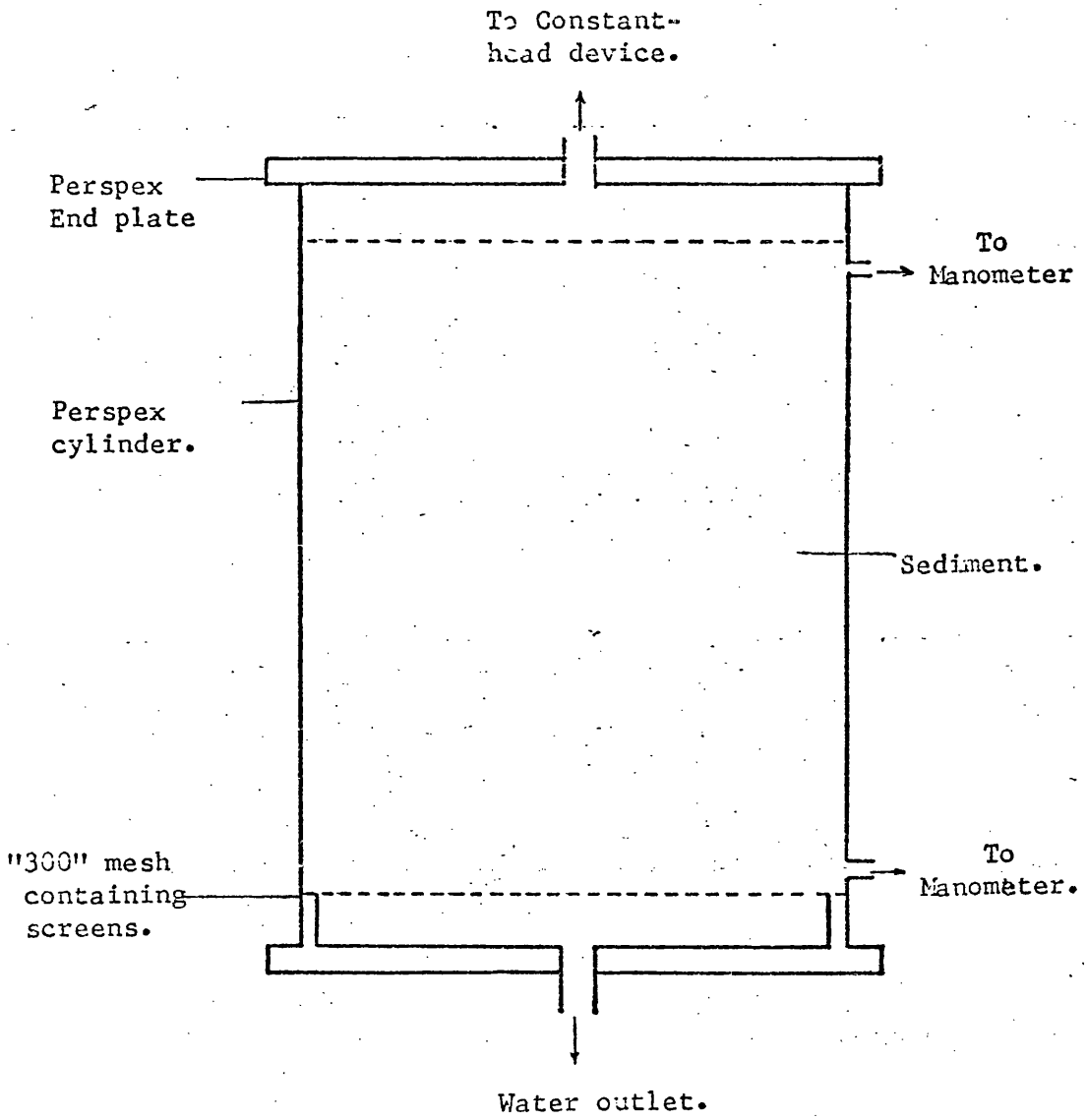

Figure 5.5 Permeability cell.

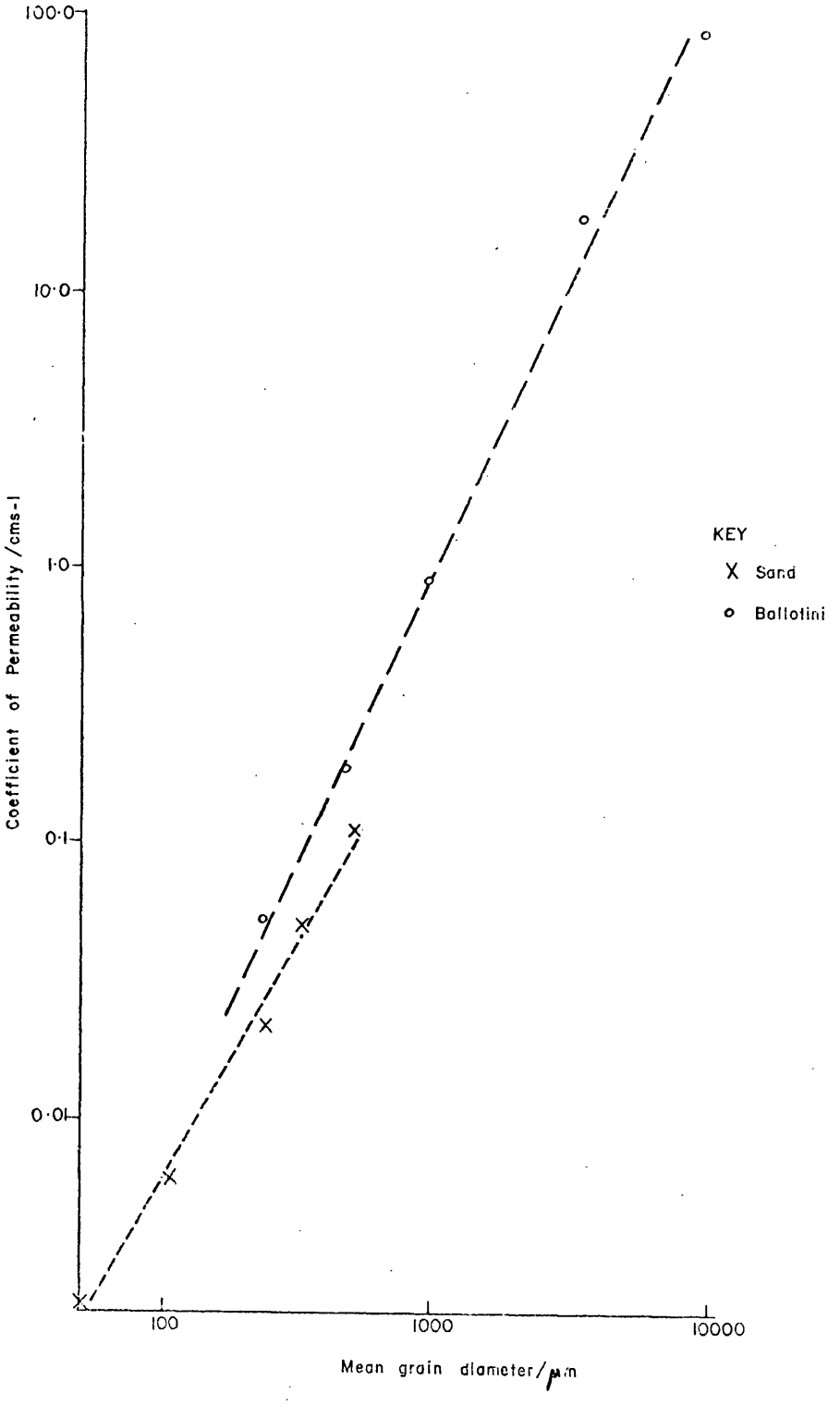

Figure 5.6 Relationship between permeability and mean grain size

and the results agreed well with the manufacturers data. The specific gravity results are shown in Table 5.3

BALLOTINI	2.48
SAND 1	2.68
SAND 2	2.67
SAND 3	2.64
SAND 4	2.64
SAND 5	2.65

Table 5.3. Specific Gravity Values

Variations in specific gravity were very small over the range of sand samples used and are hence unlikely to change the acoustic properties noticeably. The density of the Ballotini is lower however by a factor of 10%.

5.10. Packing

The acoustic properties of a particulate material are greatly dependant upon the spatial arrangement and the density of scattering centres within it. For a regularly packed ensemble these two parameters are well defined, but for an irregularly arranged mass they are more difficult to estimate and may vary throughout the medium by some small percentage.

The arrangement of the individual grains in the packed sediment columns is best described as random. The Ballotini samples exhibited a certain degree of regularity over finite volumes although this was not noticeable with the sand samples.

Attempts were made to control the packing structure of the sample using the larger sizes of Ballotini. This was done by physically placing individual grains into the sample container in a pre-determined pattern, in the first instance to produce a cubic, close-packed arrangement.

Although the sphericity of the Ballotini is fairly good and the size distribution fairly narrow it was found to be impossible to produce any quantity of sample in this manner before the cumulative effect of these minor imperfections prevented further layers being added.

If a more regularly shaped sample was used, having near perfect sphericity then it would be possible to examine this problem more carefully. This is an area of the work which needs much more development and time for a complete analysis and would be of great value.

There are several ways in which the packing structure of a granular mass can be assessed although nearly all of these, in some way, cause a change in the sample. The most successful of these involves pouring resin into the sediment. On solidification, small lumps of the granular mass can be removed for analysis. This method can directly give information

on the structure within the volume although it is debateable whether or not the infusion of the resin, done under pressure, and the setting process disturb the matrix.

5.11. Summary and Conclusions

The study was focused on two types of granular material, namely, soda glass Ballotini and natural sands. The samples had mean grain sizes ranging from 50μm, to 8mm, their size distribution being measured by seive analysis. The sand samples had a broader size distribution than the more regular and rounded Ballotini.

Porosity measurements were lower for the Ballotini than for the respective sands indicating a higher density of scattering centres, although the difference in size distribution makes this very difficult to assess quantitatively.

The change in porosity with packing is most significant for the sands because of the more irregular grain shape. The existence of high spots on the particles makes loose packing of the sand far more likely than for the more rounded Ballotini.

Considering the porosity and permeability results together it is noted that although the Ballotini packed to a lower porosity, their permeability values were higher. This implied differences in the ratio of open to 'closed' pores between the two types. There may not, in fact, be any 'closed' pores but merely almost closed areas where the porosity is high but the flow of water is restricted by narrow voids caused by larger grain to grain contact areas.

Small fluctuations in both porosity and permeability are likely to occur throughout any large quantity of irregular granular material, although, due to the size of the samples used here these fluctuations have been averaged out in the results, as also has their effect on the acoustic properties.

It is very difficult to assess the packing problem, the use of photography can give information on the surface structure with the advantage of not in any way disturbing the sample, although this can only give an indication of the bulk structure.

Chapter 6

TREATMENT OF ACOUSTIC DATA

6.1. Introduction

The previous chapter dealt with the analysis of the physical properties of the real and artificial sediments used in this study. It was, however, the measurement and computation of the acoustic data that posed some of the more demanding problems which were not always immediately apparent. This chapter explains some of the pitfalls encountered in performing the analysis and the way in which these difficulties were overcome.

The raw acoustic data consisted of impulse responses corresponding to the combined acoustic and electronic paths and from this all the necessary acoustic information regarding the different sediments was obtained.

6.2. Objectives of the Data Analysis

The objectives of the analysis were to obtain, from the cross-correlation of a pseudo-random binary sequence incident on the system with the corresponding output, all the necessary information to accurately specify the acoustic properties of the sediment samples. The secondary objective was to use these results, if possible, to show how these properties could be used to discriminate between different sediment types.

The properties of interest were the velocity of propagation of acoustic energy through the sediment and the attenuation of these signals.

The velocity of sound through the sediments was found to be not significantly dispersive over the frequency range used for the work and hence results for an individual sample were averaged to give a single estimate.

The attenuation of acoustic energy, however, varies significantly with frequency in a manner related to the physical properties of the sediment matrix.

It was noted that the attenuation is the product of two individual but related events, namely the transmission of energy through an interface and the transmission of energy through a volume mass. These two effects were separated in a manner that is described in section 6.7 into a surface transmission loss function and a volume transmission loss function, both being frequency dependent.

6.3. The Recorded Acoustic Data

The recorded data was the result of the cross-corelation of a pseudo-random binary sequence, incident on the system, with the output of the system under these conditions. This cross-correlation function is shown in Appendix A to represent the impulse response of the system. This impulse response was recorded on punched paper tape and formed the raw input data fed to the main computer (ICL 450). This impulse response was of 100μs duration digitised at 1 MHz. The sampling frequency was set at 1 MHz to prevent problems arising because of aliasing, the upper frequency limit of the combined transducer responses being 350 KHz.

6.4. Data Window

The cross-correlation of the signals shown in figure 6.1 results in an impulse response having three distinct sections (figure 6.2).

Referring to figure 6.2, section A represents the delay period corresponding to the time taken for an acoustic signal to travel directly through the water and sediment paths during which there is no correlation between the two signals. The time, To, is dependent on the acoustic path length and the velocities of propagation through the media being traversed. During section B there is a high degree of correlation between the two signals and it is this section which contains all the information regarding the transmission loss and its dependence on frequency for the sample under analysis. The duration of this section is determined by the bandwidth of the system and by the presence of multiple paths and reflections. The third section again contains no information about the sediment, there is no correlation between the two waveforms, all multiples having reduced in amplitude to negligible levels.

With the geometry used the durations of the first two sections were of the order of 600μs and 60μs respectively.

Because of the limitations imposed by the correlator (Chapter 4) there was an obvious trade-off between the digitisation frequency and the width of the 'data window' (or the length of time sequence that could be recorded) that could be used. The sampling frequency was set at 1 MHz as previously stated which restricted the data window to 100μs.

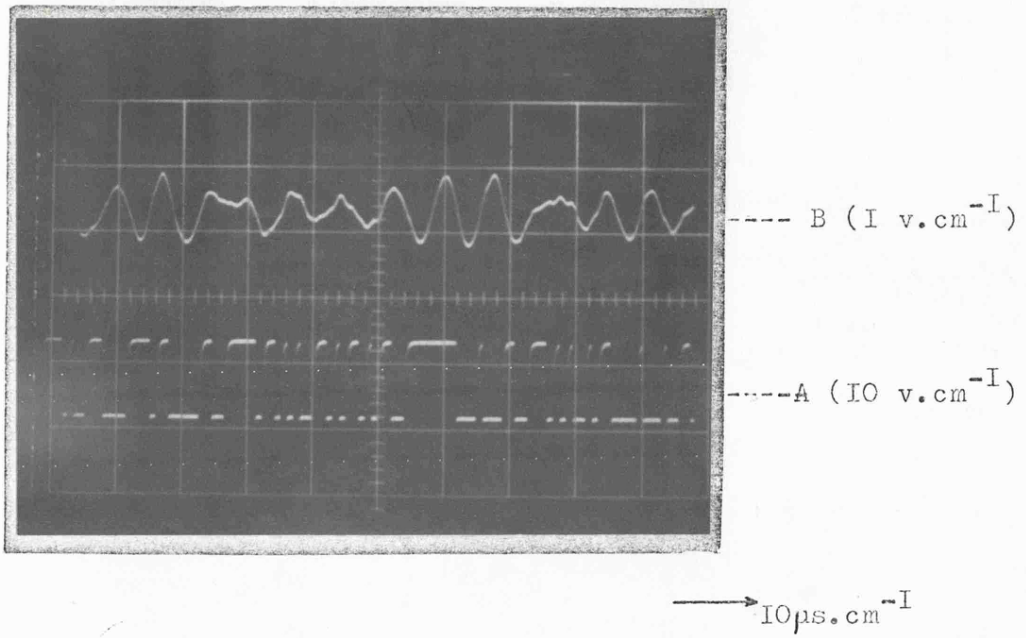

Figure 6.I A- Transmitted binary sequence.
B- Received sequence.

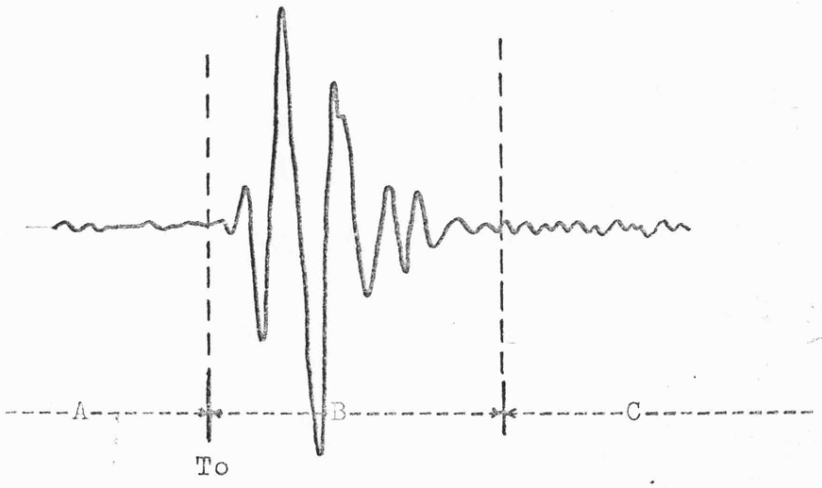

Figure 6.2 Impulse response corresponding to the correlation of the above sequences.

Referring back to figure 6.2 it is clear that if the beginning of the data window was set at $T = 0$ then the window, having a width of 100μs, would encompass none of the information containing section B.

The position of section B within the impulse response sequence affects its frequency distribution by introducing a phase shift, but has no effect on the power spectrum. For a power spectral analysis, therefore, provided the whole of the 'information section' of the impulse response is recorded it does not matter at which point in time the window begins or in fact ends.

The data window was positioned to begin approximately 10μs before the onset of section B allowing the complete section to be recorded within the data window. A picture of a typical recorded impulse response within a data window of 100μs is shown in figure 6.3.

6.5. Frequency Analysis Process

The cross-correlation of two signals x(t) and y(t) is defined by:-

$$r_{xy(t)} = \int_{-\infty}^{\infty} x(\upsilon).\, y(\upsilon + t)d\upsilon \qquad 6.1.$$

or alternatively

$$r_{xy(t)} = \int_{-\infty}^{\infty} x(\psi - t).y(\psi)d\psi \qquad 6.2.$$

Lower case letters are used to denote functions of time and upper case letters to denote their Fourier transforms (functions of frequency). The Fourier transforms of functions are indicated by square brackets. That is:-

$$G(w) = F\left[g(t)\right] \qquad 6.3.$$

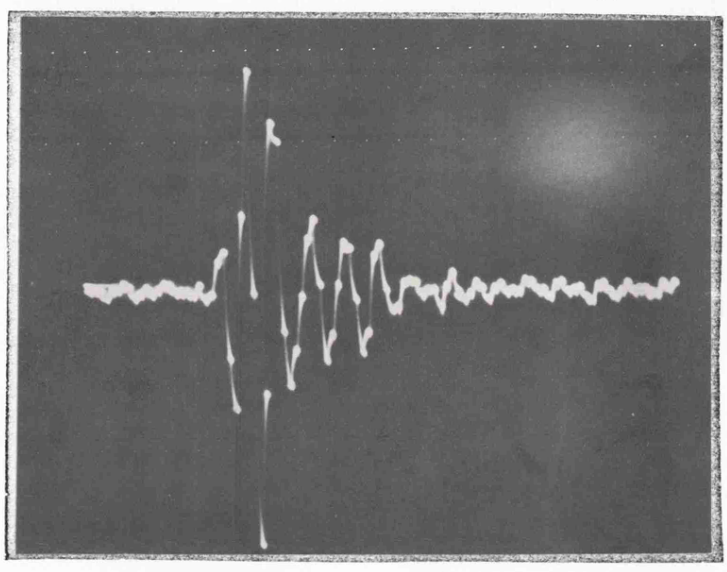

Figure 6.3 Picture showing typical position of impulse response within data window.
(width of data window --100μs.)

or G(w) is the Fourier transform of g(t).

The transform equation corresponding to equation 6.2 is:-

$$Rxy(w) = X^*(w)Y(w) \qquad 6.4.$$

where X* indicates the complex conjugate.

From this result it follows that if x(t) is white noise then the autocorrelation of x(t) is the Dirac delta function (an impulse) since X(w) = 1.

If white noise x(t) is the input to a linear system and y(t) is its output, then the autocorrelation of this output ryy(t) is the inverse Fourier transform of the squared magnitude of the systems frequency response. That is:-

$$F\left[r_{yy}(t)\right] = \left|H(w)\right|^2 \qquad 6.5.$$

where $H(w) = F\left[h(t)\right]$, h(t) being the impulse response of the system.

This result follows from equation 6.4. since:-

$$Ryy(w) = X^*(w).\ H^*(w).\ X(w).\ H(w) \qquad 6.6.$$

When X(w) = 1

and Y(w) = H(w). X(w)

$$Ryy(w) = \left|H(w)\right|^2 \qquad 6.7.$$

If white noise is the input to a linear system then the cross correlation of the input and output functions results in the impulse

response of the system.

$$r_{xy(t)} = h(t) \qquad 6.8.$$

Since from equation 6.4.

$$Rxy(w) = X^*(w).\ H(w).\ X(w) \qquad 6.9.$$
$$= H(w)$$

The above theory is limited practically as a uniform, infinite bandwidth acoustic source having sufficient output power is not available. This limitation can be overcome by noting that:-

$$Rxx(w) = X^*(w)\ X(w) \qquad 6.10$$

and that the frequency response of the system can be obtained by dividing equation 6.9. by equation 6.10.

$$H(w) = \frac{Rxy(w)}{Rxx(w)} \qquad 6.11$$

This means that a non-ideal sound source can be used (that is one not having a uniform, infinite bandwidth) to obtain the 'distorted' frequency response of the system and this response can be corrected for the imperfections of the source by measuring the autocorrelation function of the transmitted signal.

The most realistic estimate of the response of the sample is obtained if the correcting spectrum is the result of a cross-correlation measurement made between the transmitted and received signals with the sample removed. This has the additional effect of nullifying any possible spatial variations of the source. That is, a result corresponding to

a measurement made without the sediment in place is:-

$$Rxy(w) = X^*(w).\ Y(w) \qquad 6.12$$

$$= X^*(w)\ H_T(w)\ X(w) \qquad 6.13$$

Where H_T (w) contains information on the spatial response or beam patterns of the transducers used and X(w) is the amplitude variation of the source with frequency.

For a measurement made with the sediment in position

$$Rxy(w) = H^*(w).\ Hm(w).\ X(w) \qquad 6.14$$

$$= X^*(w).\ Hs(w).\ H_T(w).\ X(w) \qquad 6.15$$

Where:-

Hm(w) is the total response

and

Hs(w) is the response of the sediment

Therefore:-

$$Hm(w) = Hs(w).\ H_T(w) \qquad 6.16$$

Thus by dividing equation 6.14 by equation 6.13

$$Hs(w) = \frac{X^*(w).\ Hs(w).\ H_T(w).\ X(w)}{X^*(w).\ H_T(w).\ X(w)} \qquad 6.17$$

$$= \frac{Rxy(w)\ (\text{Sediment in place})}{Rxy(w)\ (\text{No sediment in place})} \qquad 6.18$$

This shows how the sediment response function can be separated from the response of the transducers and the electronic equipment. This equation must be treated with caution, however, as both impulse

functions contain noise. The transmitted energy is in a band between about 50 kHz and 350 KHz, in this range the real signal amplitude is large, the noise amplitude is comparatively small and the equation is valid. Outside this range, the signal amplitude decreases (figure 7.7) and the noise amplitude becomes a significant factor of the measured response. In this region equation 6.18 breaks down since two noise signals are being divided.

Estimates of the noise levels were made by performing the cross correlation firstly with the transmitting transducer disconnected (providing an indication of the acoustic noise) and secondly with the receiving transducer substituted by a dummy load (giving an indication of the electrical noise). In both cases the noise levels were -90 to -95 dBs relative to the peak of the water column measurement and hence the limits of validity of equation 6.18 are conservatively put at 80 KHz and 320 kHz.

6.6. Tapering functions

The true Fourier transform of a time series can only be obtained if the series is defined for all time. In reality Fourier analysis is usually performed on a finite length of data and hence the time series is truncated at the beginning and end of the sequence causing discontinuities at these points. This truncation can be considered to be the product of multiplying the original infinite sequence by a 'boxcar' data window having a value of unity for the length of the window and a value zero at any other point. Multiplication in the time domain is equivalent to convolution in the frequency domain and hence the Fourier transform of a truncated sequence or raw transform is the convolution of the true Fourier transform of the infinite series with

the Fourier transform of the boxcar function, a $\frac{\sin x}{x}$ function. This is not an ideal situation since 'leakage' occurs into the large side lobes of the $\frac{\sin x}{x}$ curve. The problem arises because of the discontinuities at the extremities of the data and a number of 'taper functions' have been proposed to reduce the errors involved. A taper function is designed to have unity value over the period for which the data is valid and to taper down to zero at each end of the known series. This function is then multiplied by the time series to reduce the discontinuities in the data. A number of window functions have been used, some being applied to the raw time data whilst others are designed for application as lag windows to the autocorrelation function. The choice of window is made on the basis of a compromise between the amount of leakage suppression allowed and the resolution required.

For the analysis used in this study spectral estimates were obtained identical to the Blakman-Tukey (1959) method using the following procedure:-

1. The raw transform of the impulse response function was computed.

   Xk

2. The raw spectrum was computed.

$$Gxk = \frac{2\Delta t}{N} \left| Xk \right|^2$$

3. The inverse F.F.T. was used to obtain the autocorrelation function.

$$Rxx = F^{-1}\left[Gxk \right]$$

4. The autocorrelation function was multiplied by the lag window

   Umr

5. The final smoothed spectrum was obtained from the direct F.F.T. of the weighted autocorrelation function.

The lag window used for this work was a cosine bell over the first and last 21 points of the autocorrelation function (as shown in figure 6.4) as suggested by Bingham et al (1967).

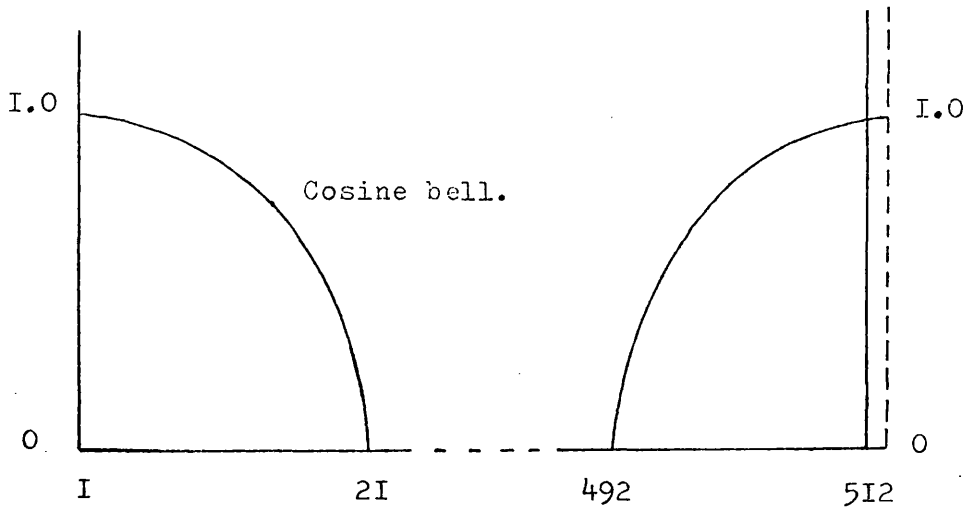

Figure 6.4 Lag window applied to autocorrelation function.

Applying this or any other form of taper changes the variance (or power) in the data since unequal weight is given to different sections of the time history. The magnitude of this reduction can be calculated by computing the ratio of the square of the area of the data window to the 'boxcar' window.

For the present study, however, this calculation is unnecessary as

all results are calculated from the ratio of the two spectra usually one measured with a sediment sample between the transducers and one measured with just a water path. Hence the constant of proportionality always cancels out.

6.7. Separation of surface and volume effects

The cross spectrum obtained from an impulse response contains information concerning the electronic equipment, the transducers used and the acoustic path along which the signal has travelled. Looking back at equation 6.17, it was shown that the effect of the transducers and electronic equipment could be removed from this frequency function using a correcting spectrum obtained from a measurement made with a water path only. The resulting function contains information solely dependent on the sediment path including the effect of the water sediment interface and the propagation through the sediment volume only.

If the correcting spectrum used is one obtained as a result of a transmission through a shallow layer of sediment then the resulting function will contain information on the acoustic propagation through the volume only, the effect of the water/sediment interface having been removed.

It was thus possible to directly obtain two frequency dependent functions, one containing information on a surface and a volume effect and the other containing information on a volume effect only. From these two results it was possible by simple division to deduce the surface and volume effects individually.

From 6.18:

$$Hs(w) = \frac{Rxy(w)\ (\text{Sediment in place})}{Rxy(w)\ (\text{No sediment in place})} \qquad 6.18$$

where

Hs(w) is the total response of the sediment

Similarly

$$Hsv(w) = \frac{Rxy(w)\ (\text{Sediment in place})}{Rxy(w)^*\ (\text{Shallow layer of sediment in place})} \qquad 6.19$$

where

Hsv(w) is the volume response of the sediment over a path length corresponding to the difference in depths of sediment corresponding to the measurements of Rxy(w) and Rxy(w)*.

If viewed in the time domain the total response of the sediment would be obtained from a convolution of surface and volume responses. In the frequency domain however this corresponds to a multiplication and hence the surface effect can be obtained by division.

$$Hss(w) = \frac{Hs(w)}{Hsv(w)} \qquad 6.20$$

where

Hss(w) is the response of the water/sediment interface.

6.8. Augmenting the time series with zeros

The computational F.F.T. method used here (H.B. Voelcker) assumes the number of data values transformed is a power of two.

That is:-

$$N = 2^P$$

Thus if the time sequence length used is not a power of two, zero values must be added to fill the sequence.

The spacing of discreet Fourier transform values is:-

$$\Delta f = \frac{1}{T} = \frac{1}{N\Delta t} \qquad 6.21$$

When zeros are added to the original sequence nothing is contributed to the basic shape of the transform envelope but because of the nature of the computational formula the spacing of the estimates is based on the augmented record length.

That is:-

$$\Delta f' = \frac{1}{(N + Nz)\Delta t} \qquad 6.22$$

where

Nz is the number of zeros added.

Further it can be shown (Bath 1974) that if the data are Gaussian then each spectrum point is the sum of two independent squared Gaussian variables and the unsmoothed estimates at a spacing $\frac{1}{T}$ are approximately uncorrelated. (The correlation being the overlap between neighbouring estimates). This is not satisfactory for most cases. In this work the original sequence of 100 data points was extended to 256 points by the addition of zeros resulting in significant smoothing.

6.9. Averaging

The digitised impulse response input to the computer was a series of values proportional to the displacement of the signal from a D.C. level on the correlator display of the discreet one microsecond points. As a result of this the average value of the impulse response was positive or negative depending on the average position of the display.

This D.C. offset was corrected for by using a simple zero-averaging routine in the programming.

The impulse response used as data for individual depth measurements was produced by averaging several results. The averaging of the responses was done by averaging the autocorrelation functions rather than the impulse responses so that cancelation due to minor time variations would not occur. This averaging was also performed during the computing stage.

6.10. The Spectral Analysis Procedure

The spectral analysis was performed using the following procedure.

1. The impulse response was extended to 256 points by the addition of zeros.
2. The raw transform of the impulse response was computed.
3. The raw spectrum was computed.
4. The inverse Fourier transform was used to obtain the autocorrelation function.
5. The autocorrelation function was multiplied by a lag window (a cosine bell as described in section 6.6).
6. The final smoothed spectrum was obtained from the direct Fourier transform of the weighted autocorrelation function.
7. The complete process was repeated using an initial response corresponding to a water transmission path only and a third time using a response corresponding to a transmission through a shallow sediment layer.
8. The surface and volume response functions were deduced and plotted.

6.11. Velocity Measurements

Velocity measurements were obtained as a result of observations of the position of the 'first arrival' within the impulse response for different depths of sediments. The time to 'first arrival' was plotted against sediment column depth.

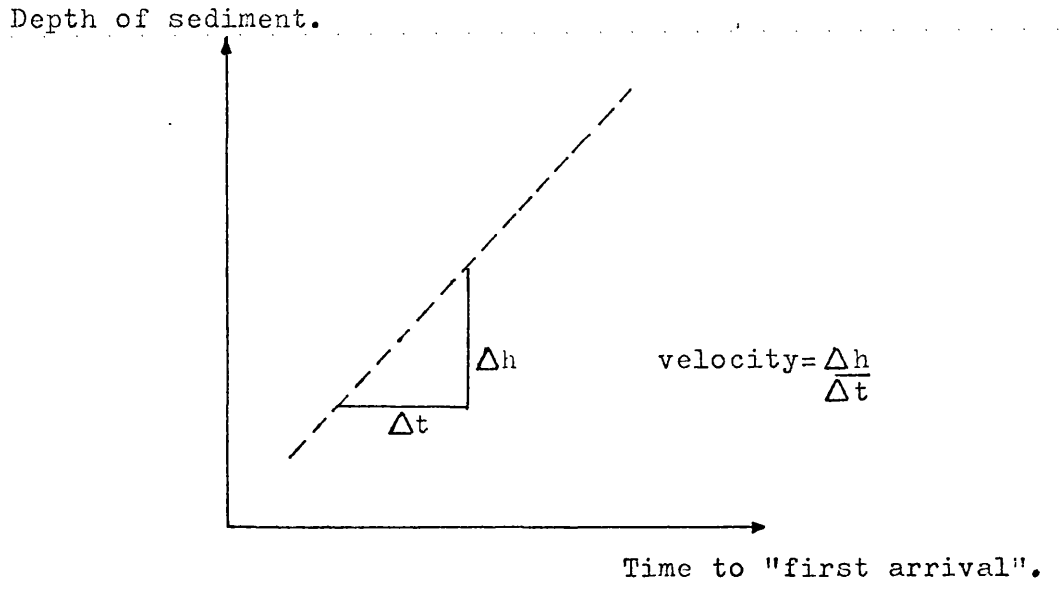

Figure 6.5. Velocity determination

The best straight line was drawn using a least squares fit and the velocity measured as the gradient of the slope.

6.12. Use of Cepstrum for Velocity Measurements

A second method used to measure velocity involved the use of 'Cepstrum' techniques.

It is noted that if a second acoustic path exists through the

sediment having a transit time slightly longer than that of the direct path then a 'second arrival' appears on the impulse response. This is caused by the high degree of correlation between the transmitted sequence and the later arrival. This multiple appears on the impulse response at a time τ after the direct arrival, the value of τ depending on the path length difference and the velocity of propagation. (figure 6.6).

The impulse responses as recorded were always of 100μs duration and so for a multiple path signal to be recorded the delay time (τ) had to be less than 100μs. The container was designed such that reflections from the side walls would not arrive within this time window and hence the only possible delayed signal was as a result of a double path through the sediment (figure 6.7.).

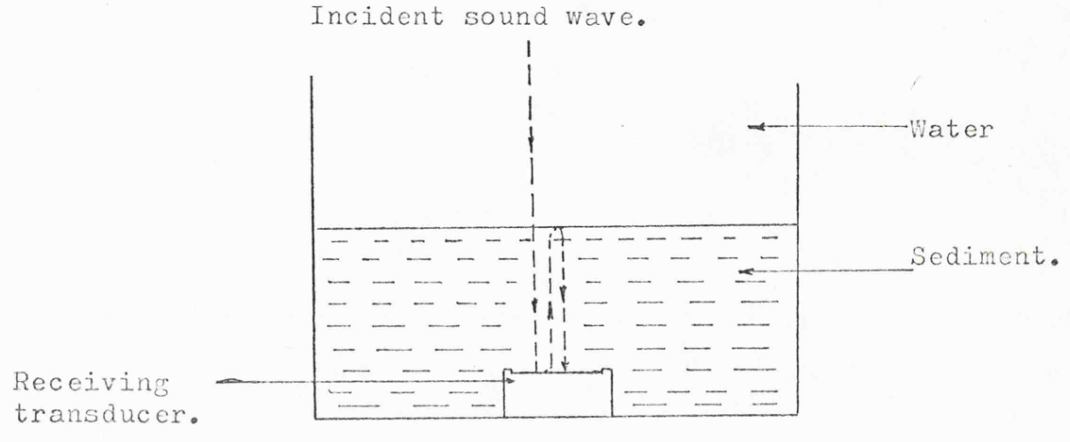

Figure 6.7 Schematic diagram showing multiple path

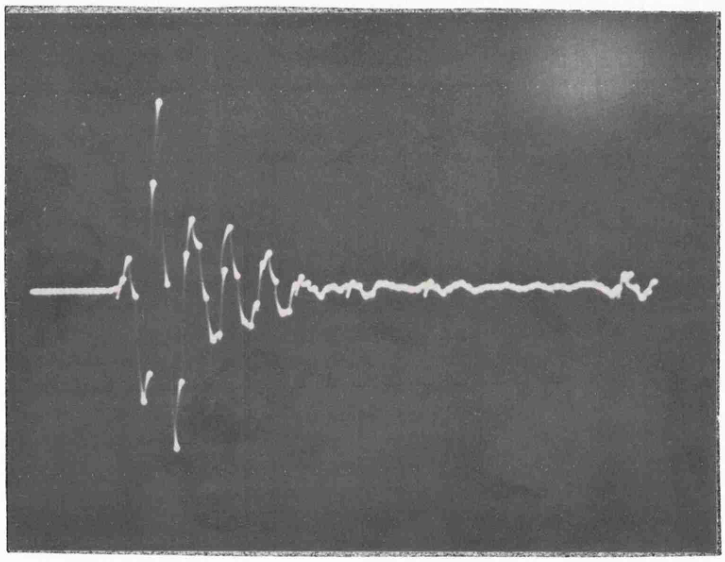

Figure 6.6 Impulse response with "multiple path" arrival.

The delay time τ in this situation corresponds to a two way travel time through the sediment column. Although it was not possible to measure this delay from the impulse response (because of overlapping) this effect was used to obtain velocity measurements using cepstrum techniques.

6.12.1. The effect on the log power spectrum of a simple echo

In the simplest echo, values of a time series y(t) are multiplied by a constant α, delayed a time difference τ and added to the original series to give a new series.

$$z(t) = y(t) + \alpha . y(t - \tau) \qquad 6.23$$

The Fourier transform of the echo is obtained from that of the original series by multiplying by $\alpha . \exp(2\pi i f \tau)$. Where f is the frequency.

Hence if $\emptyset(f)$ is the power spectrum of y(t) then that of z(t) is:-

$$\emptyset'(f) = \emptyset(f)(1 + 2\alpha \cos 2\pi f \tau + \alpha^2) \qquad 6.24$$

Whose logarithm is approximately

$$\log \emptyset'(f) = \log \emptyset(f) + 2\alpha \cos 2\pi f \tau \qquad 6.25$$

ignoring terms in α^2.

The effect of adding an echo to the original time series is thus simple in terms of the log power spectrum to which is added a cosinusoidal ripple whose parameters are simply related to the echo features α and τ. Remembering that the log spectrum is a function of frequency, f, it is clear that the 'frequency' of the ripple is just τ whose units

are ripples per cycle per second or seconds.

Hence by observation of the frequency of the ripple on the log power spectrum the delay τ was computed and thus velocity measurements were made. Measurement of the frequency of the ripple was done using Fourier analysis.

6.13. Computer Programming

A block diagram showing the essential computing operations is shown in figure 6.6. whilst the programs and descriptions of these are reproduced in Appendix C.

For ease of manipulation of data the computing was divided into three sections allowing a large degree of flexibility.

6.13.1. Section 1. Program 'INPUT'

Function

To read blocks of data from the punched paper containing up to ten impulse responses each having its own associated string of identification characters preceding it, to add this to amplification data contained on punched cards and to write the blocks into files the names of which were also specified on the cards.

Input

a. Paper tape containing impulse responses and identification information

b. Cards detailing output file name and amplifier parameters.

Output

Disc storage file containing ten impulse responses corresponding to a specified sediment type and column depth.

6.13.2. Section 2. Program "CPTRM"

Function

a. To read impulse responses from a single disc file.

b. To average these responses to zero

c. To calculate the autocorrelation function of each of the responses.

d. To average these autocorrelation functions.

e. To multiply the averaged autocorrelation function by a cosine bell type lag window.

f. To compute a spectral estimate of the power distribution within the impulse response.

g. To calculate the log spectrum and the cepstrum.

Input

a. Impulse responses and identification information from disc file generated by program 'INPUT'.

b. Punched cards specifying the name of the input disc file to be selected.

Output

a. Plot of log spectrum and cepstrum

b. Printer output of log spectrum and cepstrum.

c. Disc file containing identification characters and log spectrum.

Section 3. Program "FINSOL"

Function

a. To read log spectra and corresponding identification characters from two files generated by 'CPTRM', one spectrum corresponding to an impulse response obtained after transmission through a known height of a sediment and the other obtained using either a 'shallow layer'

or a 'water path only' response.

b. To compute, plot and print a 'corrected' function of frequency corresponding to the trasmission loss on passage through the sediment taking into account the relative amplification and correlator sensitivity values that were used in measuring the original responses.

Input

a. Log spectra and identification characters from two files created by 'CPTRM'.

b. Job control cards specifying the names of input files to be used.

Output

Printed output and plot of corrected log transmission loss.

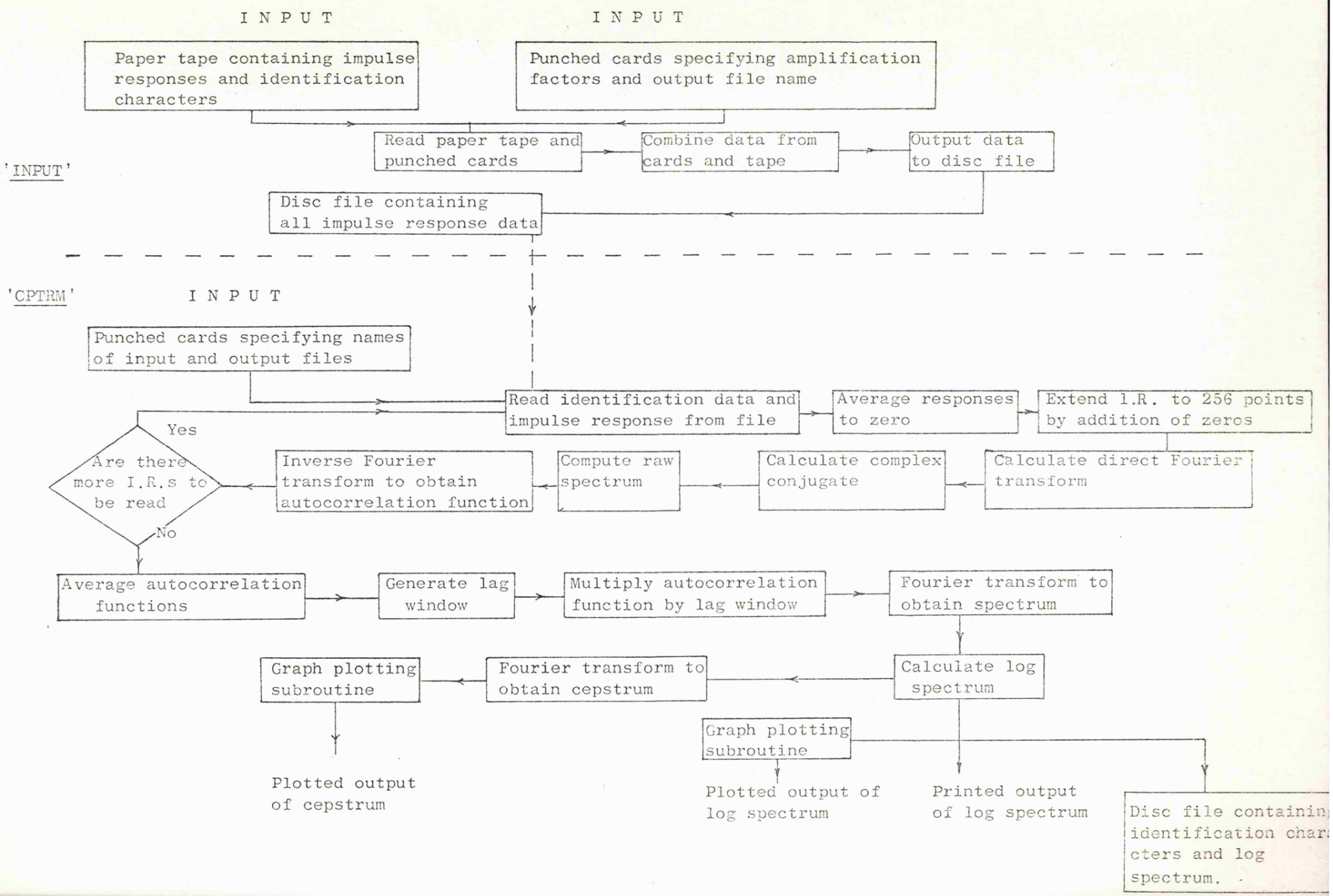
INPUT
INPUT
Paper tape containing impulse responses and identification characters
Punched cards specifying amplification factors and output file name
'INPUT'
Read paper tape and punched cards
Combine data from cards and tape
Output data to disc file
Disc file containing all impulse response data
'CPTRM'
INPUT
Punched cards specifying names of input and output files
Read identification data and impulse response from file
Average responses to zero
Extend I.R. to 256 points by addition of zeros
Yes
Are there more I.R.s to be read
No
Inverse Fourier transform to obtain autocorrelation function
Compute raw spectrum
Calculate complex conjugate
Calculate direct Fourier transform
Average autocorrelation functions
Generate lag window
Multiply autocorrelation function by lag window
Fourier transform to obtain spectrum
Graph plotting subroutine
Fourier transform to obtain cepstrum
Calculate log spectrum
Graph plotting subroutine
Plotted output of cepstrum
Plotted output of log spectrum
Printed output of log spectrum
Disc file containing identification characters and log spectrum.

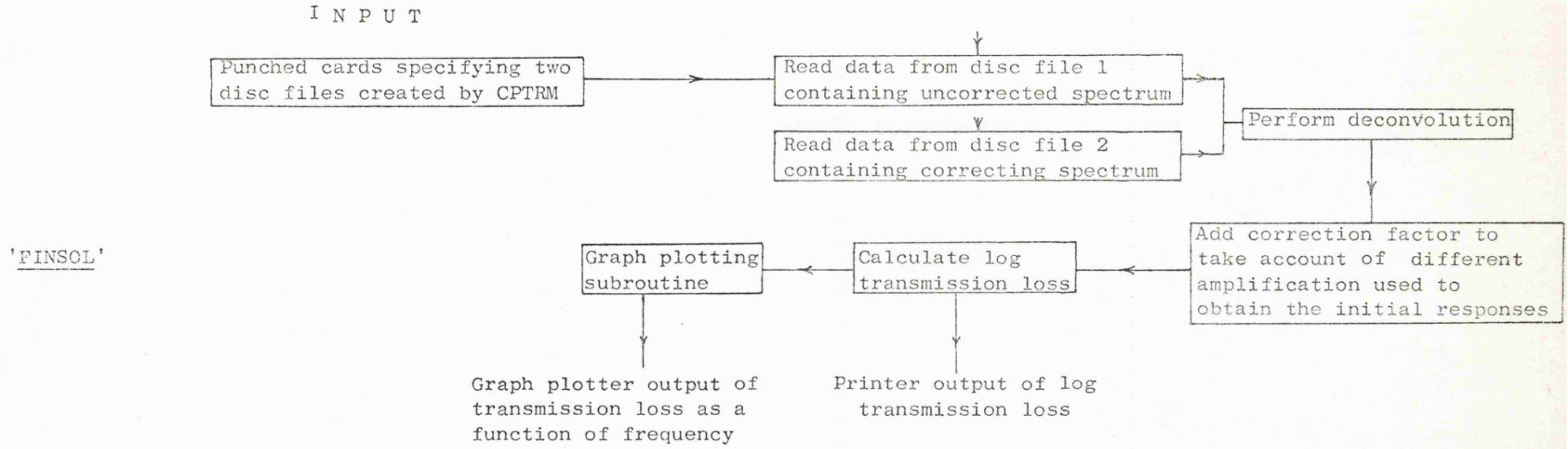

Figure 6.8. Block diagram showing the three computing blocks broken down to indicate the major program steps.

6.14. System check

To verify that the equipment was functioning correctly and the processing was valid, single frequency attenuation measurements were made on some of the sediment samples using a sinusoidal generator and a gating unit. Velocity measurements were also checked using direct measurements through a water column. The results of these checks backed up the cross-correlation results.

Chapter 7

RESULTS AND DISCUSSION

7.1. Introduction

The results of the velocity and attenuation measurements that were made during this study are presented in this chapter. The chapter is divided up into two sections, the first contains velocity measurements and shows their relationship with the sediment physical parameters whilst the second sets out to discuss the attenuation measurements and their implications. In each case the results obtained with artifical and real sediments are shown side by side and any differences contrasted.

Amongst the earliest theoretical work on the subject of the velocity of propagation of sound waves in unconsolidated sediments is that performed by Swikker and Kosten (1949), Ament (1953), Biot (1956 a & b) and Patterson (1956). These studies were generally based on work done by Wood (1941) on the propagation of compressional waves in emulsions.

Experimental studies on porous media soon followed. This included investigations on artifical and real sediments performed in the laboratory and in situ. Notable work by Hamilton (1956, 1972), Sutton et al (1957), Shumway (1956 & 1960) and Schreiber (1968) is discussed in relationship to the data presented here where appropriate.

7.2. Velocity Results

7.2.1. Velocity Measurements (see section 6.11)

The averaged values of the measured sound wave velocities are presented in tabular form for both real and artifical samples in Table 7.1.

Sediment Type		Mean Diameter (μm)	Average Measured Velocity (ms^{-1})
Ballotini	No. 1	250	1640
	No. 2	490	1682
	No. 3	1200	1698
	No. 4	4000	1744
	No. 5	8000	1782
Sand	No. 1	50	1538
	No. 2	130	1628
	No. 3	250	1660
	No. 4	330	1705
	No. 5	480	1762

Table 7.1. Results of velocity measurements

7.2.2. Dependence of Acoustic Velocity on Mean Grain Size

The velocity measurements are plotted against mean grain size for each of the sediments in figure 7.1. For both the sand and the Ballotini samples, velocity is shown to increase with increasing mean grain size, that is with decreasing values of M_{ϕ} (measured in phi units, as explained in 5.4). The relationship between velocity and the mean grain diameter, expressed in phi units is linear to within the limits of experimental error. The use of a linear regression analysis for each set of results shows that for:-

Sand samples

Rate of change of velocity with increasing grain size $= \frac{dv}{dM_{\phi}} = -64.56\ ms^{-1}$

Coefficient of determination = 0.97

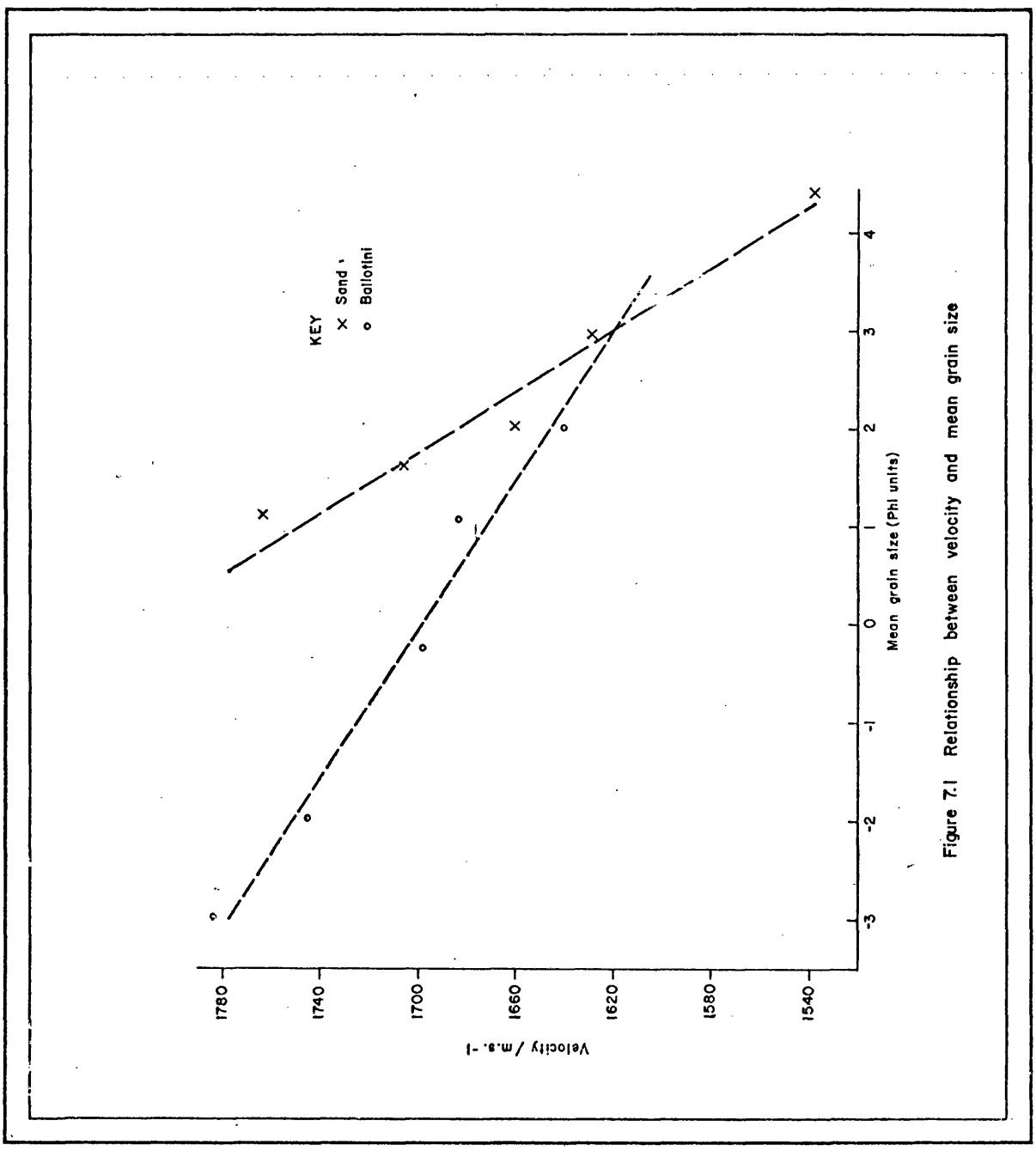

Figure 7.1 Relationship between velocity and mean grain size

Ballotini samples

Rate of change of velocity with increasing grain size $= \frac{dv}{dM_{\phi}} = -26.35\ ms^{-1}$

Coefficient of determination = 0.98

It must be noted that these results represent the total change of velocity caused by the variation of a number of physical parameters that differ between the samples and hence the partial derivative, $\frac{\partial v}{\partial Md_{\phi}}$, cannot be directly obtained from this unless the effects of the variations of all other significant parameters can be assessed. In the case of the artificial sediments, the variation of porosity between the samples is small and hence the velocity variation from sample to sample is more likely to give a good estimate of the partial derivative of velocity with respect to mean grain size.

7.2.3. Dependence of Acoustic Velocity on Porosity

The velocity measurements for each of the samples are plotted against the appropriate porosity value, (see sections 5.6 and 5.7) in figure 7.2. The porosity range of the sand samples is much greater than that of the Ballotini. This is to be expected since porosity tends to be less dependent on grain size for matrices of packed spherical particles.

Urick (1947) was amongst the first to obtain experimental data on the relationship between porosity and velocity. He measured velocity in suspensions of kaolin using an interferometer and produced results which agreed well with the emulsion equation of Wood (1941)

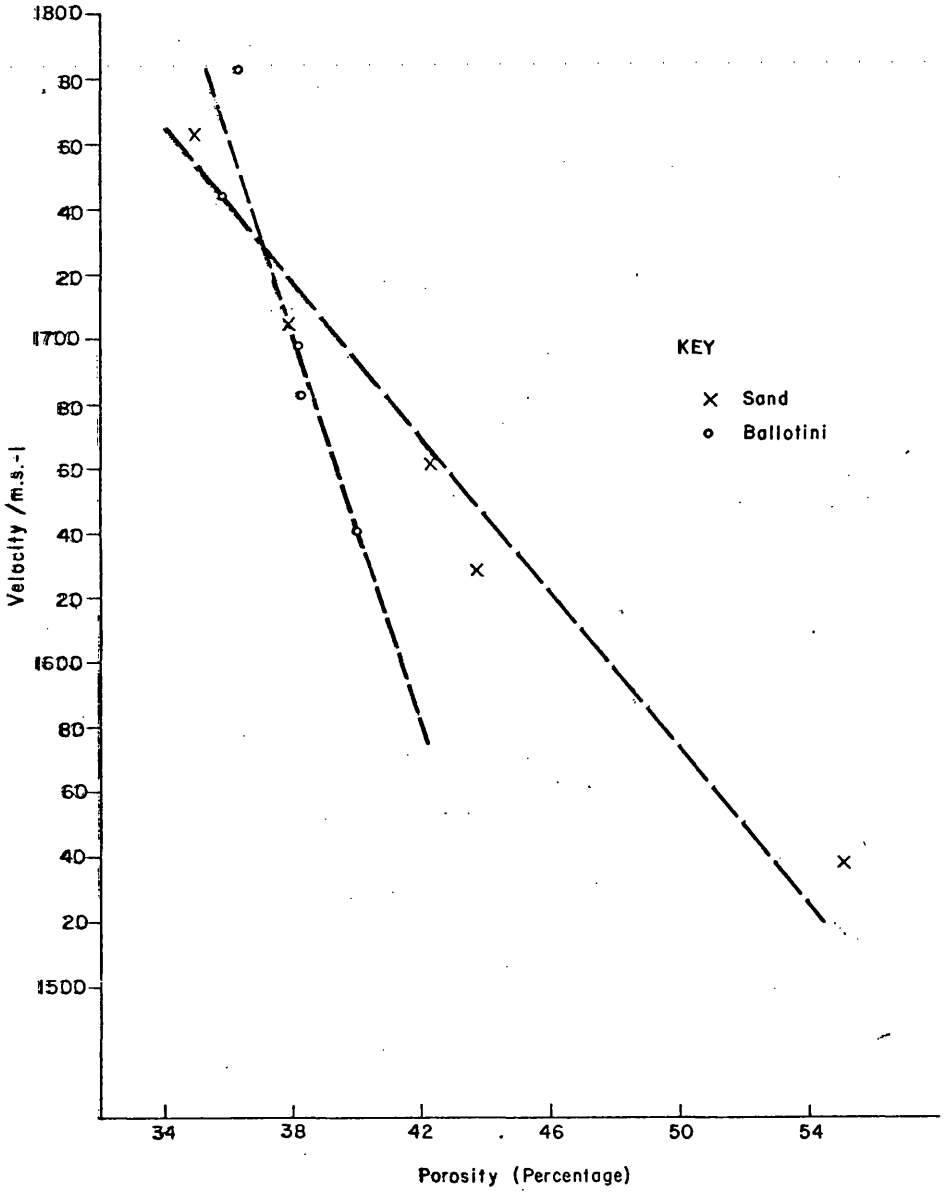

Figure 7.2 Relationship between velocity and porosity

$$Cws = \sqrt{\frac{1}{(\sum fsi\ \rho\ si + fw\ \rho_w)\ (\sum fsi\ Bsi + f_w\ B_w)}} \quad - 7.1$$

where Cws = sound velocity in the water-sediment mixture

fsi = volume fractions of sediment particles of the i mineral types

fw = volume fraction of water

Bsi = sediment particle compressibilities for the i minerals

Bw = water compressibility

ρsi = sediment particle densities for the i minerals

ρw = water density

The equation predicts a parabolic relationship between sound speed and porosity, minimum velocity occurring at a porosity of about 80%.

The results of the present study (figure 7.2) follow the trend of the Wood equation and are in agreement with Schreiber (1968). Figure 7.3 shows the results of the present work contrasted with the measurements of Shumway (1960). The figure also indicates the two relationships proposed by Wood and by Shumway, which embrace the results of this work.

The range of measured porosity values for the artificial samples is limited but the relationship between velocity and porosity shows a similar trend to that indicated by the real sediment results. It is notable that the porosity effect is more significant in the case of the Ballotini but it should be remembered that porosity is a dependent variable and the observed relationships are distorted by, for example, the grain size effect, porosity being dependent on grain size as shown in figure 7.4.

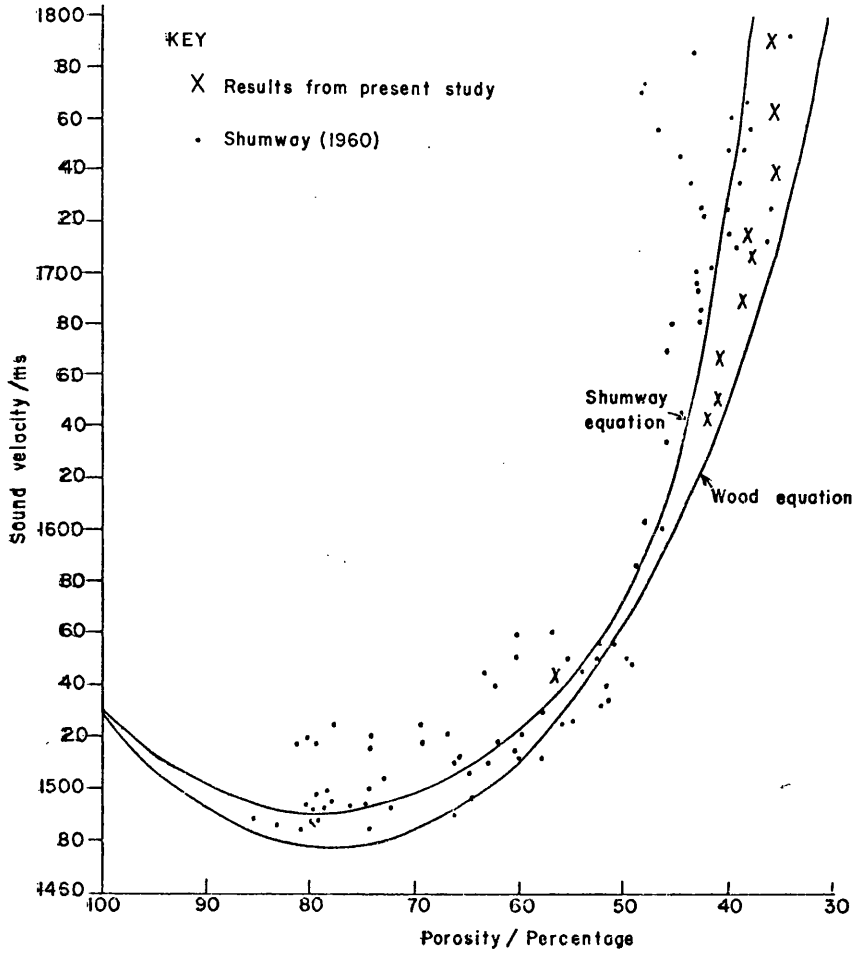

Figure 7.3 Comparison of Velocity / Porosity results

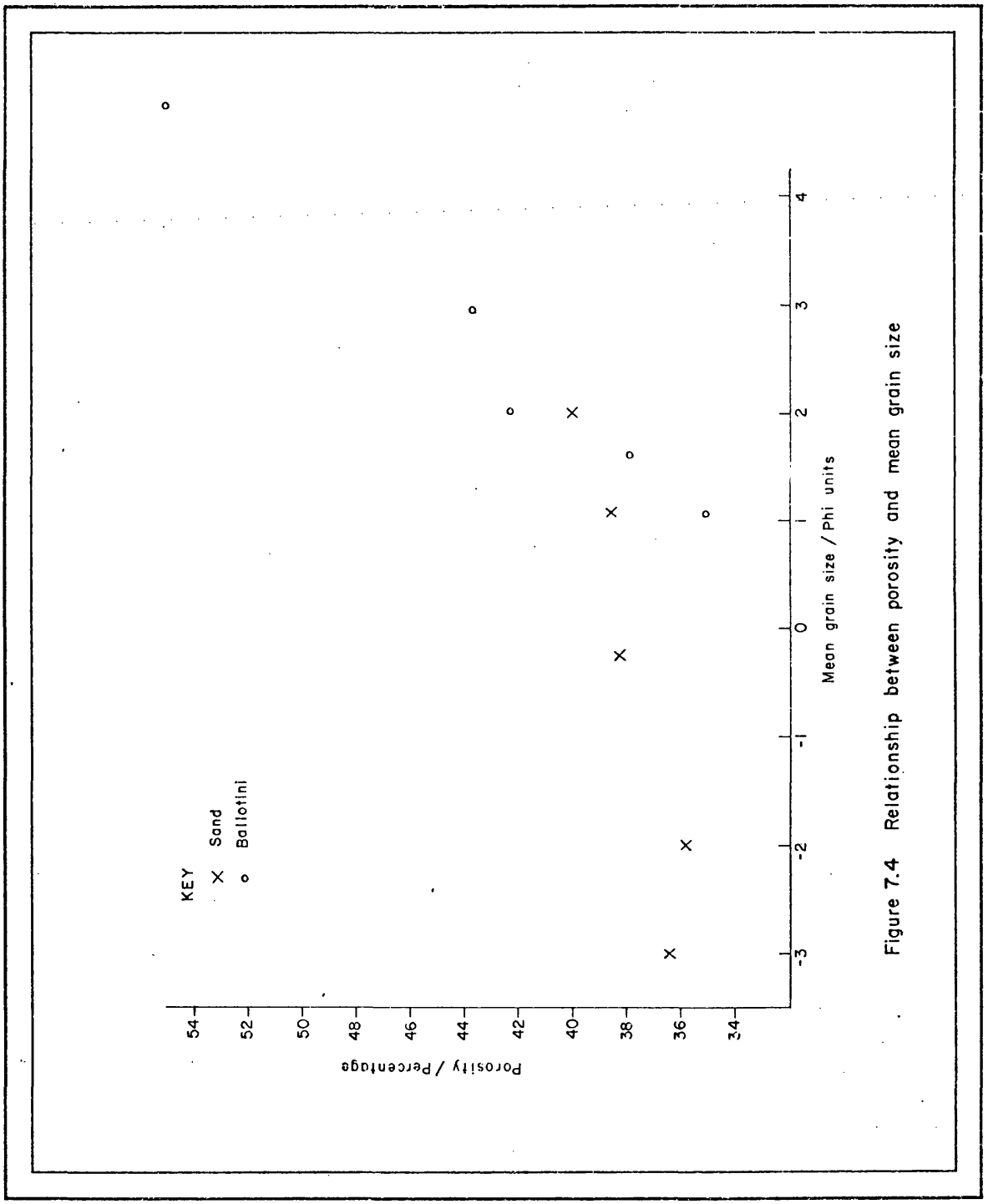

Figure 7.4 Relationship between porosity and mean grain size

7.2.4. Dependence of Acoustic Velocity on Phi Deviation

Phi-deviation is a measure of the degree of sorting of a sediment mass and is described in section 5.14.

It is known (Schreiber 1968) that well sorted sediments exhibit poorest packing and conversely that poor sorting yields the best packing. It is reasonable, therefore, to assume that poorly sorted sediments might give rise to higher acoustic velocities, velocity tending to increase as packing becomes tighter.

The results of plotting acoustic velocity against phi deviation are shown in figure 7.5. This indicates that velocity is highly influenced by the range of particle sizes within the sample but again this is an effect interrelated with the variation of mean grain size. The relationship between phi deviation and mean grain diameter for the sands used in this study (figure 7.6) is typical for marine sediments in general, (e.g. Inman and Chamberlain 1955) the most well sorted sediments being those having the largest mean diameters. For the Ballotini, however, this trend does not apply and there is no obvious trend of variation of phi deviation with mean grain size. This is most likely due to the manner in which the artificial samples were manufactured.

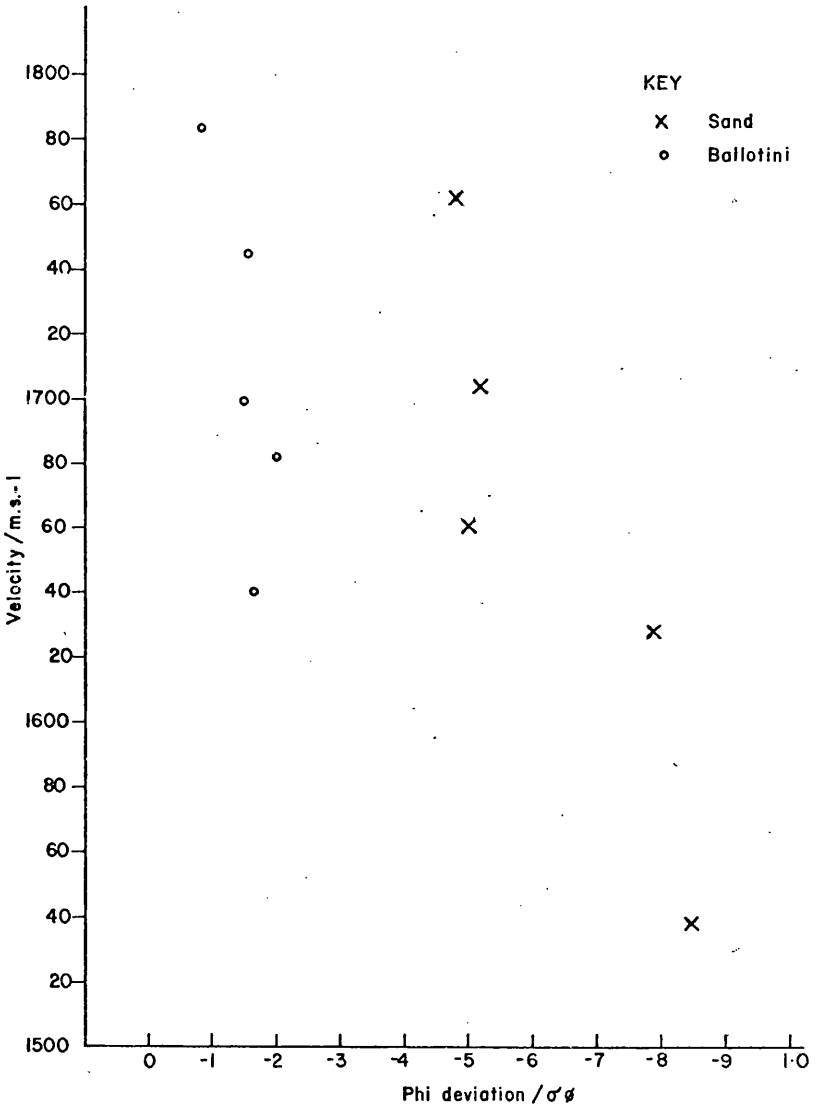

Figure 7.5 Relationship between velocity and phi deviation

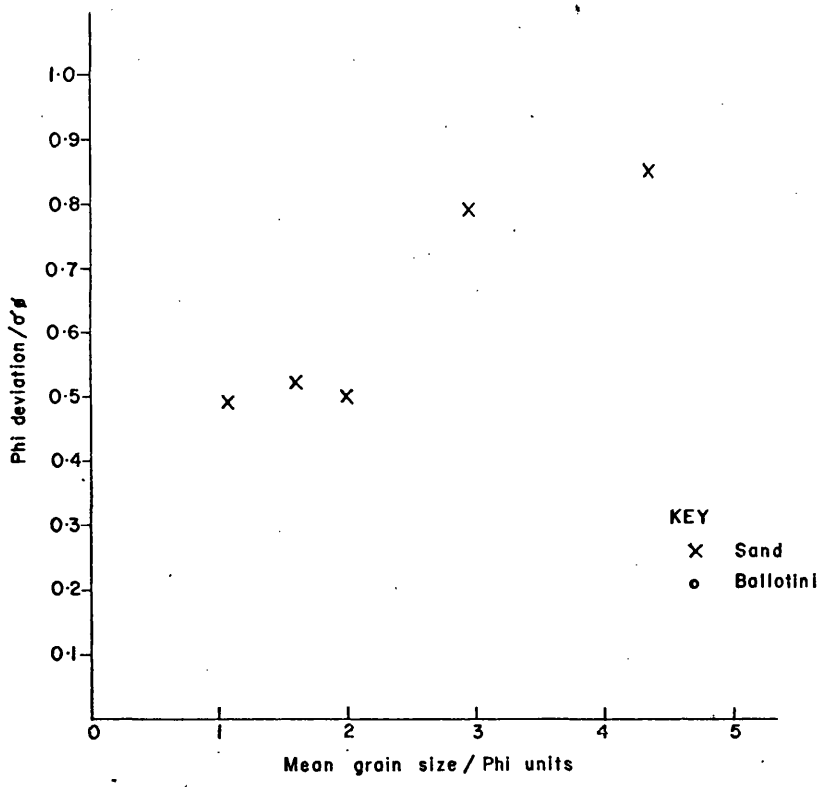

Figure 7.6 Relationship between phi deviation and mean grain size

7.2.5. Estimation of Acoustic Velocity

Using multiple linear regression techniques equations can be developed relating velocity to other measured physical parameters (e.g. porosity, mean grain size). Such equations should be treated with caution since the interrelationship between variables in such an analysis should be linear but it is clear that, for example, the relationship with porosity is not linear, although an approximation over a specified range may be valid. In spite of this objection there is some merit in such equations provided limitations are observed.

Sutton et al (1957) using an elaborate statistical analysis technique developed an equation relating sound velocity in kms^{-1} (Cws) to the independent variables phi median diameter (Mdϕ), percentage of material soluble in HCI (ζ), and porosity (η):

$$Cws = 2.093 - (0.414 \pm 0.006)Md\phi + (0.00135 \pm 0.00038)\zeta - (0.44 \pm 0.15)\eta$$

Shumway (1960) noted that phi mean diameter correlates better to sound velocity than phi median diameter and developed an equation relating velocity to phi mean diameter (Mϕ), porosity (η) and phi deviation ($\sigma\phi$).

$$Cws = 1.87295 - 0.0287\ M\phi - 0.0036\ \eta - 0.0472\ \sigma\phi \qquad 7.3$$

Using the data obtained from this study it is possible to deduce a similar relationship. The parameters chosen in this case are the same as those selected by Shumway, the volume of HCI soluble material in the samples used not being a significant value.

The linear regression equation obtained from these results is thus:-

$$Cws = 1.9958 - 0.0212\ M\phi - 0.00827\ \eta + 0.1049\ \sigma\phi \qquad 7.4$$

Where:-

Cws is the sound velocity in $km.s^{-1}$

Mø is the mean grain diameter in phi units

η is the porosity (percentage)

$\sigma\phi$ is the phi deviation.

7.3. Attenuation Results (Volume and Surface Losses)

7.3.1. Measurements

The following block diagram summarises the analysis procedure

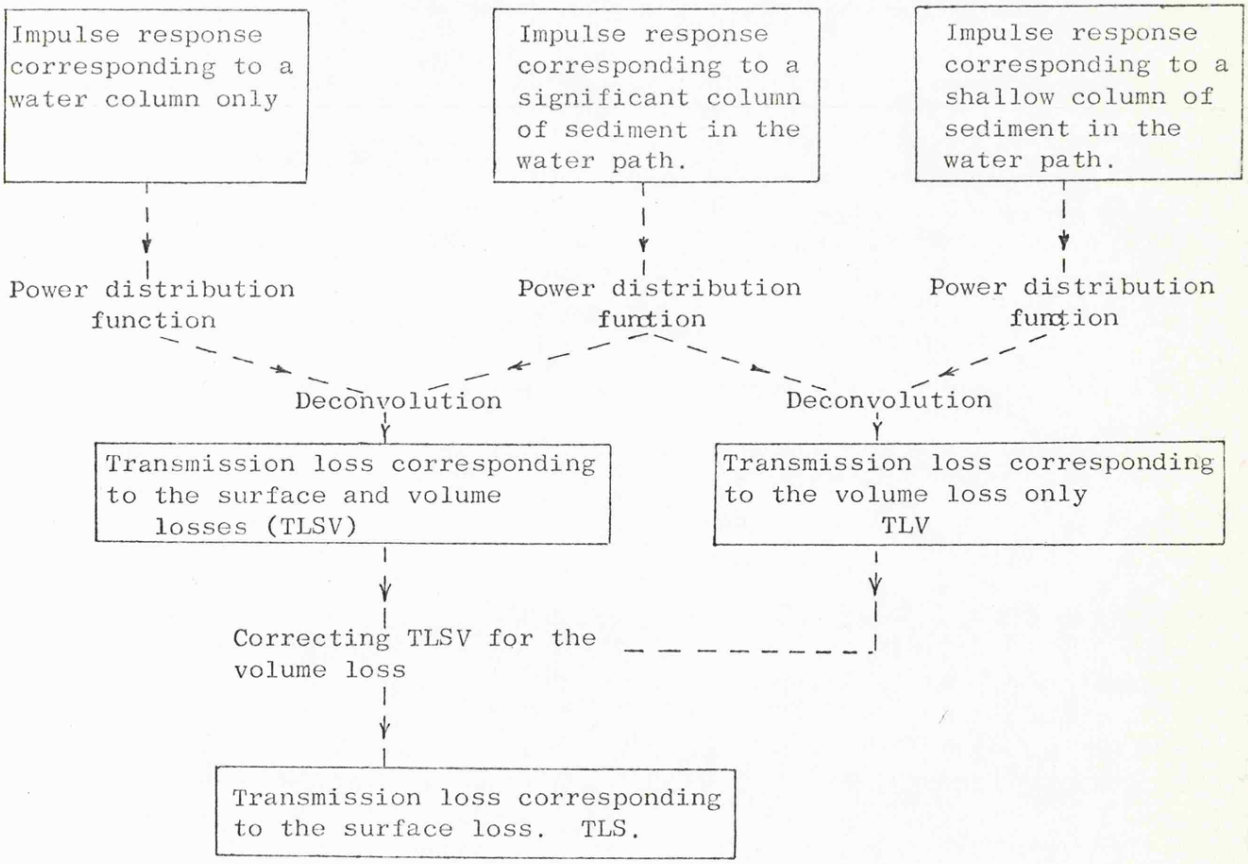

The surface and volume transmission loss functions were computed for each of the sediment samples in this manner. Figure 7.7. shows an example of a computer drawn plot of power distribution function corresponding to a measurement made with 300mm of 250um sand.

Examples of transmission losses plotted as a function of frequency are shown in figures 7.8 to 7.10. Figure 7.8 represents the sum of surface and volume effects, figure 7.9 represents the volume effect only and figure 7.10 represents the surface effect only. Figure 7.10 is typical of the surface loss results showing that the energy loss at the interface is independent of frequency for the majority of samples over the range of 80 KHz to 320 KHz.

7.3.2. Acoustic Transmission Loss at the Water/Sediment Interface

The transmission loss at the water/sediment interface was computed for a number of measurements for each of the samples. To these measurements two correction factors were applied firstly to take account of refraction at the water/sediment interface and secondly to compensate the acoustic mismatch at the sediment/transducer faceplate interface. These corrections were assessed in the following manner:-

1. To take account of refraction losses caused by the insertion of a higher velocity layer resulting in a lower sound intensity being transmitted. This correction was calculated on the basis of Snell's Law using the measured values of velocities for the samples (figure 7.11).

Figure 7.7 Computer drawn plot of the smoothed power spectrum corresponding to a measurement made through 300mm. of 250μm sand.

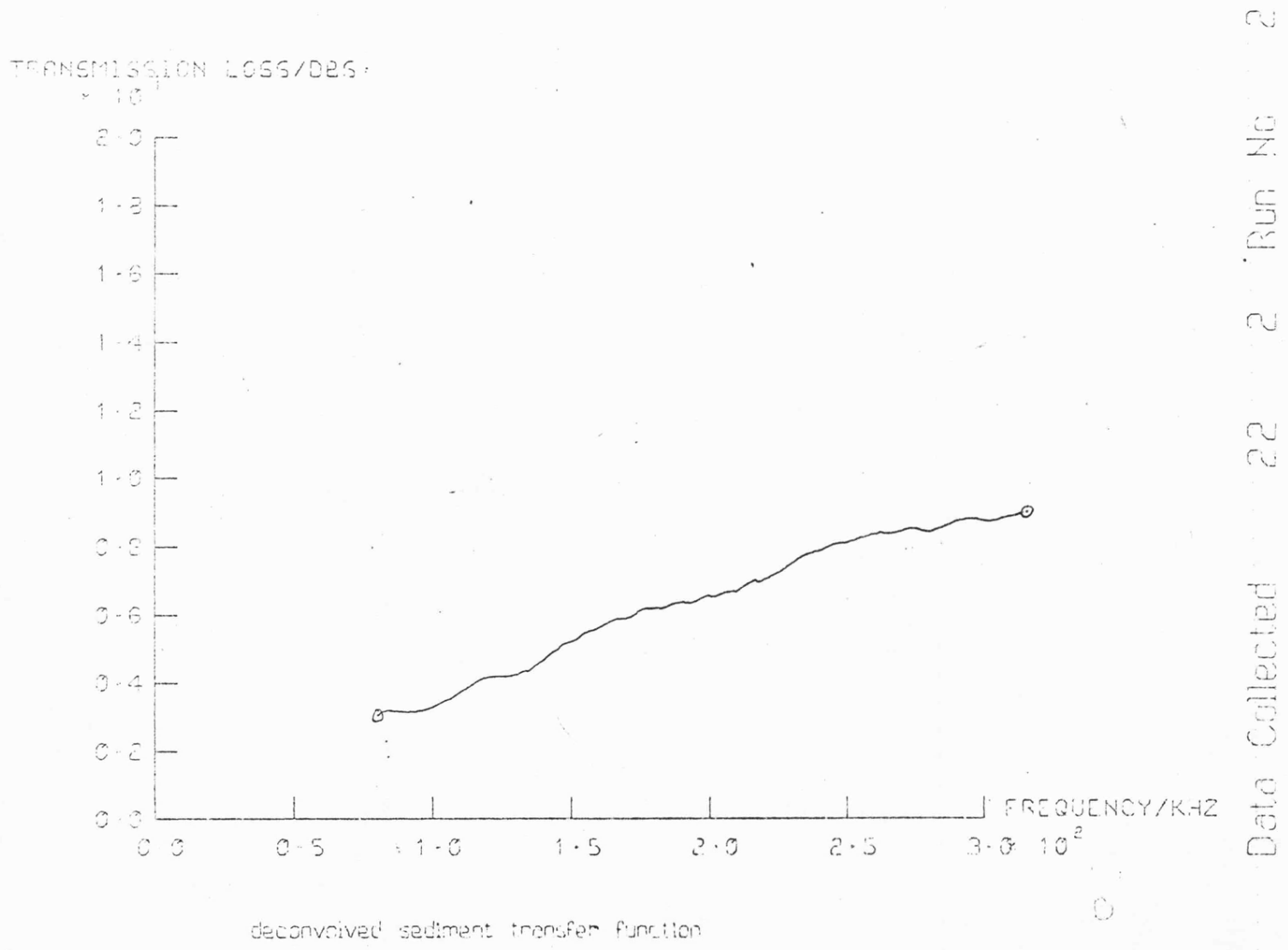

Figure 7. 8 Computer drawn plot corresponding to a measurement made through 90 mm. of 480μm sand. (surface and volume losses)

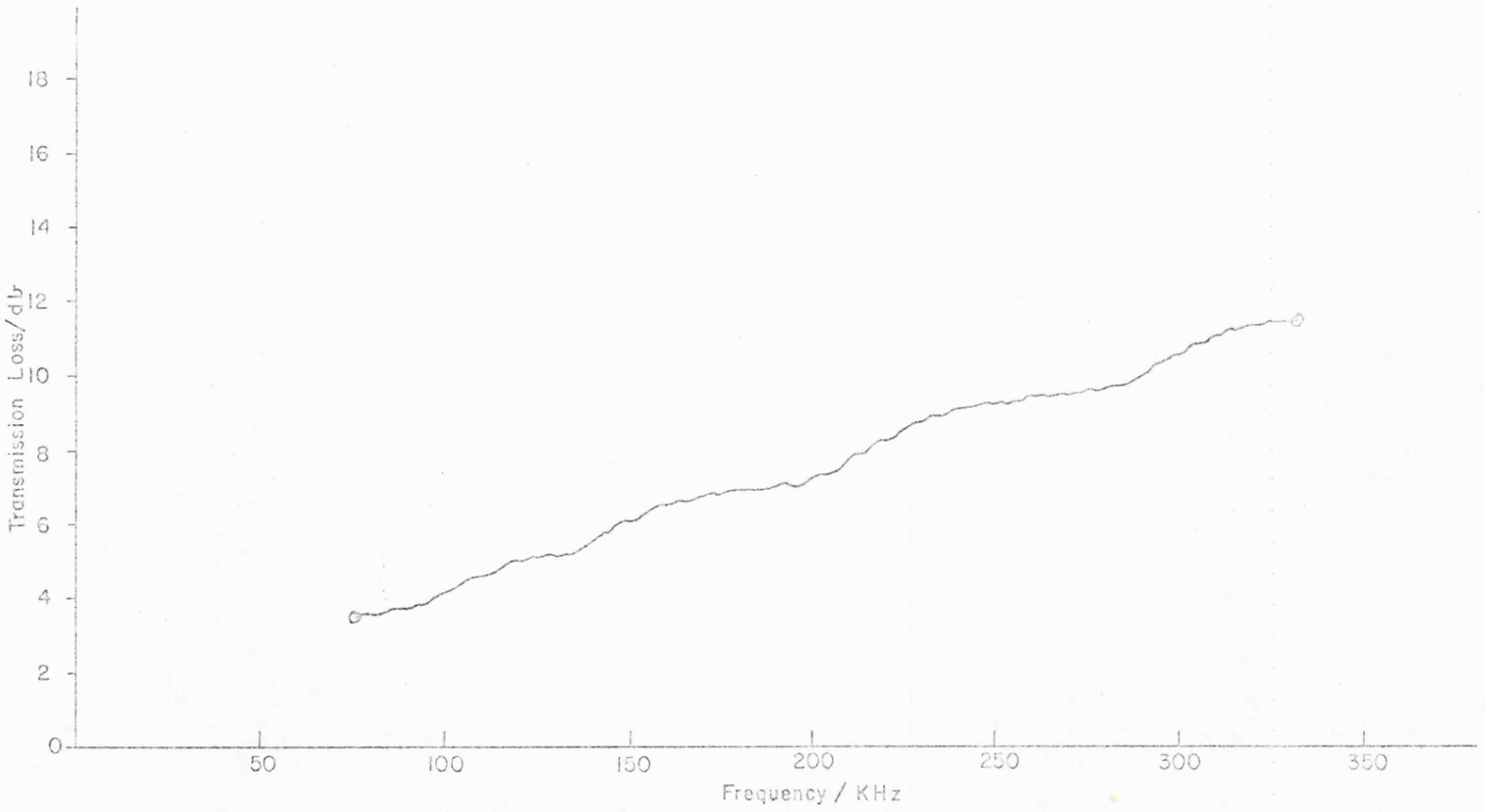

Figure 7.9 Transmission loss as a function of frequency for 90mm of 480mm sand (volume effect only).

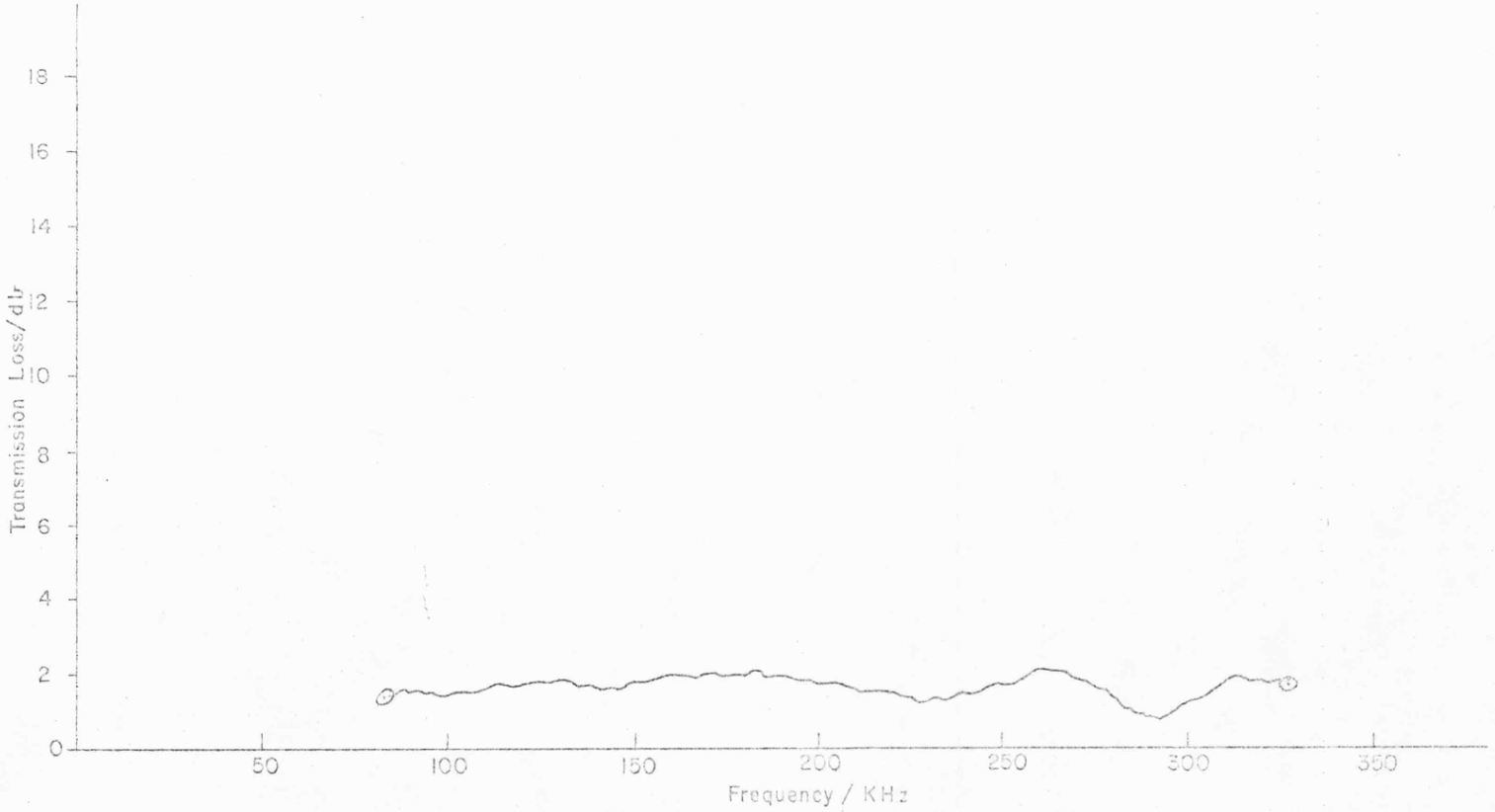

Figure 7.10 Transmission loss as a function of frequency for 480mm sand (surface effect only)

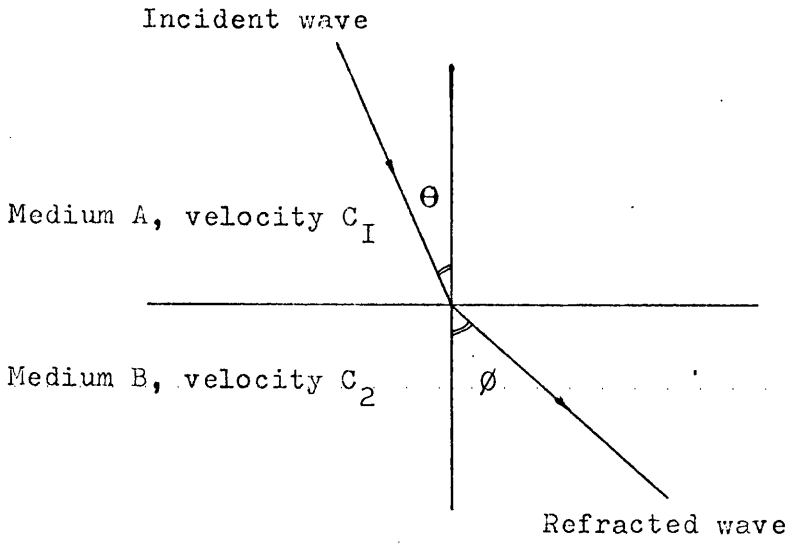

Figure 7.11. Refraction at the water/sediment interface.

$$\frac{\sin \theta}{\sin \phi} = \frac{C_1}{C_2} \qquad 7.5.$$

2. To take account of the transmission loss occurring at the sediment/transducer interface. This factor was calculated using the Rayleigh reflection coefficient for a simple harmonic plane wave incident on a plane boundary between two media across which there is a density and velocity change. At normal incidence the Rayleigh reflection coefficient, R, is expressed:-

$$R = \frac{P_2}{P_1} = \frac{Z_2 - Z_1}{Z_2 + Z_1} \qquad 7.6$$

Where:-

P_1 is the incident pressure amplitude

P_2 is the reflected pressure amplitude

Z_1 is the characteristic impedence of the first medium.

Z_2 is the characteristic impedence of the second medium

The characteristic impedence being theproduct of density and compressional wave velocity

$$Z = \rho.c. \qquad 7.7$$

The experimental values for transmission loss at the water/sediment interface are plotted in figure 7.12. It can be seen that with the exception of the 8mm Ballotini the surface loss for each of the sediments is independent of frequency for the range of frequencies used. The 8mm example is different in that the particle diameter is of the same order as the wavelength of the acoustic energy and Rayleigh scattering is becoming the dominant energy loss mechanism. Above 200 kHz the volume and surface losses for this sample increase very rapidly with frequency and estimation of the individual effects is difficult. The frequency averaged experimental values for the transmission loss at the water sediment interface are shown in table 7.2. together with the theoretical values computed from the measured densities and velocities. These theoretical values were calculated using the Rayleigh reflection coefficient for the water/sediment interface using equation 7.6. and from these calculating a transmission coefficient:-

The reflection coefficient is

$$R = \frac{P_2}{P_1} = \frac{Z_2 - Z_1}{Z_2 + Z_1} \qquad 7.6$$

The ratio of the reflected and incident sound intensities is given by:-

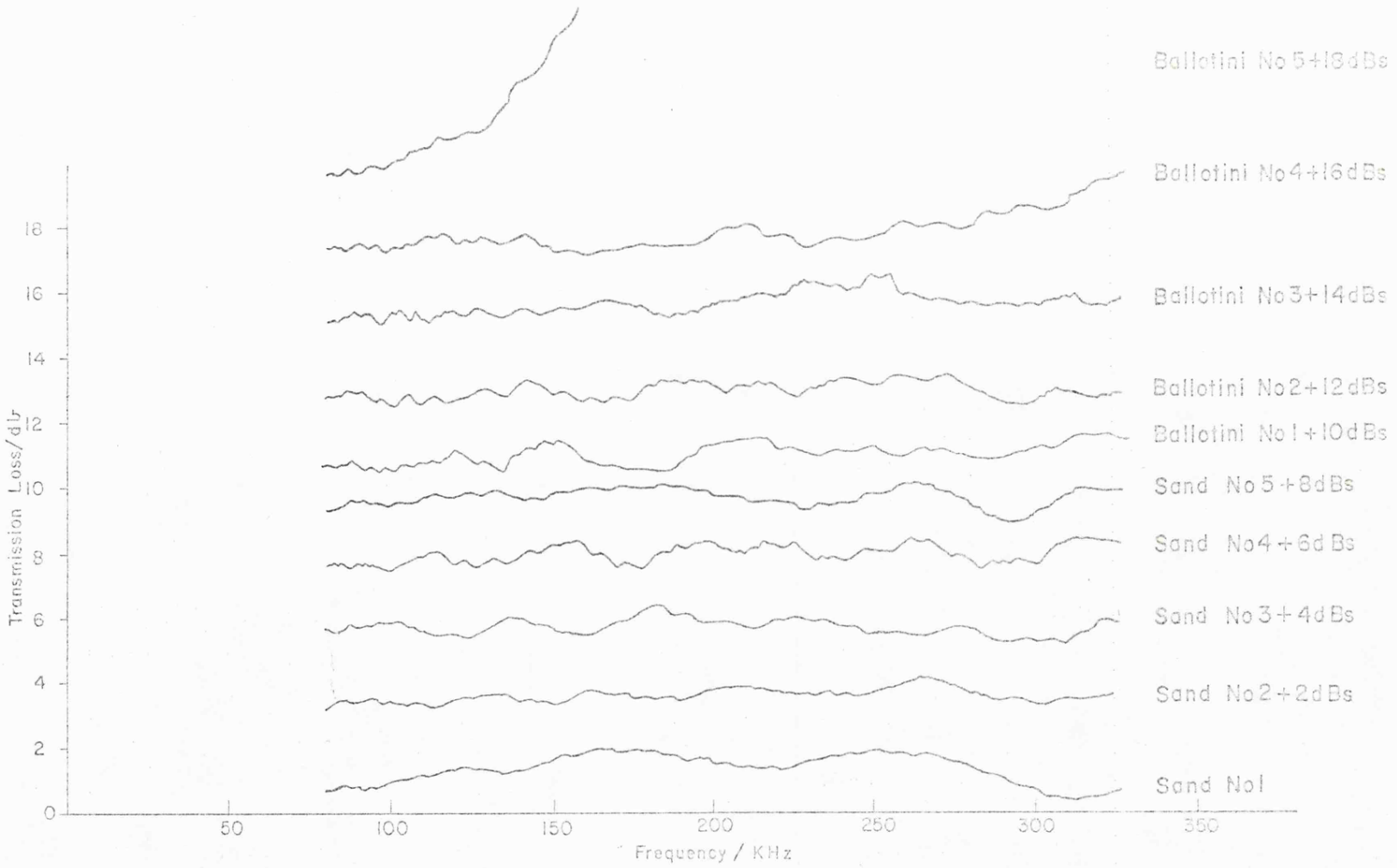

Figure 7.12 Transmission loss as a function of frequency for Ballotini and Sand (surface loss only)

Sediment	Wet Density sat kgm^{-3}	Velocity C/ms^{-1}	Reflectivity (Calculated from measured ρ and c values)	Bottom Loss	Transmission Loss	Transmission Loss (measured)	Bottom Loss (from measured T.L)
Sand No. 1	1656	1538	27.42%	11.54 dB	0.32 dB	0.37 dB	10.88 dB
Sand No. 2	1940	1628	36.19%	8.82 dB	0.61 dB	0.65 dB	8.57 dB
Sand No. 3	1946	1660	37.03%	8.62 dB	0.64 dB	0.67 dB	8.45 dB
Sand No. 4	2018	1705	39.85%	7.99 dB	0.75 dB	0.80 dB	7.74 dB
Sand No. 5	2072	1762	42.32%	7.47 dB	0.86 dB	0.91 dB	7.23 dB
Ballotini No. 1	1888	1640	35.32%	9.04 dB	0.58 dB	0.62 dB	8.76 dB
Ballotini No. 2	1913	1682	36.99%	8.64 dB	0.64 dB	0.69 dB	8.33 dB
Ballotini No. 3	1915	1698	37.44%	8.53 dB	0.66 dB	0.71 dB	8.22 dB
Ballotini No. 4	1950	1744	39.36%	8.10 dB	0.73 dB	0.79 dB	7.79 dB
Ballotini No. 5	1943	1782	40.10%	7.94 dB	0.76 dB	0.84 dB	7.55 dB

Table 7.2 Bottom Loss and Transmission Loss figures calculated from measured density and velocity values compared with direct results.

$$\alpha r = \frac{Iref}{Iinc} = \left(\frac{Z_2 - Z_1}{Z_2 + Z_1}\right)^2 \qquad 7.8$$

Where

Iref is the reflected sound intensity

Iinc is the incident sound intensity

The ratio of the transmitted and incident intensities, αt, is given by:-

$$\alpha t = 1 - \alpha r \qquad 7.9$$

Combining 7.9 and 7.8 it can be shown that

$$\alpha t = \frac{4Z_1Z_2}{(Z_1 + Z_2)^2} \qquad 7.10$$

The theoretical transmission loss at the interface is:-

$$T.L. = -10 \log \alpha t \qquad 7.11$$

When considering the amplitude of a signal reflected from the sea-bed the more usual figure that is used is the Bottom Loss (B.L.). This figure is directly related to the Transmission Loss at the interface through equation 7.9 and is defined:-

$$B.L. = -10 \log \alpha r \qquad 7.12$$

The equivalent Bottom Loss figures calculated from the measured transmission loss figures are also presented in table 7.2.

The theoretical values for the Transmission Loss are in close agreement with the measured values. The theoretical values are always

lower, however, the greatest inconsistency being in the case of the largest diameter sediments. The difference is most likely due to a scattering loss at the interface which is not accounted for in the Rayleigh reflection coefficient. If energy is scattered at the interface then the observed transmission loss must be higher than a theoretical value assuming no scattering.

Figure 7.13 shows the relationship between the reflectivity of the interface and the mean sediment diameter. The reflectivity values (Reflection coefficient x 100 percent) are those computed from the measured porosity, density and velocity values.

Saturated density and acoustic velocity both increase with increasing grain size (decreasing Mø) so it is not surprising to see reflectivity increasing with increasing median diameter. Correlation between these two factors is high and linear regression analysis of the results indicates a relationship of the form:-

For sand samples

$$M\phi = 10.47 - 0.21\ R \qquad 7.13$$

For Ballotini samples

$$M\phi = 39.92 - 1.05\ R \qquad 7.14$$

The gradients of the two regression lines are very different indicating that reflectivity is probably not directly related to mean grain size alone but is related to other parameters which may themselves be related to mean grain size.

Reflectivity values are plotted against porosity for Ballotini and

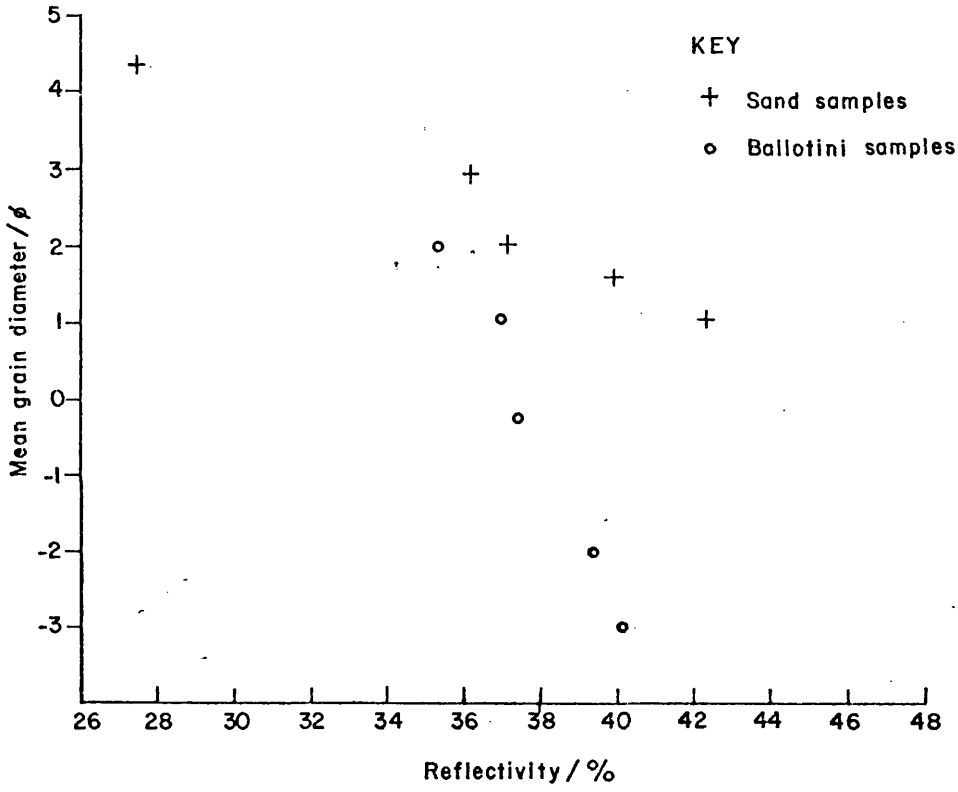

Figure 7.13 Relationship between mean grain diameter and reflectivity

sand samples in figure 7.14. In section 7.1., acoustic velocity was shown to be highly correlated with sediment porosity and reflectivity is also seen to be related to porosity. Using linear regression analysis for these results the following relationships were obtained

For sand samples.

$$\eta = 92.27 - 1.35\ R \qquad 7.15$$

for $27\% < \eta < 43\%$

For Ballotini samples

$$\eta = 70.16 - 0.86\ R \qquad 7.16$$

for $35\% < \eta < 41\%$

The relationships for the sand samples are in reasonable agreement with figures suggested by other authors for real sediments, e.g.

Taylor Smith 1975

$$M\phi = 10.73 - 0.12\ R \qquad 7.17$$

$$\eta = 98.8 - 1.53\ R \qquad 7.18$$

Hamilton 1956

$$\eta = 97.6 - 1.44\ R \qquad 7.19$$

for $36\% < \eta < 75\%$

Morgan (1964)

$$\eta = 98.4 - 1.48\ R \qquad 7.20$$

for $25\% < \eta < 85\%$

Differences in these regression equations are partly due to the different ranges of porosity values over which the measurements were made. The lower reflectivities for the Ballotini samples are

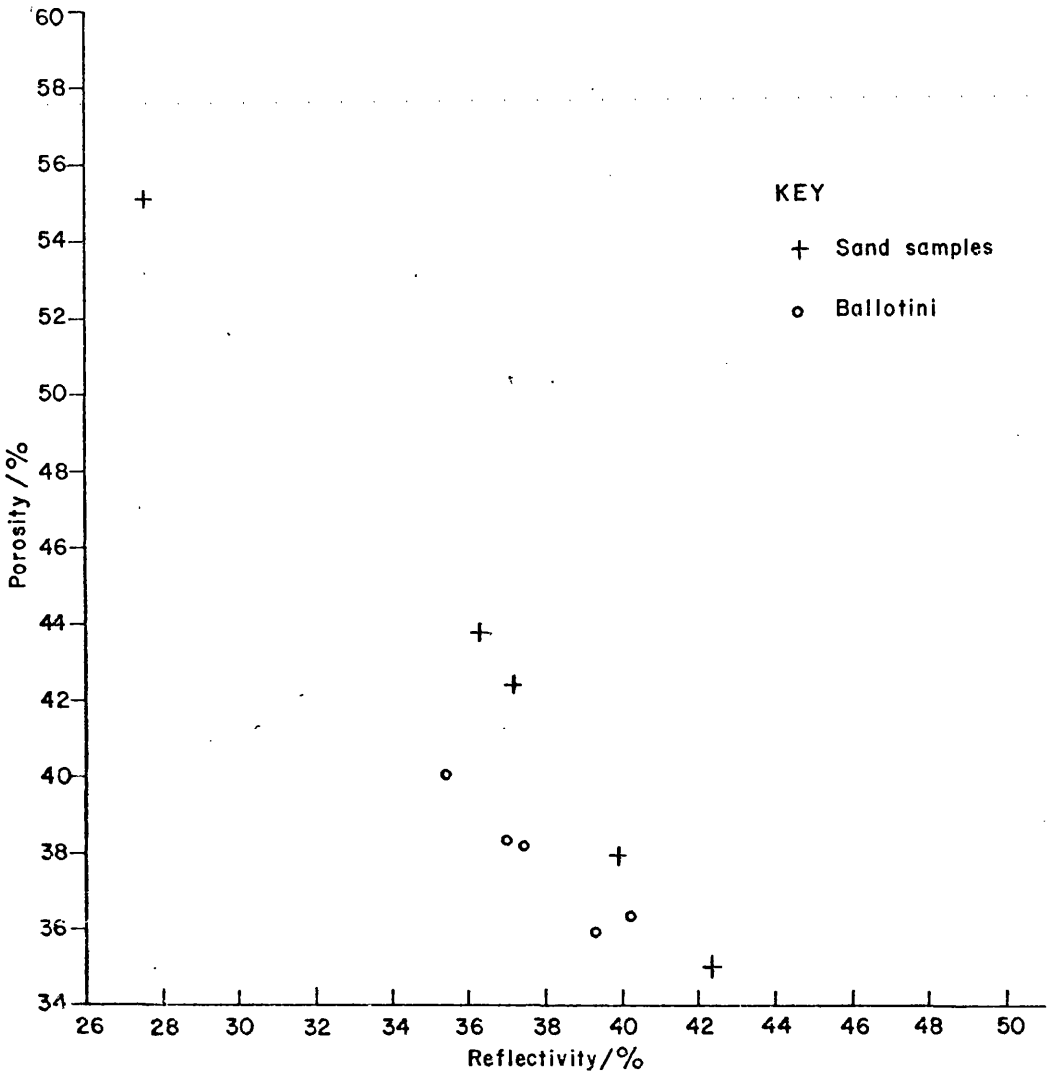

Figure 7.14 Relationship between porosity and reflectivity

directly due to the lower saturated density values which give rise to a lower specific impedence contrast at the boundary.

The density values for the Ballotini samples are independent of particle size, a characteristic which is not true of real sediments. As a result of this the rate of change of acoustic impedence with grain size is not as high as would be expected in similar real materials. This causes the effect observed in figure 7.13 where the rate of change of reflectivity with change in mean grain size is lower for the Ballotini than for the sands.

Looking at figure 7.2, it is observed that the effect of change of porosity on acoustic velocity for the Ballotini samples is more significant than for the sand samples. Despite the fact that the solid density values for the Ballotini are independent of size, the velocity/porosity ratio has an overiding effect resulting in the reflectivity versus porosity graph (figure 7.14) having a smaller gradient for the Ballotini than for the sands.

Finally reflectivity is plotted against Coefficient of Permeability in figure 7.15. The apparent trend of increasing reflectivity with increasing permeability is probably solely due to the permeability/ mean grain size relationship (figure 5.6).

7.3.3. Acoustic Transmission Loss incurred in propagation through sediments

For comparison and later discussion all values of attentuation are listed in decibels per metre (dB/m) and the equations showing

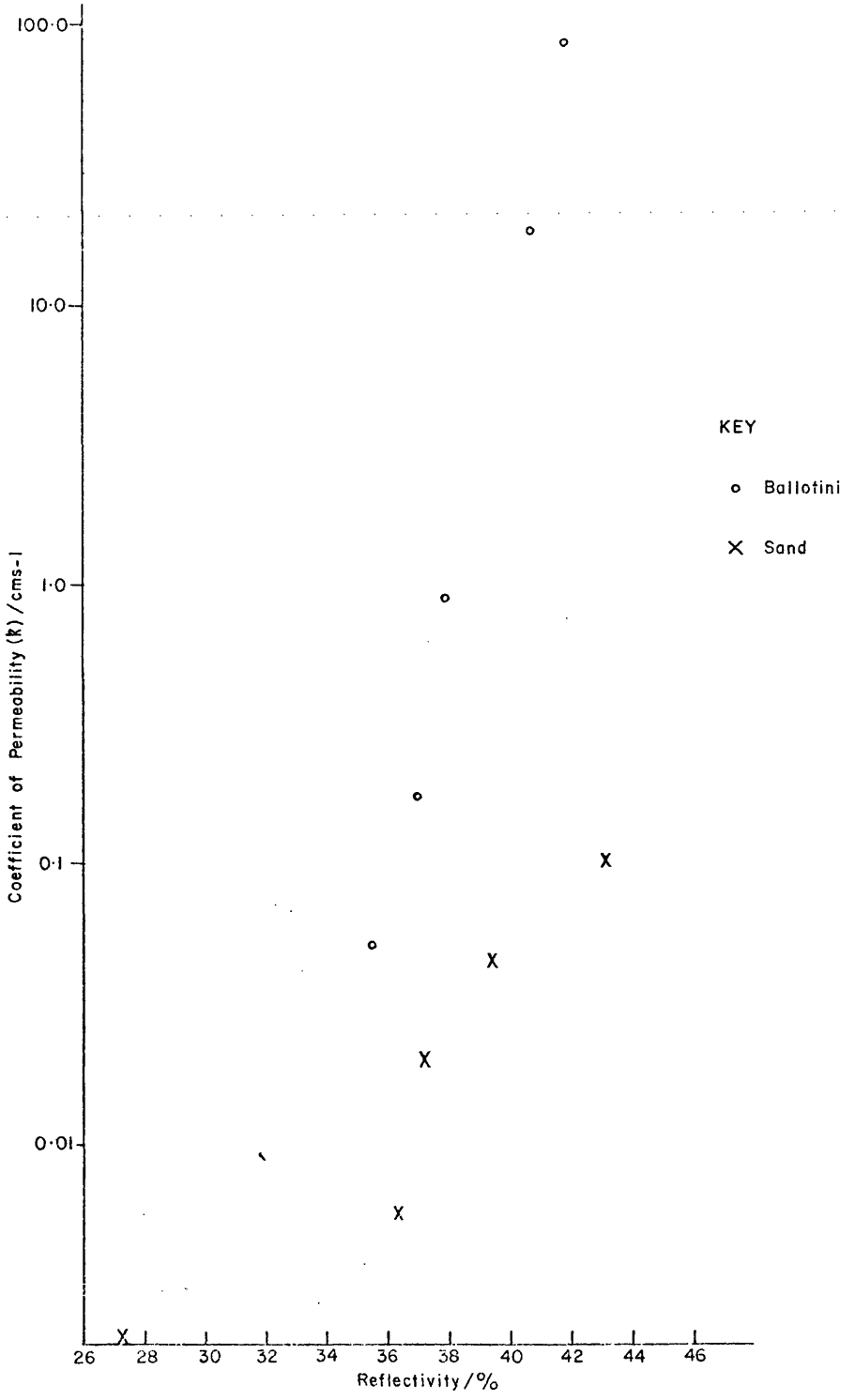

Figure 7.15 Relationship between reflectivity & permeability

dependence of attenuation on frequency are in the form

$$\alpha = kf^n \qquad 7.21$$

Where α is the attenuation of compressional waves in dB/m, k is constant, f is the frequency in kHz and n is the exponent of frequency.

The acoustic transmission loss incurred as a result of the propagation of sound through each of the samples was obtained by spectral analysis of a number of impule responses corresponding to transmission through different depths of sediment as described in section 7.3.1. The measured Transmission Loss (expressed in dBs per metre) was then plotted as a function of frequency for each of the samples.

Figures 7.16 to 7.25 show the measured transmission loss functions for each of the samples on a log/log scale. Each plot represents the weighted average of between ten and twenty transmission loss functions obtained with different column thicknesses as the sediment layer was built up, each individual measurement being based on the average of ten recorded impulse responses.

The gradients of the log/log plots of attenuation against frequency, with the exception of 7.25, indicate an approximate first power dependence of attenuation on frequency. The exact values of the exponent n in equation 7.21 calculated from these plots are indicated in table 7.3.

The relationship between attenuation and frequency has been debated at great length in several papers on the subject of the acoustic

Sediment	Mean grain diameter (μm)	n
Sand No. 1	50	1.00
Sand No. 2	130	0.82
Sand No. 3	250	0.95
Sand No. 4	330	0.95
Sand No. 5	480	0.92
Ballotini No. 1	250	0.80
Ballotini No. 2	490	0.91
Ballotini No. 3	1200	1.10
Ballotini No. 4	4000	1.05
Ballotini No. 5	8000	-

Table 7.3 Values of the exponent of frequency (n) for the sediment samples.

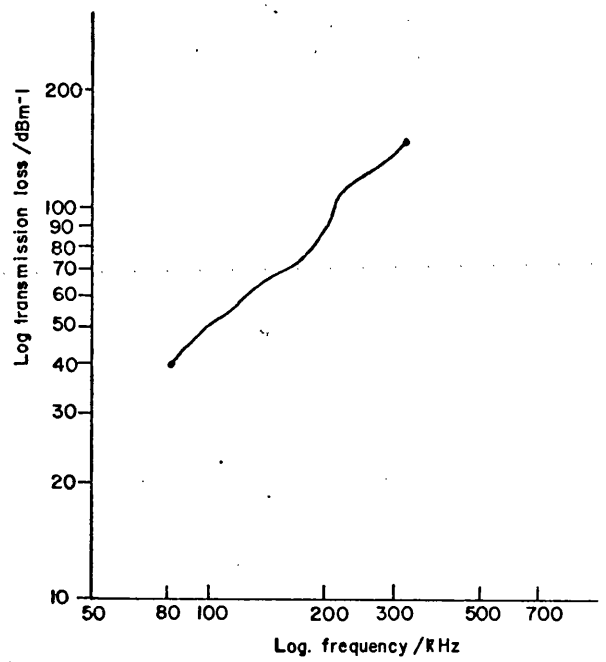

Figure 7.16 Logarithmic plot of volume transmission loss for 50μm. sand samples

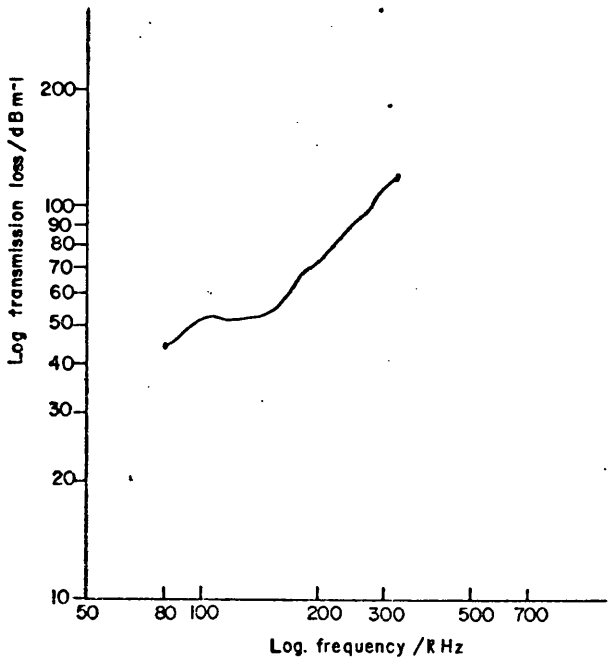

Figure 7.17 Logarithmic plot of volume transmission loss for 130μm sand samples

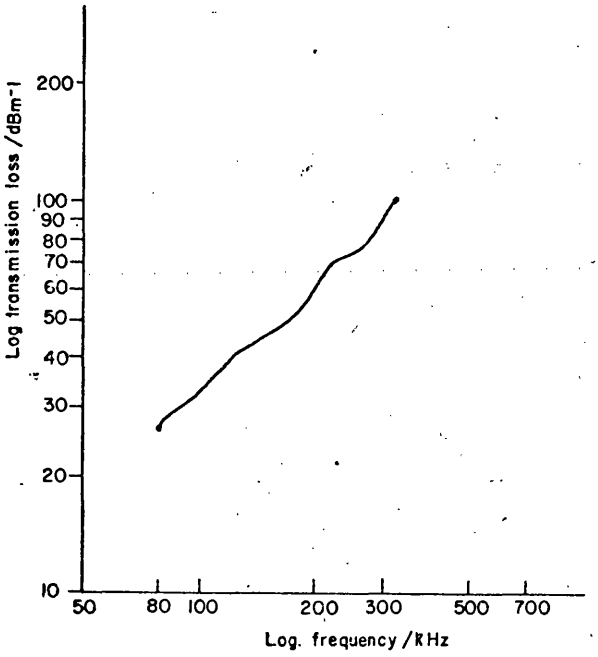

Figure 7.18 Logarithmic plot of volume transmission loss for 250μm sand samples

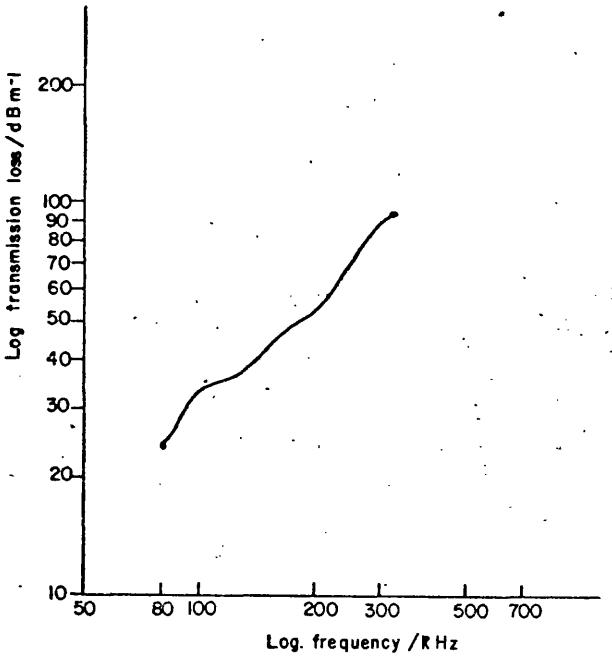

Figure 7.19 Logarithmic plot of volume transmission loss for 330μm sand samples

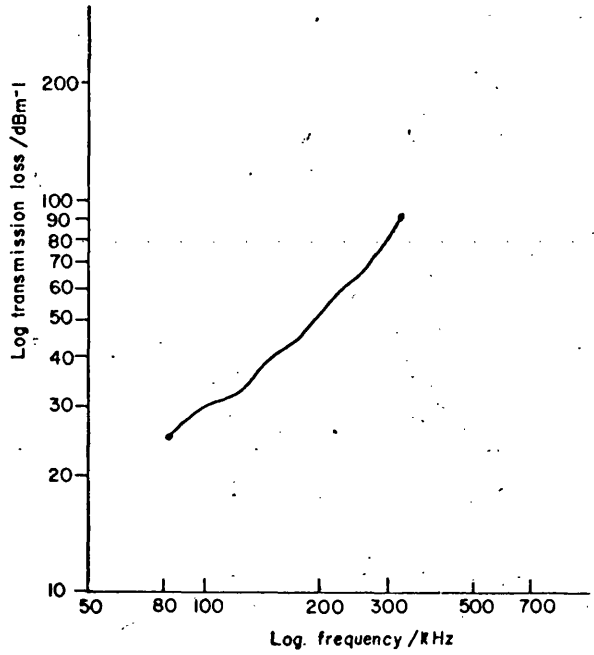

Figure 7.20 Logarithmic plot of volume transmission loss for 480μm. sand samples

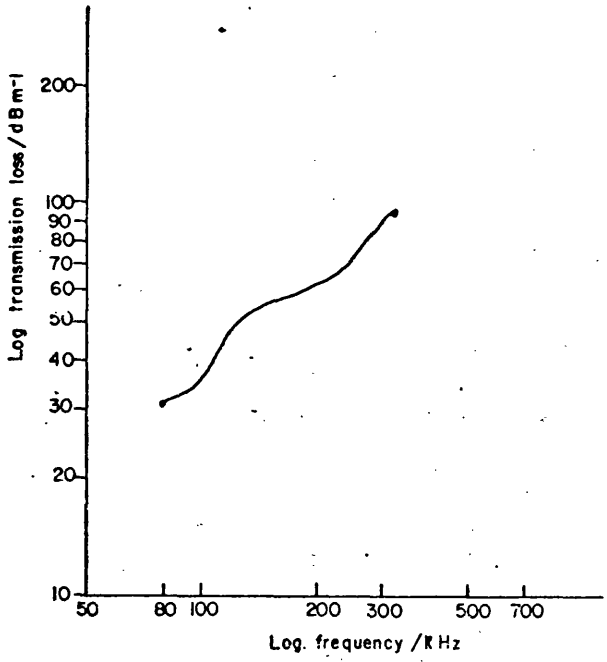

Figure 7.21 Logarithmic plot of volume transmission loss for 250μm. ballotini samples

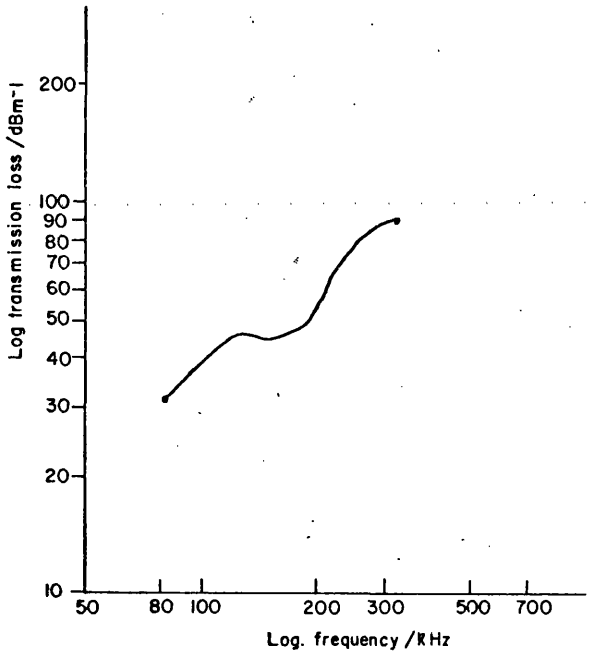

Figure 7.22 Logarithmic plot of volume transmission loss for 490μm ballotini samples

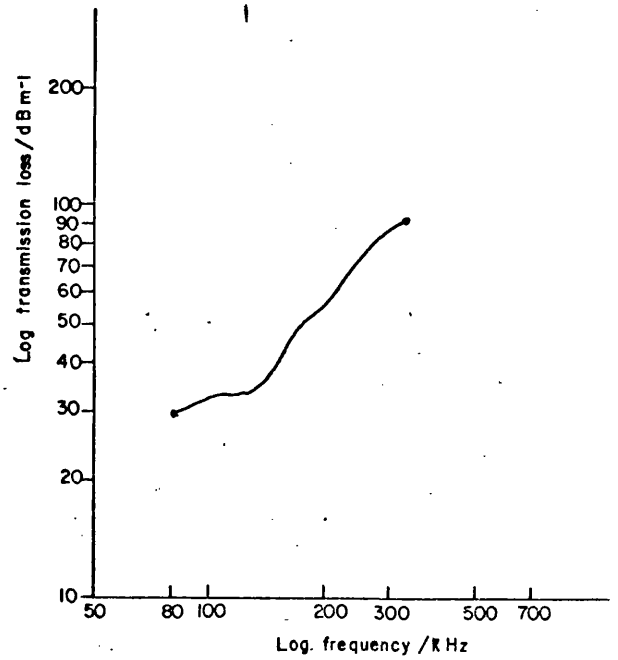

Figure 7.23 Logarithmic plot of volume transmission loss for 1200μm ballotini samples

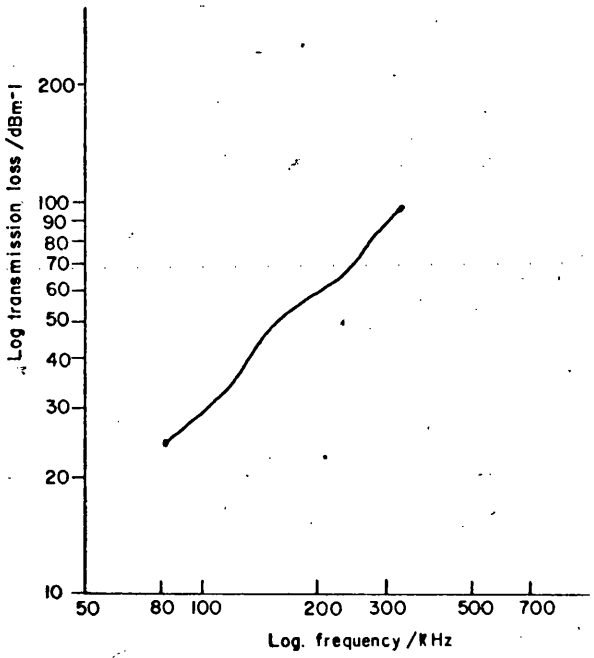

Figure 7.24 Logarithmic plot of volume transmission loss for 4mm ballotini samples

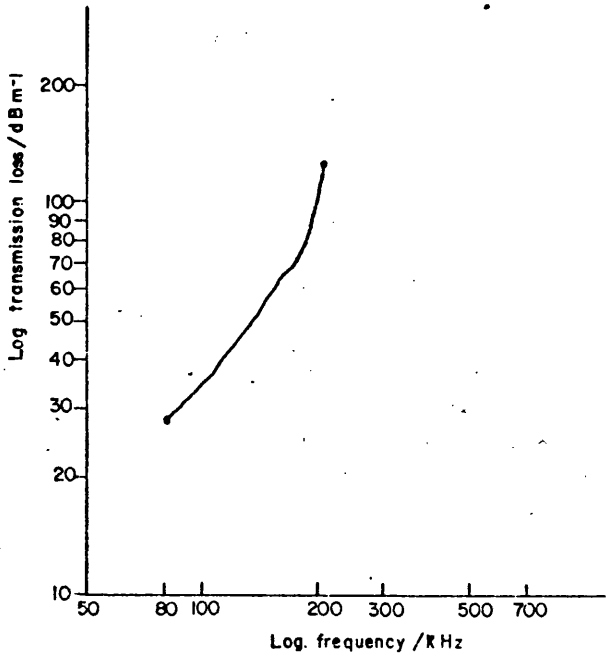

Figure 7.25 Logarithmic plot of volume transmission loss for 8mm ballotini samples

properties of marine sediments. Because of the difficulties encountered in making accurate measurements of attenuation (both in situ and in the laboratory) the computations of k and of the exponent n based on these results show considerable scatter. In predicting attenuation and extrapolating measurements to other frequencies the most important factor is the exponent of frequency, n. Busby and Richardson (1957) made measurements of attenuation in compacted sediments (mean grain sizes 120 μ to 450 μ) between 500 kHz and 3 MHz and concluded that acoustic attenuation increased with frequency but that the experimental evidence was insufficient to draw an exact relationship. However, measurements in sediments composed of glass beads indicated an approximate relationship of the form

$$\alpha = kf^4 \qquad 7.22$$

The high value of n in this account may be due to Rayleigh scattering becoming a significant factor in the MHz range. Nolle (1963) measured attenuation in quartz sands (mean grain sizes 100 μ to 700 μ) between 400 kHz and 1 MHz and proposed an experimental relationship of the form

$$\alpha = 3.7 \times 10^{-7} \, w^{\frac{1}{2}}/a \qquad 7.23$$

where α is the attenuation coefficient

w is the angular frequency

a is the average particle radius

In the same paper Nolle backed up this experimental data with a theoretical analysis suggesting a relationship of the form

$$\alpha = 3.1 \times 10^{-7} \, w^{\frac{1}{2}}/a \qquad 7.24$$

A study by Hampton (1967) also suggested a square root dependence of attenuation on frequency, although this data has been questioned by

other authors (e.g. Mizikos 1971 and Hamilton 1972) who have pointed out that these results are more in accord with a first power dependence.

Shumway (1960) using the resonant chamber method obtained attenuation data at two and sometimes three frequencies for each of 65 samples and obtained a value for the exponent n of 1.79 (standard deviation of n being 0.98).

McCann (1972) made measurements of attenuation in small sediment samples between 350 and 1000 kHz using a pulse technique (as discussed in Chapter 2) and showed the dependence of attenuation on frequency to vary between the first and second powers. An average value for n of 1.63 was obtained.

The most extensive study of the dependence of attenuation on frequency in marine sediments has been performed by Hamilton. In a series of papers (1956, 1970 a & b, 1971, 1972, and 1976), Hamilton has collected together an extensive array of frequency and attenuation data from his own studies of marine sediments off San Diego, in the Japan Sea and in the Indian Ocean Central Basin, North together with selected data from the literature. To summarise these results figure 7.26 shows figure 1 of Hamilton's 1976 paper.

Neprochnov (1971) summarised Soviet measurements of attenuation coefficient at low frequencies in the main sediment layers of the Black Sea, Japan Sea, Arabian Sea, Bay of Bengal and in other areas of the Indian Ocean. These measurements, based on the amplitudes of compressional waves reflected from main boundaries, indicated a general linear relation-

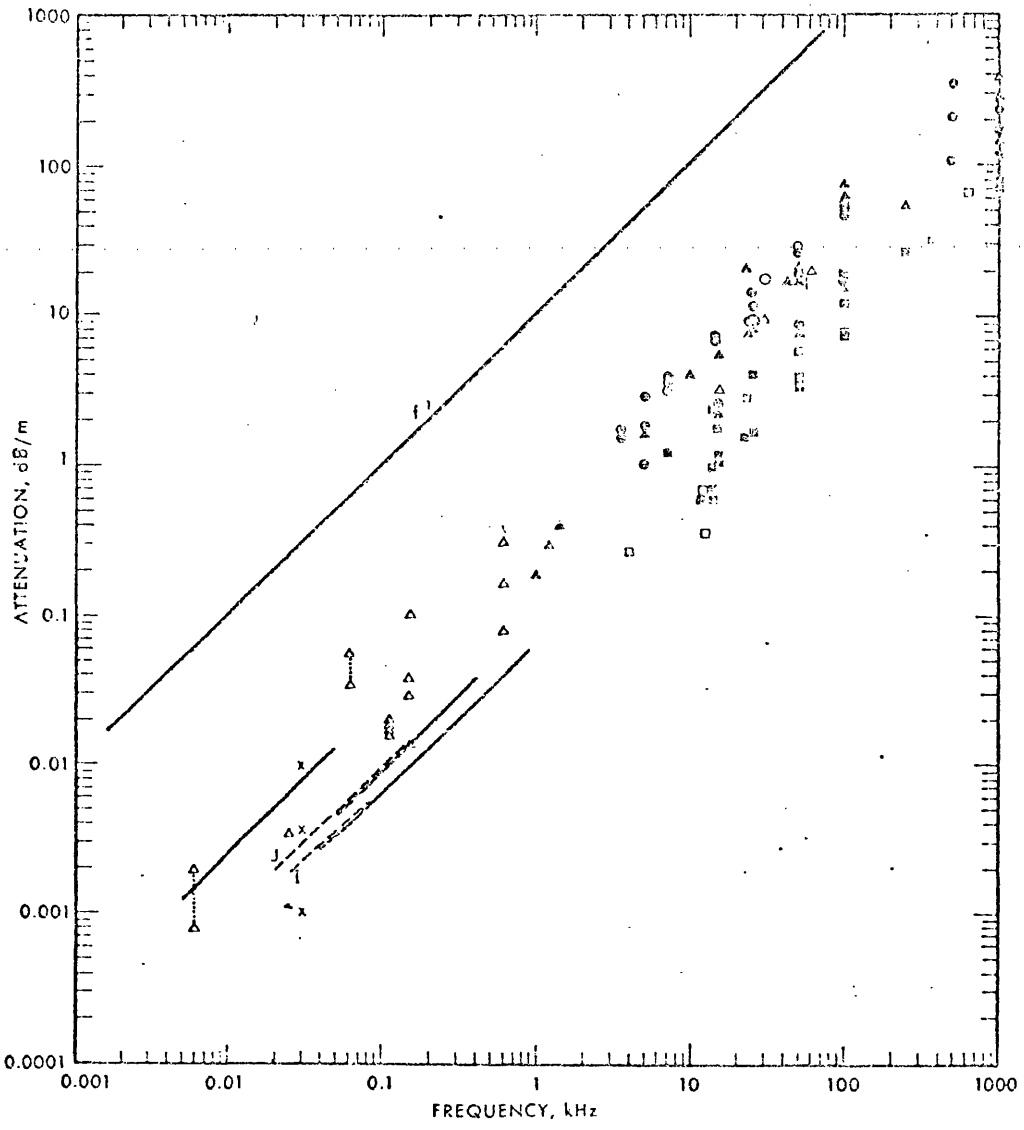

Figure 7.26 Attenuation of compressional waves vs. frequency in natural, saturated sediments and sedimentary strata. Symbols: circles- sand(all sizes); squares-clay-silt (mud); triangles--mixed sizes.
After Hamilton(1976).

ship between effective absorption coefficient and frequency in the range 20 Hz to 400 Hz.

The data listed in this work backs up the findings of Neprochnov, Hamilton and cited references indicating an approximate first power dependence of attenuation on frequency. If the exponent of frequency in equation 7.21 is taken as unity then the only variable in the relationship is the constant k. Attenuation varies considerably from one sediment type to another inferring that the constant k must be related to the physical parameters of the sediment.

Linear plots of attenuation against frequency for each of the sediments are reproduced in figures 7.27 to 7.36.

Assuming a linear dependence of attenuation on frequency the values of the constant k were calculated and the results are shown in table 7.4.

Sediment	$k/s.m^{-1}$
Sand No. 1	0.470
Sand No. 2	0.376
Sand No. 3	0.310
Sand No. 4	0.300
Sand No. 5	0.240
Ballotini No. 1.	0.310
Ballotini No. 2	0.275
Ballotini No. 3	0.280
Ballotini No. 4	0.280
Ballotini No. 5	0.30 up to 130 KHz

Table 7.4 Computed values of k assuming a linear dependence of on frequency.

The value equated for the largest Ballotini sample is debatable as Rayleigh scattering is occurring and an f^1 relationship is thus invalid.

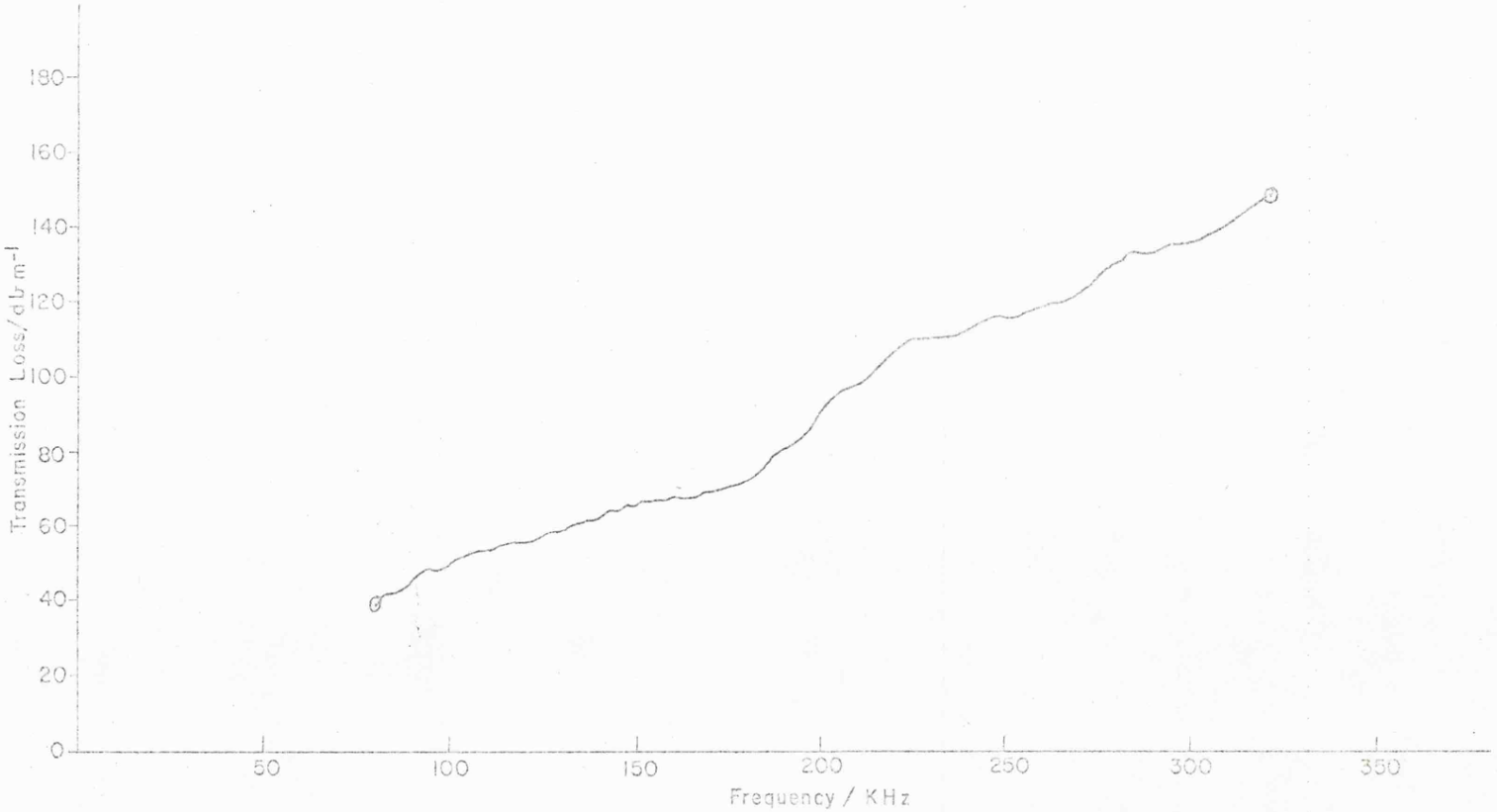

Figure 7.27 Transmission loss as a function of frequency for the 50 mm sand (volume effect only)

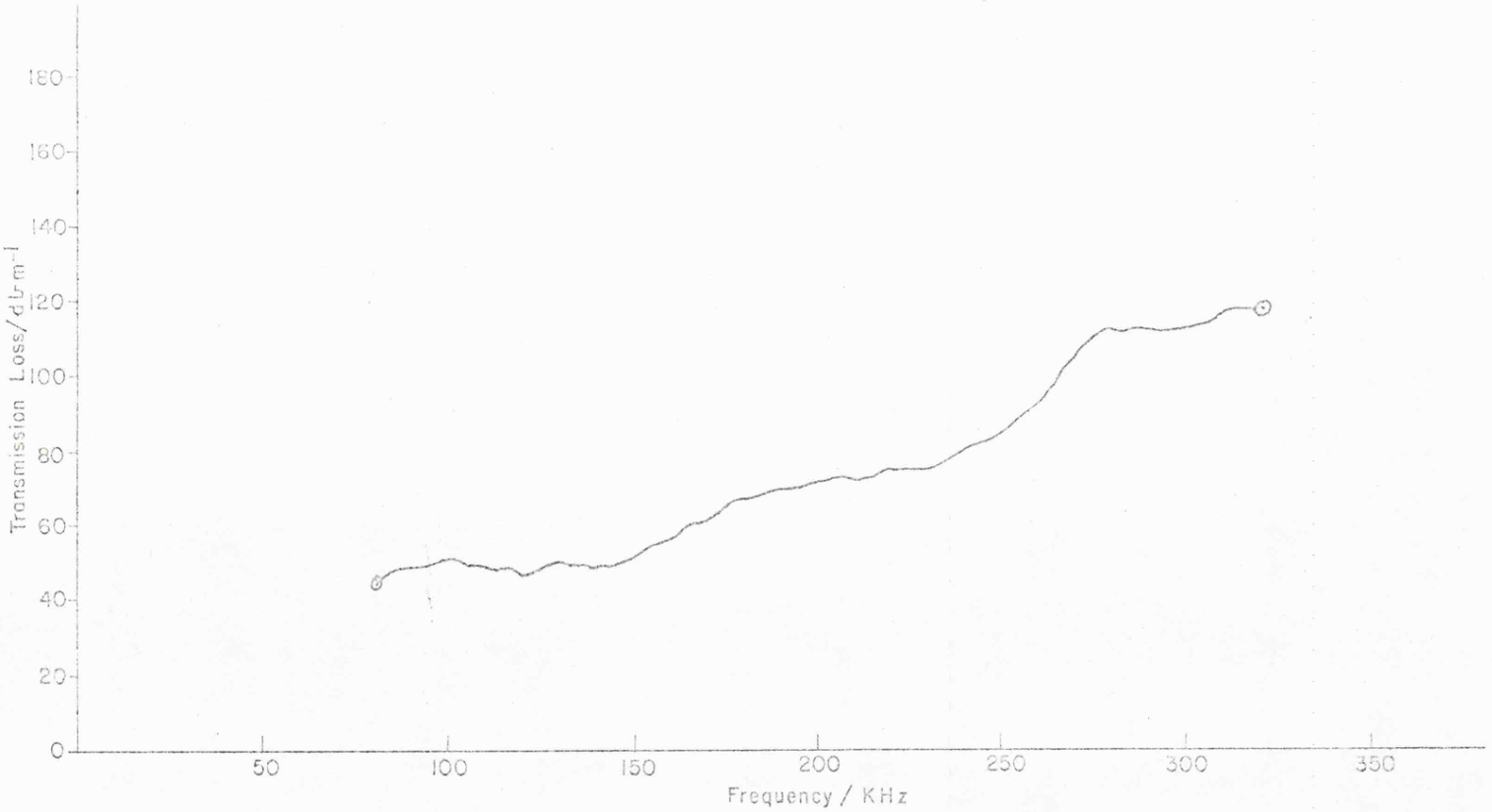

Figure 7.28 Transmission loss as a function of frequency for the 130 mm sand samples (volume effect only)

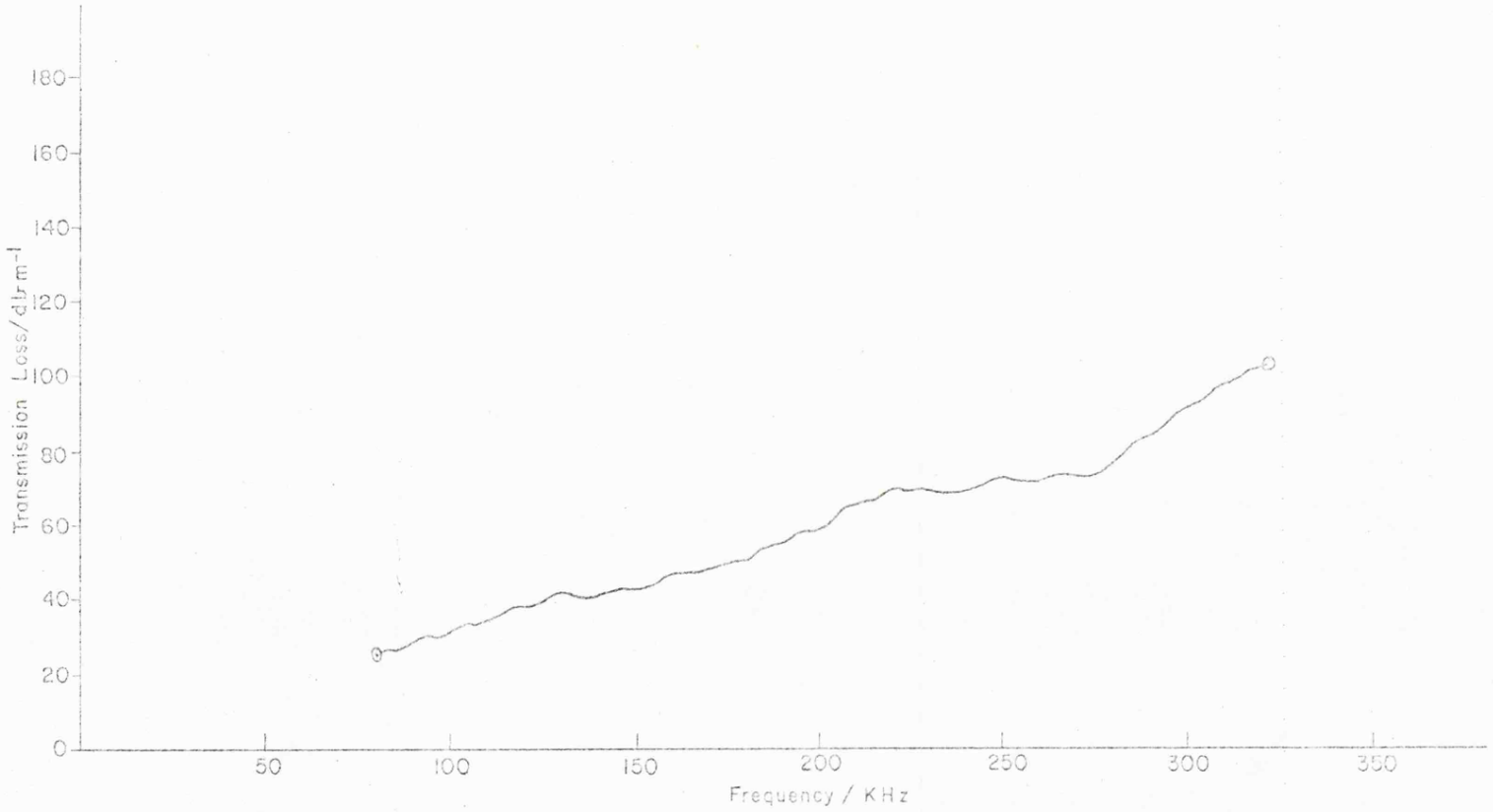

Figure 7.29 Transmission loss as a function of frequency for the 250mm sand samples (volume effect only)

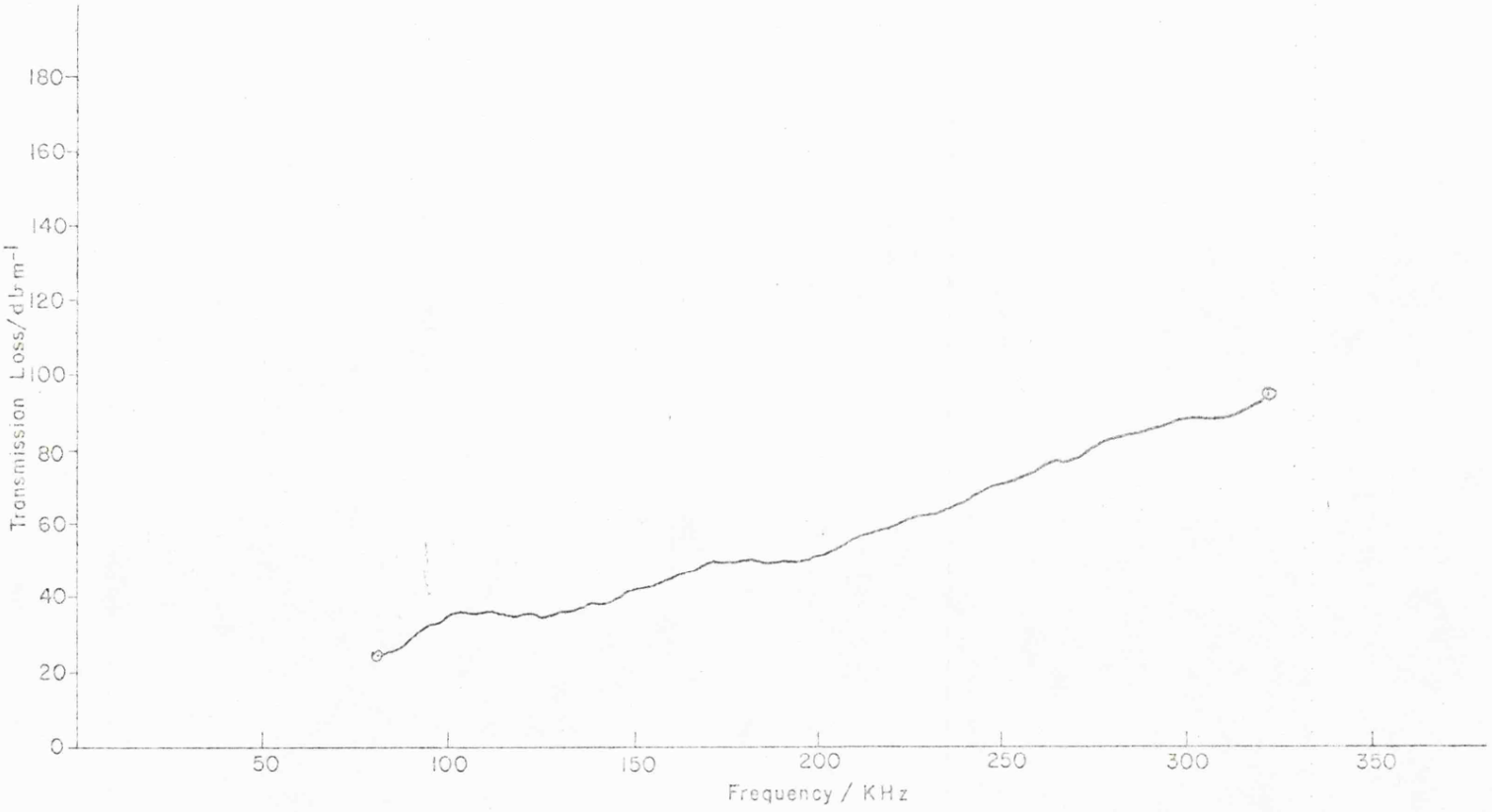

Figure 7.30 Transmission loss as a function of frequency for the 330mm sand samples (volume effect only).

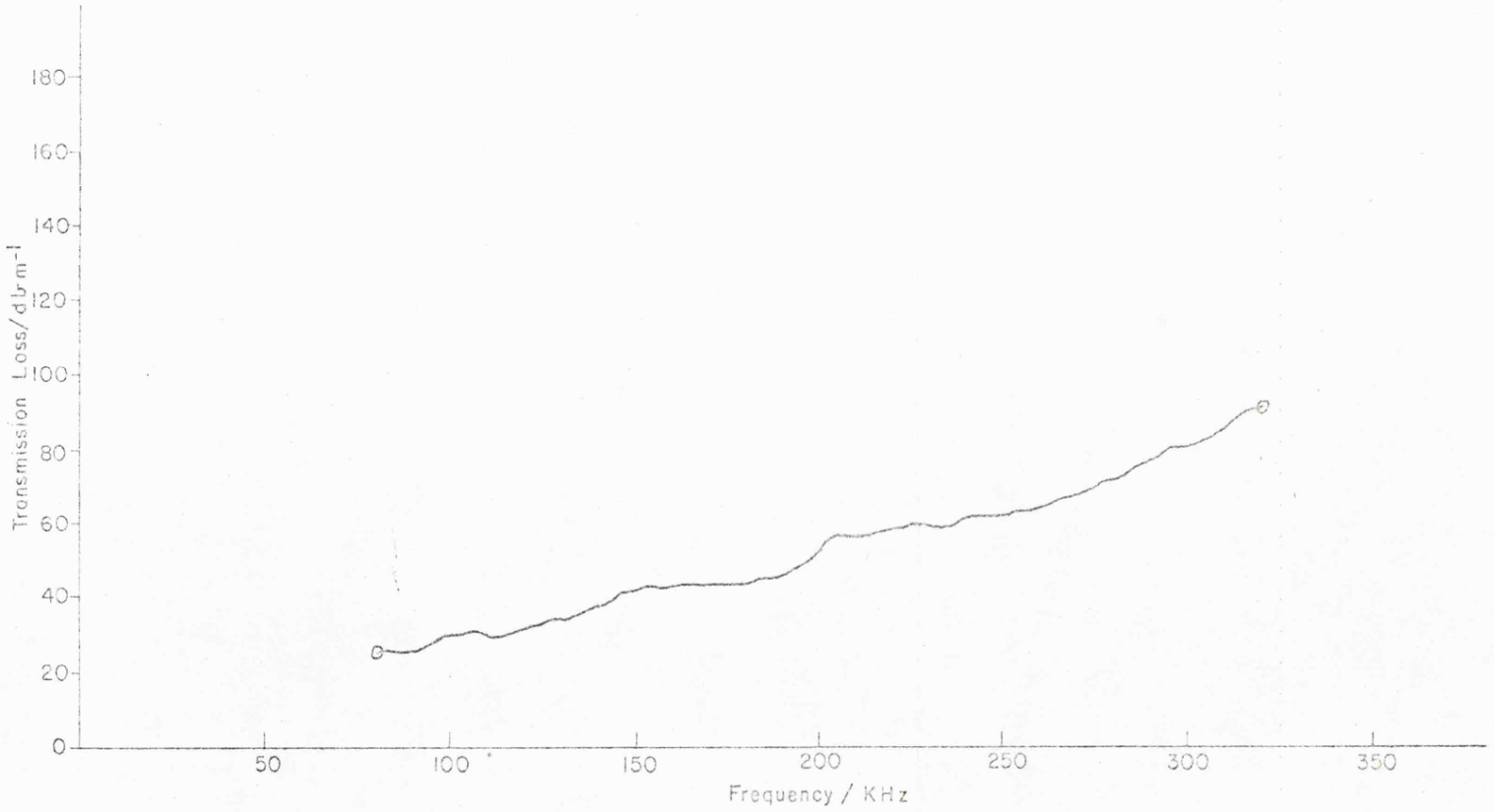

Figure 7.31 Transmission loss as a function of frequency for the 460mm sand samples (volume effect only).

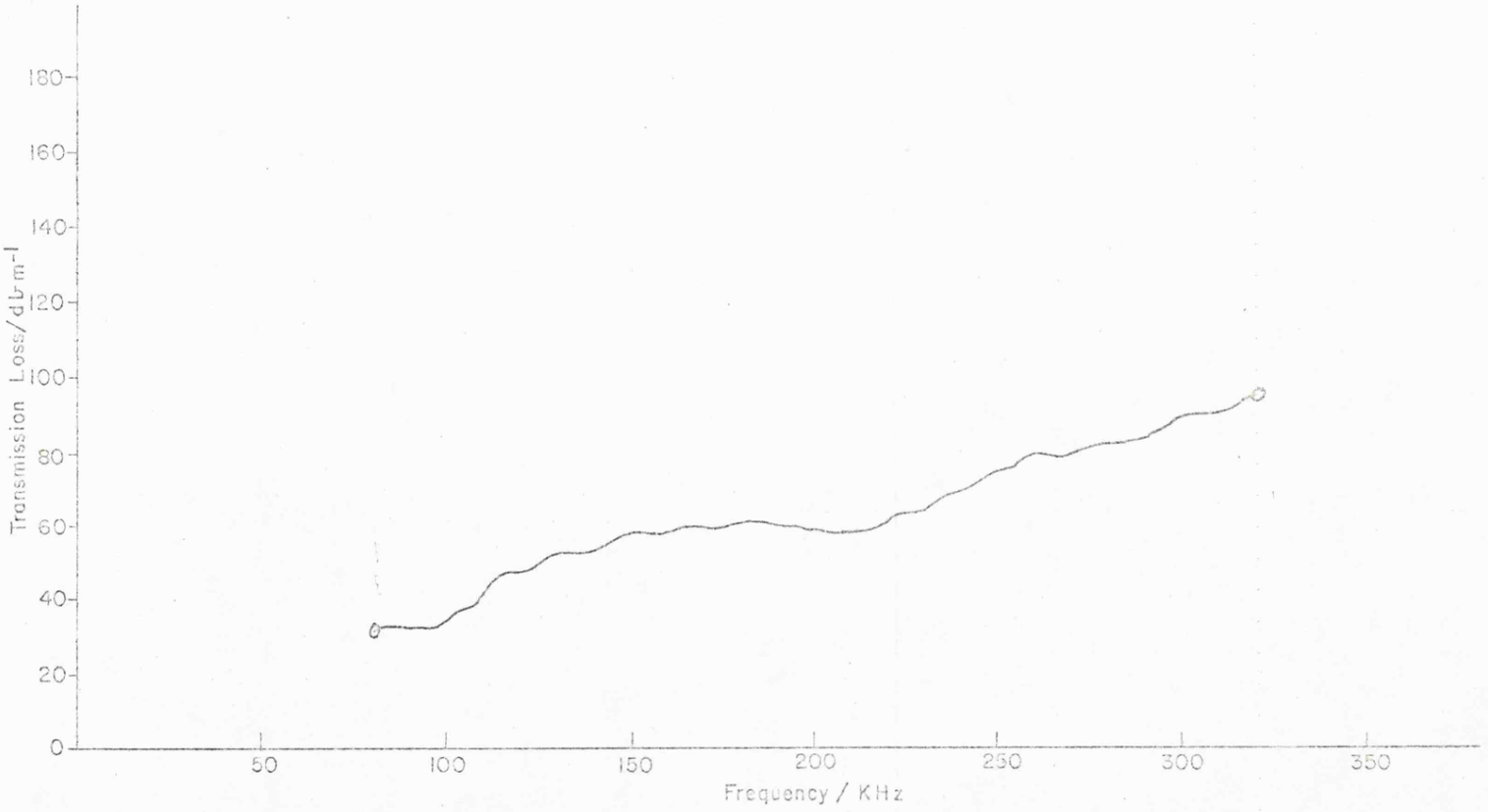

Figure 7.32 Transmission loss as a function of frequency for the 250mm ballotini samples (volume effect only).

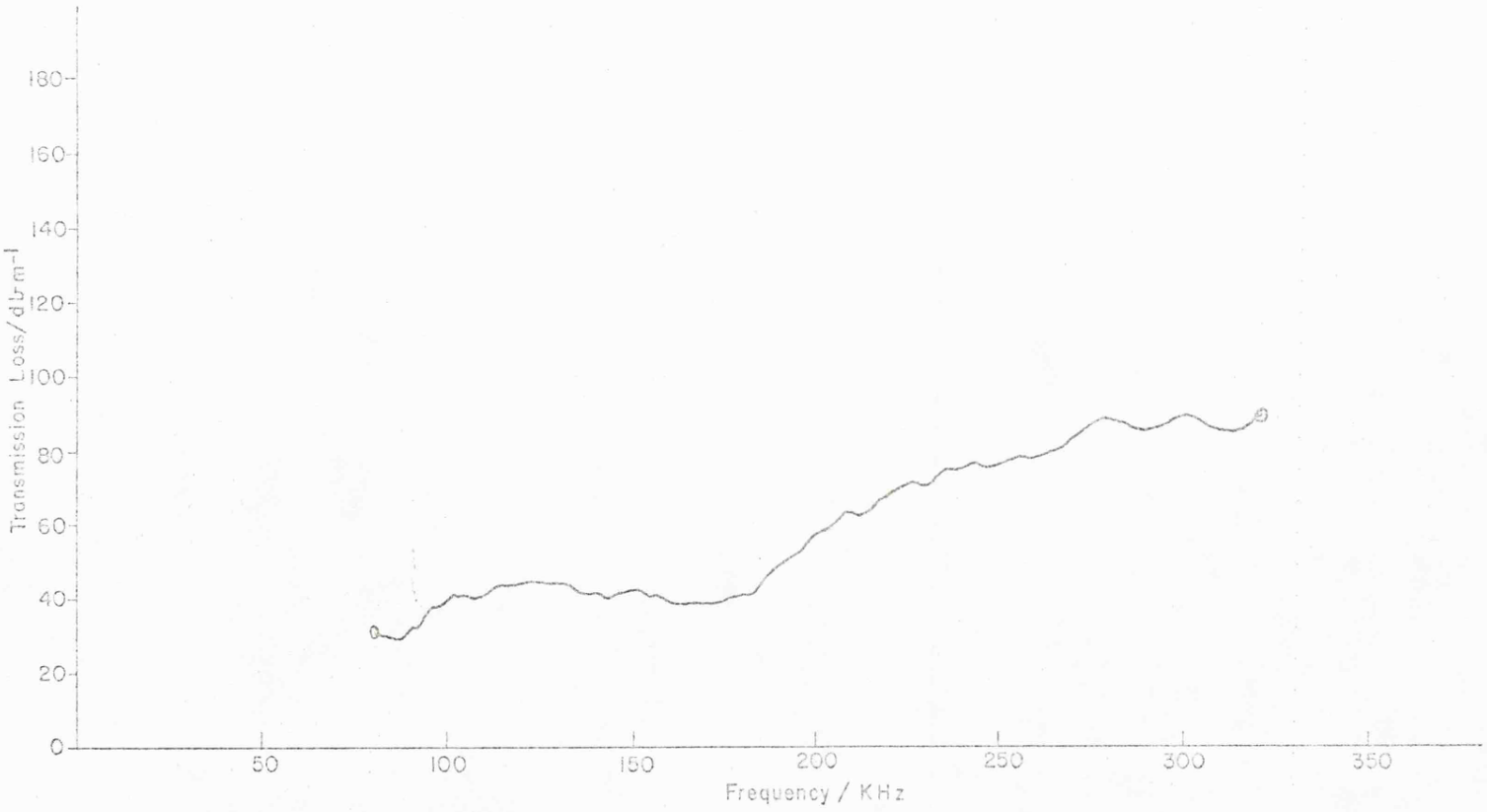

Figure 7.33 Transmission loss as a function of frequency for the 490mm ballotini samples (volume effect only).

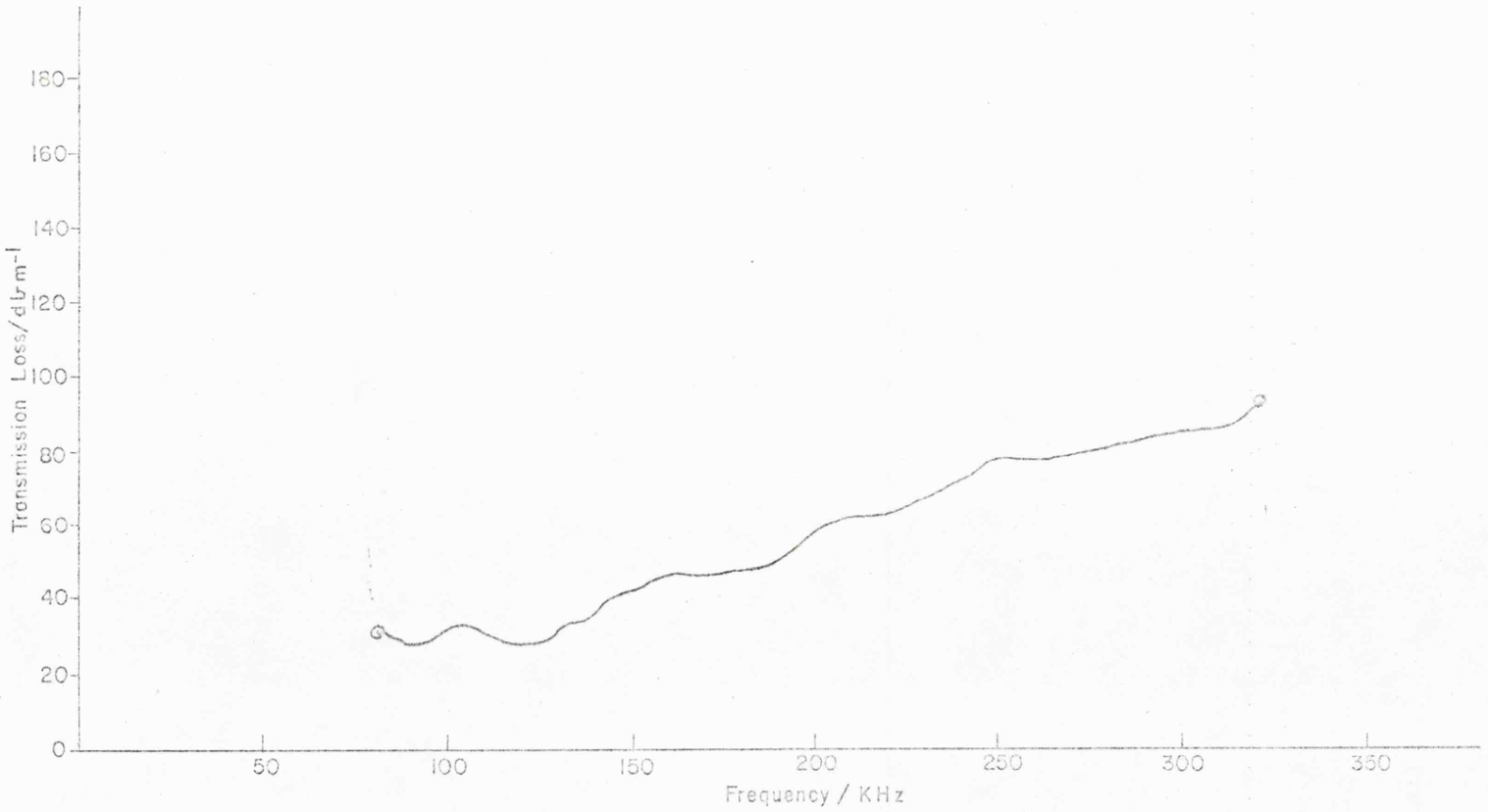

Figure 7.34 Transmission loss as a function of frequency for the 1·2mm ballotini samples (volume effect only).

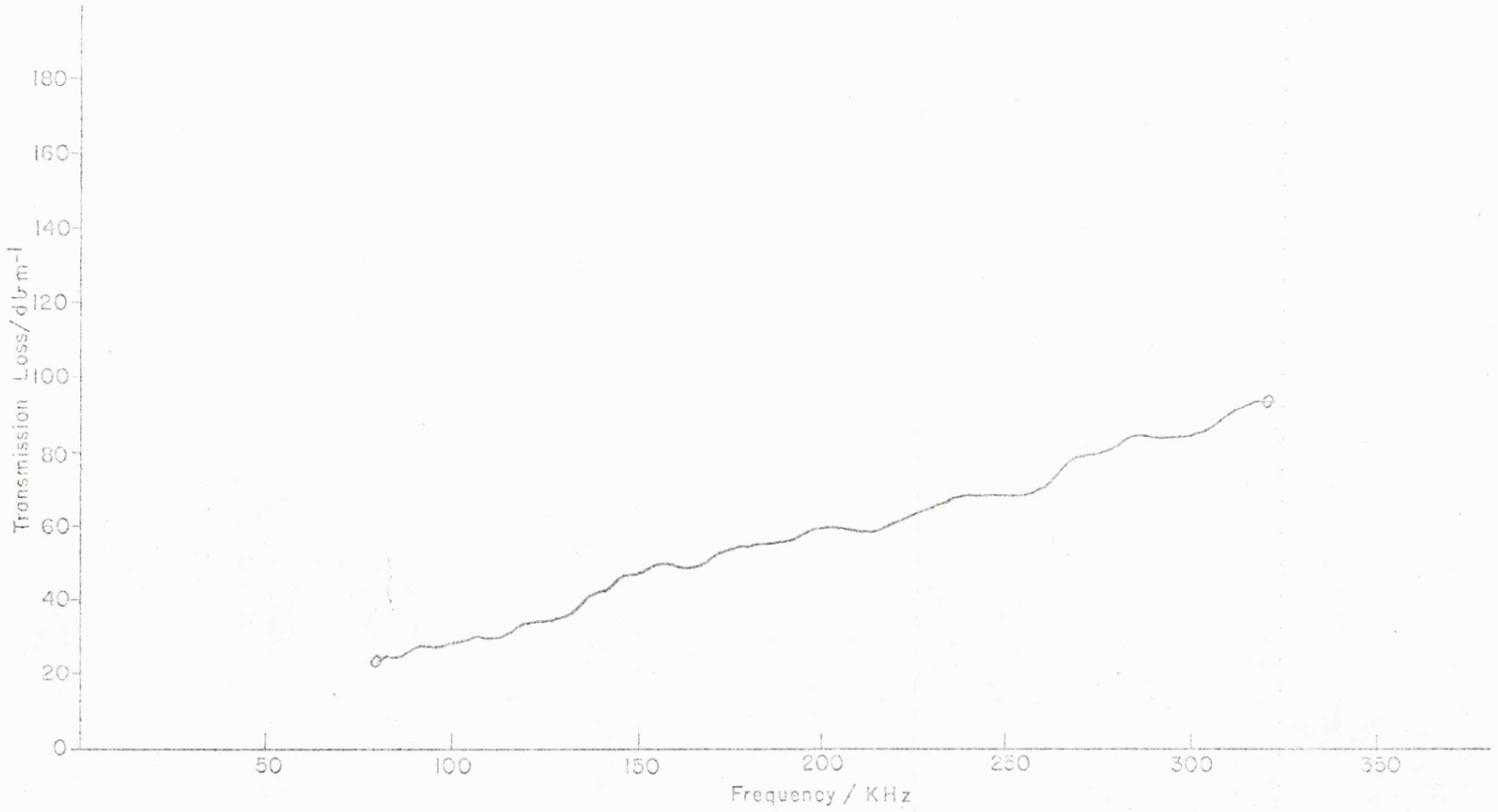

Figure 7.35 Transmission loss as a function of frequency for the 4mm ballotini samples (volume effect only).

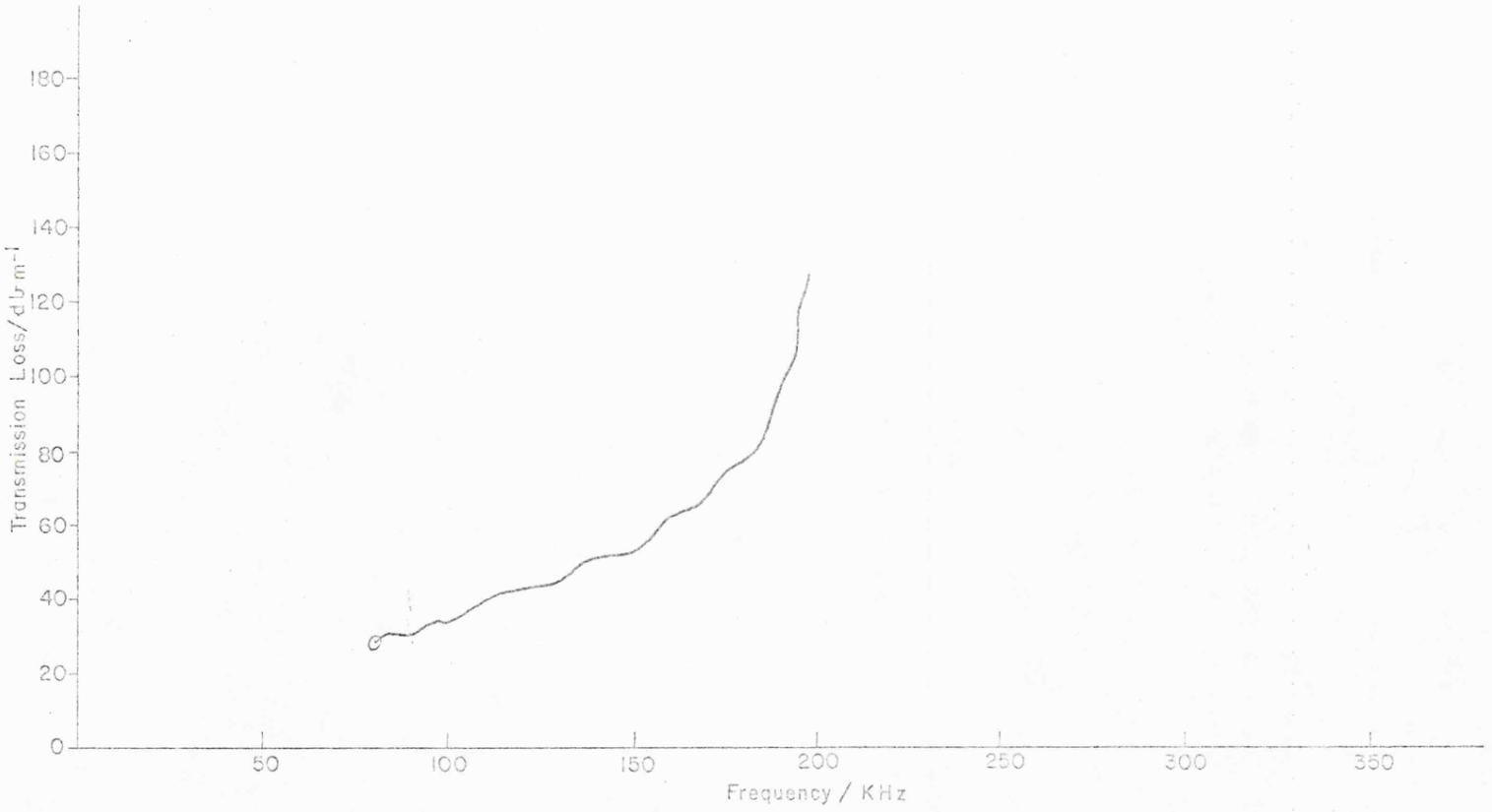

Figure 7.36 Transmission loss as a function of frequency for the 8mm ballotini samples (volume effect only).

Figure 7.37 illustrates the variation of the constant k with sediment mean grain size. (Mø) For phi values less than 2.5, k increases gradually with ø (decreasing grain size), above this value of ø, k tends to increase more rapidly although the number of data points is limited. Other investigators have measured increasing attenuation in sands with decreasing grain size (e.g. Hamilton 1972, Shumway 1960, Hampton 1967 and McCann and McCann 1969). Hamilton's results (1972 figure 3) suggested a maximum in the k versus mean grain size curve at between 3.5 and 4.5 ø indicating maximum attenuation in very fine sand and mixtures of sand, coarse silt and clay. If this is in fact the case then a maximum attenuation would occur in the present study for a sand having a mean grain size between sand sample No. 1 and sand sample No. 2 the corresponding value of k being approximately 0.5.

Figure 7.38 shows a summary of results presented by Hamilton (1972) covering his own work and other results from the literature together with the data accumulated in this study. The results here are lower than the average values predicted by Hamilton but follow the same trend.

Figure 7.39 illustrates that the variation of k with porosity is similar to the variation with mean grain size. Again k increases with increasing porosity over the range 34% to 55%. Porosity and mean grain size are well correlated for the sediments used here and hence the similarity between these last two figures (7.38 and 7.39) is not surprising. Similarly if a maximum occurs in the k versus mean grain size curve then a similar maximum should occur at a corresponding porosity.

The values of k and porosity are superimposed on figure 5 from

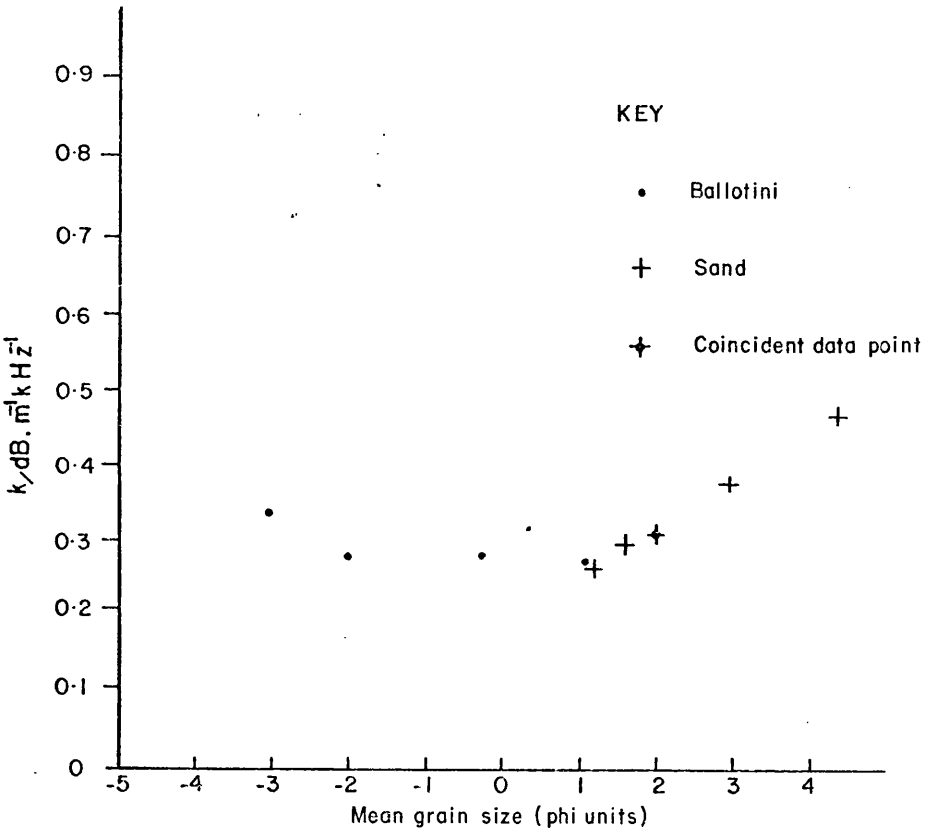

Figure 7.37 Relationship between k and mean grain size

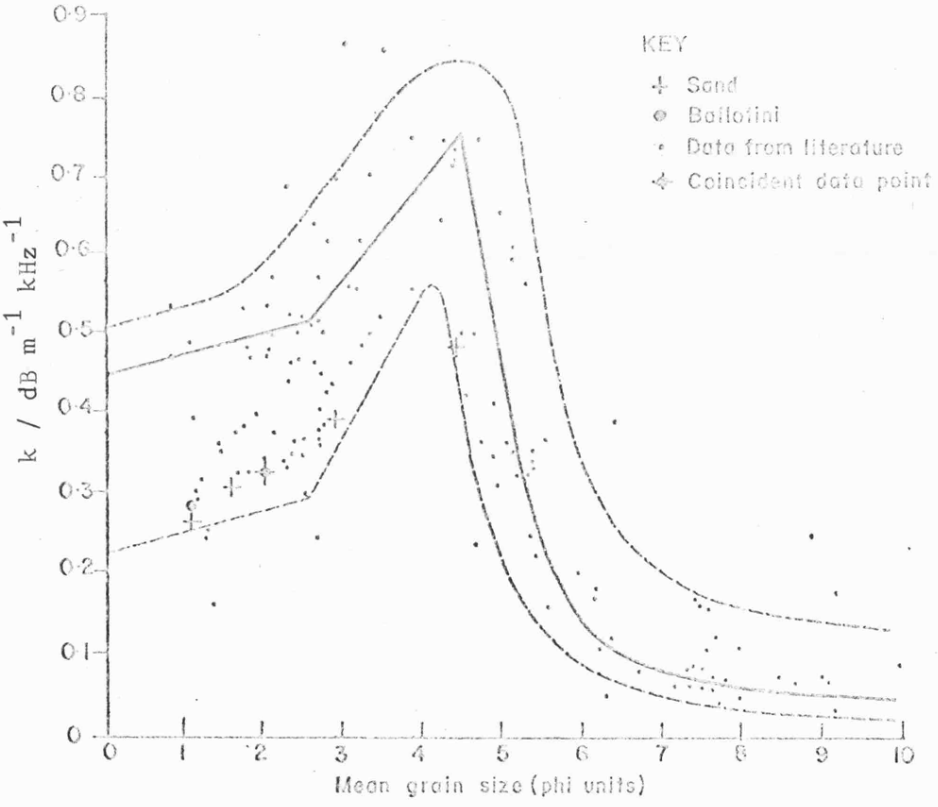

Figure 7.38 Comparison of mean grain size/attenuation results with data presented by Hamilton(1972) and Shumway(1960). The lines, suggested by Hamilton, indicate "the area within which most data should fall" and the averaged data values from the literature.

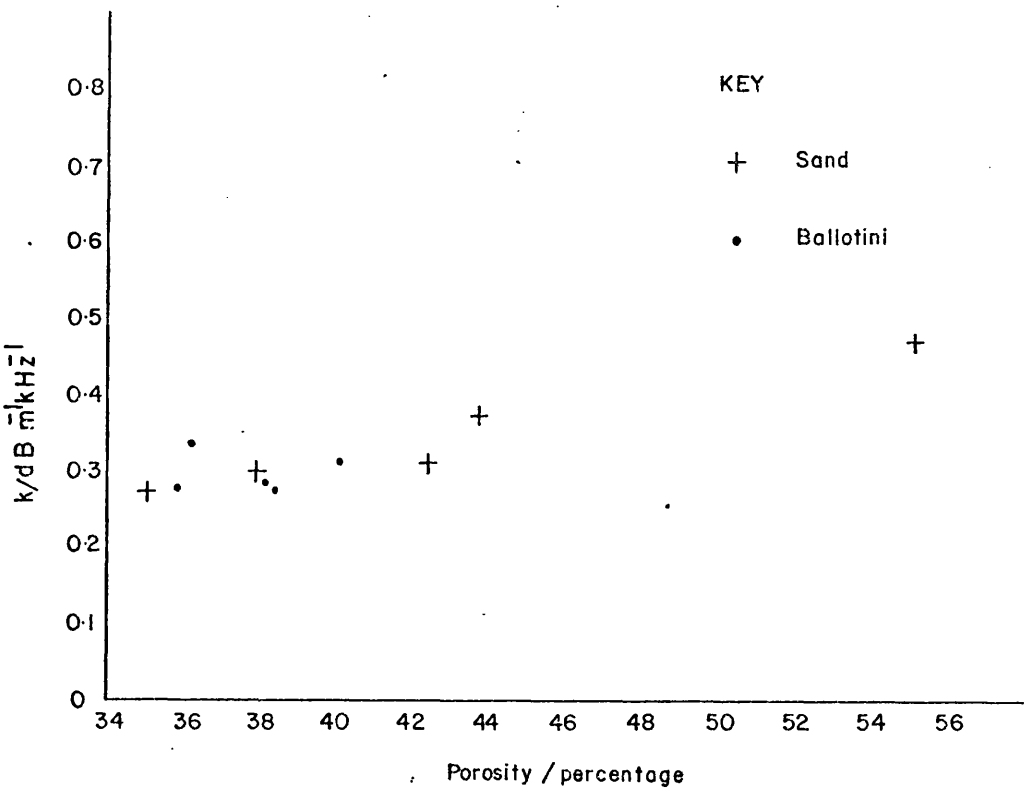

Figure 7.39 Relationship between k and porosity

Hamilton (1972) (figure 7.40) indicating that the results obtained are again lower than those obtained by Hamilton but follow the same general trend. The maximum value of k that might be expected from these results (if the trend indicated by Hamilton held good) would occur at a porosity of about 51% and the corresponding maximum value of k would be approximately 0.5.

Figure 7.41 shows the variation of k with permeability for all the sand samples and for the smaller 3 Ballotini samples. Attenuation is seen to increase with decreasing permeability, attenuation tending to be higher in the Ballotini samples than in sand samples having the same permeability.

7.4. Implications of Results

Perhaps the most interesting aspect of the results is the implication of the attenuation/frequency measurements on the selection of energy loss mechanisms for the transmission of sound through marine sediments. Outside the region where Rayleigh scattering is a significant factor, there are two main mechanisms that can give rise to acoustic energy losses. These are interactions between particles at the particle boundaries, sometimes called solid friction losses, and viscous losses which occur as a result of relative movements of the solid framework and the pore fluid.

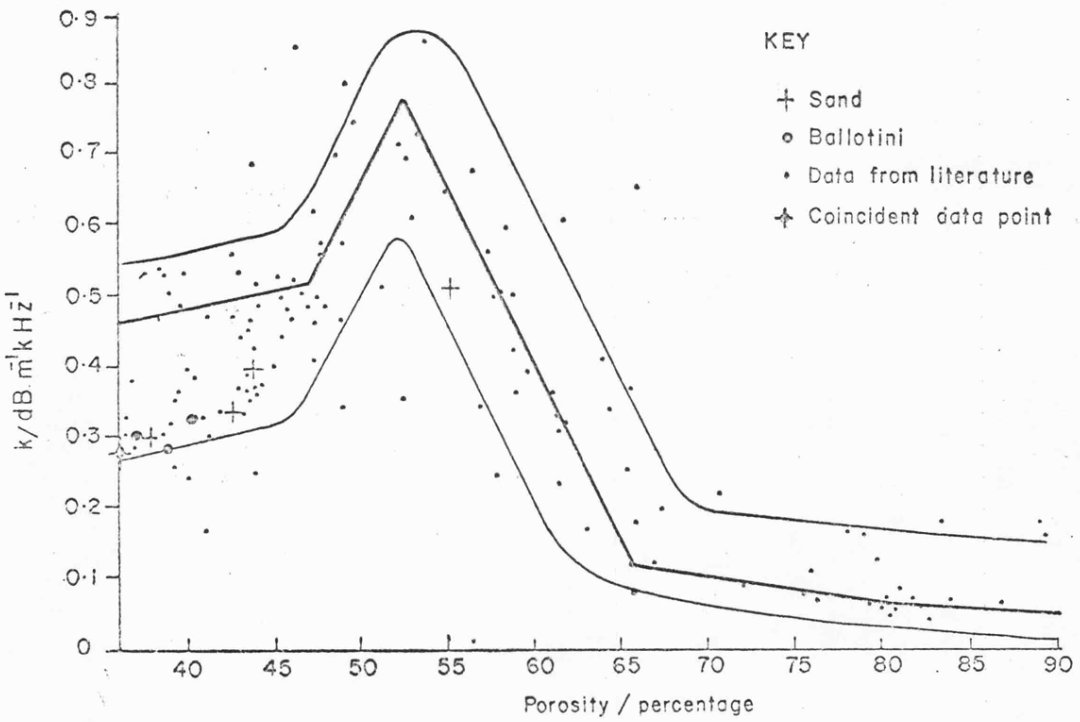

Figure 7.40. Comparison of attenuation/porosity results with data presented by Hamilton (1972) and Shumway (1960). The lines, suggested by Hamilton, indicate "the area within which most data should fall" and the averaged data values from the literature.

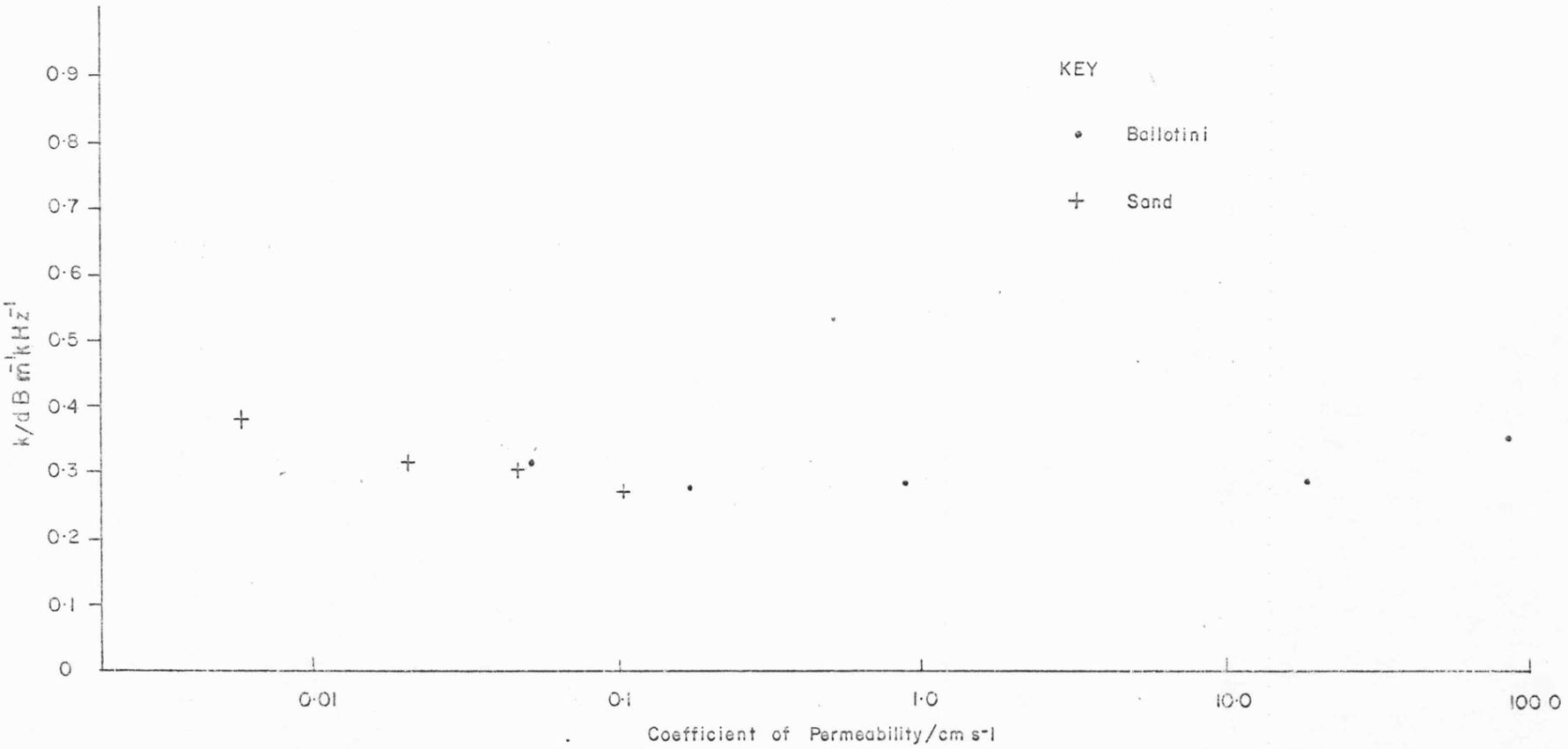

Figure 7.41 Relationship between k and permeability

Solid Friction Losses

Solid friction losses occur at the points of contact of particles and it has been shown (Hunter et al 1961, Duffy and Mindlin 1957) that these losses are identical in nature to the losses encountered in poly-crystaline rocks. Such losses are characterised by a linear variation of attenuation with frequency and a small velocity dispersion. (Attwell and Ramana 1966).

Viscous Losses

Viscous losses occur as a result of a velocity differential between particle and fluid movements. This mechanism was studied by Biot (1956 a and b) who derived an expression for the viscous losses encountered in a porous solid. Biot considered the elastic modulii of the fluid and the solid matrix and indicated that in the particle size range between 6 phi and 1 phi and at frequencies greater than 5 kHz the viscous loss is proportional to the square root of frequency.

It is concluded that these two mechanisms both contribute to the total energy loss under any particular set of conditions but the relative importance of each of the two parameters depends on the porosity and the mean grain size of the material and the frequency of the acoustic energy. McCann and McCann (1969) proposed that the attenuation can be expressed in the form

$$= k_1 f + k_2 f^{\frac{1}{2}} \qquad 7.25$$

The results of this study indicate that the solid friction term giving rise to a linear increase of attenuation with frequency dominates the viscous term in equation 8.1. for sediments of mean diameter greater

than 6 phi. Relative movement between the solid particles and the fluid cannot however be excluded on the basis of these results but if present is probably small. It is interesting to note that the viscous loss term if present will be higher in sands than in most other sediment types as these are most permeable. Permeability and fluid viscosity in this case should to some extent dictate the attenuation. A square root dependence was not observed however even for the highly permeable Ballotini and it must be concluded that the viscous term is very small.

If solid friction losses dominate then attenuation should be related to the number of integrain contacts and the sliding and rolling friction between the grains. The number of interparticle contacts are related to the mean grain size, sorting and the density of packing, the latter being related to porosity. Interlocking of grains is also important and in general this increases with increasing density and angularity of the grains. In general, for natural sands, angularity increases with decreasing grain size (Pettijohn 1957). Thus as grain size decreases the resistance to shear stress at the particle contacts increases but as porosity increases with decreasing grain size the number of intergrain contacts per unit volume decreases. There are in this case two conflicting trends which can, to an extent, be estimated.

As the grain size decreases from 1 to 2.5 ø there is a 6 to 8 percent increase in porosity. Shumway and Igelman (1960) showed that over the same range grain surface areas increase by 240 percent. It must be remembered that the grain surface area is not the same as the total contact area although the two are closely related and this infers that over the range of sizes considered attenuation is likely to increase with decreasing mean grain size as observed in the experimental results.

Chapter 8

SUMMARY

A system has been developed which enabled velocity and attenuation measurements to be made on air-free samples of both artifical and real sediments using an impulse response technique. The method adopted has several advantages over most other laboratory techniques in that attenuation measurements are acquired between 80 kHz and 320 kHz during a single experimental run. The identical sediment matrix is therefore used for all the frequency measurements on an individual sample, the sample is not disturbed and the transducers are not substituted.

The broadband acoustic transmission measurements indicated that the attenuation in the volume of the sediment increases linearly with frequency provided the wavelength of the acoustic energy is greater than the mean particle diameter of the sediments. This is demonstrated in figures 7.27 to 7.35.

Volume attenuation was shown to increase with increasing porosity according to the relationship shown in figure 7.39 and to decrease with increasing mean grain size as shown in figure 7.37.

The transmission loss at the water/sediment interface, indicated in figure 7.12, was shown to be frequency independent provided the wavelength of the acoustic energy is greater than the mean particle diameter. This transmission loss agreed well with the theoretically predicted values for a plane wave incident on a smooth boundary as indicated in table 7.2.

Velocity was shown to increase with decreasing porosity (figure 7.3), to increase with increasing mean grain size (figure 7.1) and to increase with decreasing phi-deviation (figure 7.5). The interrelationship of these parameters is best summarised by the linear regression equation 7.4.

APPENDIX A

Determination of Impulse Response by Cross Correlation

Consider a linear system with impulse response sequence h(j)

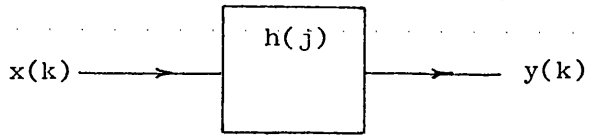

The output sequence y(k) is given by the convolution of x(k) with the impulse response sequence.

$$y(k) = \frac{1}{\ell} \sum_{j=0}^{\ell-1} x(k - j).h(j) \qquad A1$$

The cross correlation between input and output sequences is:-

$$rxy(k) = \frac{1}{m} \sum_{j=0}^{m-1} x(j - k)\, y(j) \qquad A2$$

If the Fourier Transforms of both sides of equation (A1) are taken:-

$$Y(n) = X(n).H(n) \qquad A3$$

$$n = 0, 1, 2, 3, \ldots N-1$$

and similarly the transform of equation A2 is:-

$$Rxy(n) = X^*(n).Y(n) \qquad A4$$

where * denotes complex conjugation. Using equation A2 Rxy(n) can be written as

$$Rxy(n) = \left| X(n) \right|^2 H(n) \qquad A5$$

If the spectral density of the input sequence x(k) is constant then

$$Rxy(n) = C.H(n) \qquad A6$$

where C is a constant.

On taking the inverse Fourier Transform of equation A6

$$rxy(k) = \frac{1}{\ell} \sum_{j=0}^{\ell-1} C(k - j)\, h(j)$$

where $C(k) = 0$ for all k except $k = 0$, and $C(o) = a$, where a is constant.

Therefore rxy(k) is in fact given by

$$rxy(k) = a.h(k)$$

That is to say the impulse response of the system is the cross-correlation function between input and output sequences multiplied a constant when the input sequence has a constant spectral density.

APPENDIX B

BRITISH STANDARD SIEVES

Phi values, and relation to Wentworth's Grade Scale

BRITISH STANDARD SEIVES			WENTWORTH'S GRADE SCALE		
Sieve No.	Mesh Aperture mm.	Phi	Diam mm	Grade term	Phi
			4.0	.....	-2
5	3.353	1.75	3.36		-1.75
6	2.812	-1.49	2.83	Granule	-1.5
8	2.057	-1.04	2.0	.....	-1
10	1.676	-0.75	1.69		-0.75
12	1.405	-0.49	1.41	Very Coarse Sand	-0.5
14	1.204	-0.27	1.19		-0.25
16	1.003	-0	1.0	.....	0
18	0.835	0.23	0.84		0.25
22	0.699	0.52	0.71	Coarse Sand	0.5
25	0.599	0.74	0.595		0.75
30	0.5	1.0	0.5	.....	1
36	0.422	1.24	0.420		1.25
44	0.353	1.50	0.351	Medium Sand	1.5
52	0.295	1.76	0.297		1.75
60	0.251	1.99	0.25	.....	2
72	0.211	2.24	0.21		2.25
85	0.178	2.49	0.177	Fine Sand	2.5
100	0.152	2.72	0.149		2.75
120	0.124	3.01	0.125	.....	3
150	0.104	3.26	0.105		3.25
170	0.089	3.49	0.088	Very Fine Sand	3.5
200	0.076	3.71	0.074		3.75
240	0.066	3.91	0.0625	.....	4
300	0.053	4.25	0.053	Silt	4.25

APPENDIX C

Computer programs used in this study.

Program I "INPUT"

```
0100        DIMENSION IR(100),IA(1000)
0150        INTEGER ATCOR
0200        READ(5,100)ATCOR
0250        READ(5,100)NP
0300        DO 300 N=1,NP
0400        L=N*100
0500        J=L-99
0600        CALL READFT(N1,N2,N3,N4,N5,IR)
0700        M=0
0800        DO 101 K=J,L
0900        M=M+1
1000        IA(K)=IR(M)
1100 101    CONTINUE
1200 300    CONTINUE
1300        WRITE(7,200)ATCOR,NP,N1,N2,N3,N4,N5
1340        NN=NP*100
1350        WRITE(7,500)(IA(N),N=1,NN)
1400 100    FORMAT(I5)
1500 200    FORMAT(7I3)
1550 500    FORMAT(1H ,10I6)
1600        STOP
1700        END
```

Subroutine "READFT" is a fortran linked paper tape reading module. The first five numbers are separated by commas and are put into the locations given as the first five parameters. In the calling module the third parameter specifies the number of numbers to follow on the tape. These are put into the array specified by the sixth parameter.

Program 2 "CPEAK"

```
00000100        DIMENSION IR(100),KY(100),W(512),L(512),AVPS(512),PSDB(51
     2)
00000120        DIMENSION PSDBP(121,2),FREQ(121),TIME(121),IDENT(13)
00000130        DIMENSION CPST(121,2)
00000140        DIMENSION WW(512)
00000150        COMPLEX CPS(512)
00000160        COMPLEX Y(512)
00000200        COMPLEX X(512)
00000300        COMPLEX CUMACF(512)
00000400        COMPLEX AVACF(512)
00000450        INTEGER ATCDR
00000500        DO 90 I=1,20
00000510 90     WW(I)=COS(3.14152*(I-1)/40)
00000520        DO 91 I=21,493
00000530 91     WW(I)=0.0
00000540        DO 92 I=494,512
00000550 92     WW(I)=COS(3.14152*(I-433)/40)
00000600        READ(3,350)ATCDR,NP,N1,N2,N3,N4,N5
00000610        DO 12 I=1,512
00000620 12     CUMACF(I)=CMPLX(0.0,0.0)
00000700 350    FORMAT(7I3)
00000800        DO 351 J=1,NP
00000900        READ(3,352)(IR(I),I=1,100)
00001100        WRITE (6,700)
00001200        WRITE (6,720)N1,N2
00001300        WRITE (6,740)
00001400        WRITE (6,760)N4
00001500        WRITE (6,780)
00001600        WRITE (6,800)N5
00001700        WRITE (6,820)
00001800        WRITE (6,200)(IR(I),I=1,100)
00001900        DO 6 I=1,100
00002000 6      KY(I)=IR(I)
00002050        CALL ZERDAV(KY,N3)
00002080        DO 7 I=1,100
00002100 7      X(I)=CMPLX(KY(I),0.0)
00002200        CALL FTCMPX(512,100,-1,X,W,L,1)
00002300        DO 8 I=1,512
00002400 8      X(I)=X(I)*CONJG(X(I))
00002450        WRITE (6,150)X
00002500        CALL FTCMPX(512,512,1,X,W,L,2)
00002600        DO 8 I=1,512
00002800 8      CUMACF(I)=CUMACF(I)+X(I)
00002900 351    CONTINUE
00002930        WRITE (6,920)
00003000        DO 9 I=1,512
00003050        CUMACF(I)=CUMACF(I)*WW(I)
00003100 9      AVACF(I)=CUMACF(I)/NP
00003200        CALL FTCMPX(512,512,-1,AVACF,W,L,2)
00003300        DO 10 I=1,512
00003400 10     AVPS(I)=REAL(AVACF(I))
```

"CPPRM" continued.

```
00003402          AVPS(I)=1.0
00003405          WRITE (6,900)
00003410          WRITE(6,420)(WW(I),I=1,512)
00003420          WRITE(6,420)(AVPS(I),I=1,512)
00003427          DO 14 I=1,512
00003430          PSDB(I)=10*ALOG10(AVPS(I))
00003435          CPS(I)=CMPLX(PSDB(I),0.0)
00003436 14       CONTINUE
00003440          CALL FTCMPX(512,512,-1,CPS,W,L,2)
00003445          DO 16 I=1,121
00003450          PSDBP(I,1)=PSDB(I+40)
00003460          FREQ(I)=(I+40)*1.95695
00003465          TIME(I)=I
00003470 16       CPSP(I,1)=REAL(CPS(I))
00003540          DATA IDENT/47,'0D~ATA 0C~OLLECTED                    0F~UN 0N~0
                 '/
00003550          WRITE(88,100) N1,N2,N5
00003555 352      FORMAT(10I0)
00003560 100      FORMAT(3I4)
00003570          READ(88,101) IDENT(7),IDENT(3),IDENT(12)
00003580 101      FORMAT(3A4)
00003590          CALL PPPLTI('LINF','LINF',6,5,FREQ,PSDBP,121,2,121,1,1,-5
                 ,0,
00003591         +'FREQUENCY/KHZ','POWER DISTRIBUTION/DBS',
00003592         +'POWER DISTRIBUTION FUNCTION',IDENT(2))
00003600          CALL PPPLTI('LINF','LINF',6,5,TIME,CPSP,121,1,121,1,1,-5,
                 0,
00003601         +'TIME/MICROSECS','CEPSTRUM','CEPSTRUM',IDENT(2))
00003790 900      FORMAT(1H0,'AVERAGE POWER SPECTRUM COMPUTED')
00004000 500      FORMAT(8E10.3)
00004100 700      FORMAT(1H1,'DATE DATA COLLECTED')
00004200 720      FORMAT(1H ,2I3,' 1975')
00004300 740      FORMAT(1H0,'SEDIMENT TYPE')
00004400 760      FORMAT(1H ,I3)
00004500 780      FORMAT(1H0,'RUN NUMBER')
00004600 800      FORMAT(1H ,I3)
00004700 820      FORMAT(1H0,'IMPULSE RESPONSE AVERAGED TO ZERO')
00004800 900      FORMAT(1H ,10I8)
00004750 920      FORMAT(1H0,'CUMULATIVE AUTOCORRELATION FUNCTION COMPUTED
                 )
00004260 150      FORMAT(1H0,'POWER SPECTRUM OF IMPULSE RESPONSE',I3,'COMP
                 TED')
00004870          WRITE(12,410)ATCOR,NF,N1,N2,N3,N4,N5
00004880          WRITE(12,500)(PSDB(I),I=1,512)
00004690 410      FORMAT(7I3)
00004900 420      FORMAT(1H ,8E12.4)
00004910          STOP
00004920          END
***END
?//
```

Program 3 "FINSOL"

```
00000100       DIMENSION PSDB(121),WSPS(121),FREQ(121)
00000200       DIMENSION TLDBP(121,2),IDENT(13)
00000300       INTEGER ATCDR
00000500       READ(3,350)ATCDB,NP,N1,N2,N3,N4,N5
00000600       READ(7,352)(WSPS(I),I=1,121)
00000700       READ(3,352)(PSDB(I),I=1,121)
00000800       DO 1 I=1,121
00001000  1    PSDB(I)=TLDBP(I)-ATCDB-WSPS(I)
00001100       DO 2 I=1,121
00001200       TLDBP(I,1)=-TLDBP(I)
00001300  2    FREQ(I)=(I+40)*1.95695
00001400       DATA IDENT/47,'@D~ATA @C~OLLECTED                    @R~UN @N~U
     */
00001500       WRITE(88,100)N1,N2,N5
00001700  100  FORMAT(3I4)
00001800       READ(88,101)IDENT(7),IDENT(8),IDENT(12)
00001900  101  FORMAT(3A4)
00002000       CALL PBPLTI('LINF','LINF',6,5,FREQ,TLDBP,121,2,121,1,1,-5
     .0,
00002100      +'FREQUENCY/KHZ','TRANSMISSION LOSS/DBS',
00002200      +'DECONVOLVED SEDIMENT TRANSFER FUNCTION',IDENT(2))
00002250       WRITE(6,353)(TLDBP(I,1),I=1,121)
00002300  350  FORMAT(7I3)
00002400  352  FORMAT(8E10.3)
00002500  353  FORMAT(1H ,8E10.3)
00002600       STOP
00002700       END
***END
?//
```

Subroutine "ZEROAV"

```
0100        SUBROUTINE ZEROAV(RY,N3)
0200        DIMENSION RY(100)
0300        SUM=0.0
0400        DO 1 I=1,N3
0500  1     SUM=SUM+RY(I)
0600        AVER=SUM/N3
0700        DO 2 I=1,N3
0800  2     RY(I)=RY(I)-AVER
0900        RETURN
1000        END
```

Subroutine "FTCMPX"

```
0100        SUBROUTINE FTCMPX(M,N,ISIGN,X,W,L,ICALL)
0200        DIMENSION W(I),L(I)
0300        COMPLEX X(I)
0400        IF(M.EQ.N)GO TO 6
0500        LL=N+1
0600        DO 2 I=LL,M
0700  2     X(I)=CMPLX(0.0,0.0)
0800  6     CALL CFAHRT(X,W,L,M,M,ISIGN,ICALL)
0900        RETURN
1000        END
```

Subroutine "CFAHRT" is an F.F.T. program written by Professor H.B. Voelcker, Department of Electrical Engineering, University of Rochester, New York.

BIBLIOGRAPHY

Albers, V.M., 1965, Underwater Acoustics Handbook II: Pennsylvania State University Press, University Park, Pa.

Ament, W.S., 1953, Sound propagation in gross mixtures: J. Acoust. Soc. Amer., v. 25, p. 638.

Anderson, O.K., On the distortion of measured correlation function caused by the frequency response of the measured system: D.I.S.A. Information.

Anderson, O.L., Lieberman, R.C., 1968, Sound velocities in rocks and minerals: experimental methods, extrapolations to very high pressures and results, in Physical Acoustics, principles and methods: W.P. Mason, editor, New York, Academic Press, p. 330-466.

Attwell, P.B., Ramana, Y.V., 1966, Wave attenuation and internal friction as functions of frequency in rocks: Geophys., v. 31, p. 1049-1056.

Bath, M., 1974, Spectral analysis in geophysics: Elsevier.

Bedford, A., Ingram, J.E., 1971, A continuum theory of fluid saturated porous media: J. App. Mech., v. 40, p. 657-661

Bennett, L.C. Jnr., 1967, In situ measurements of acoustic absorption in unconsolidated sediments (abstract): Trans. Am. Geophys. Union, v. 48, p. 144.

Bergland, G.D., 1969, A guided tour of the fast fourier transform: I.E.E.E. spectrum, V. 7, p. 41-51.

Bertram, S., 1970, Frequency analysis using the discrete fourier transform: I.E.E.E. Transactions on Audio and Electroacoust., V.Au. - 18, No. 4, p. 495-500

Bevington, M., 1969, Data reduction and error analysis for the Physical Sciences: McGraw Hill.

Bingham, C., Godfrey, M.D., Tukey, J.W., 1967, Modern techniques for power spectrum estimation: I.E.E.E. Trans. Audio. Electroacoust. V. Au-15, p. 56-66.

Biot, M.A., 1941, General theory of three dimensional consolidation: J. App. Phys. v. 12, p. 155-161.

Biot, M.A., 1955, Theory of elasticity and consolidation for a porous anisotropic: J. Appl. Phys., v. 22 (2).

Biot, M.A., 1956a, Theory of propagation of elastic waves in a fluid saturated porous solid (Low frequency case): J. Acoust. Soc. Amer., v. 28, p. 168-178.

Biot, M.A., 1956b, Theory of propagation of elastic waves in a fluid saturated porous solid (High freqency case): J. Acoust. Soc. Amer. v. 28, p. 179-191.

Biot, M.A., 1962a, Mechanics of deformation and acoustic propagation in porous media: J. Appl. Phys., v. 33, p. 1482-1498.

Biot, M.A., 1962b, Generalised theory of acoustic propagation in porous dissipative media: J. Accoust. Soc. Am., v. 34, p. 1254-1264.

Birch, F., 1961, The velocity of compressional waves in rocks to 10 kilobars Part 2., J. Geophys. Res., v. 66, p. 2199-2224.

Birch, F., 1966, Compressibility; elastic constants in handbook of physical constants. S.P. Clark Jnr., editor, Geol. Soc. Am. Memoir, v. 97, p. 98-174.

Blackman, R.B., Tukey, J.W., 1959, The measurement of power spectra: Dover, New York.

Blitz, 1964, Elements of acoustics: Butterworth and Co.,

Bobber, R.J., 1970, Underwater electroacoustic measurements: Naval Research Laboratory, A.D. 717-318.

Bogart, B.P., Healey, M.J.R., Tukey, J.W., 1962, The quefrency analysis of time series for echoes: Ceptstrum, Pseudo-autocovariance, cross-cepstrum and saphe cracking Time series analysis, Murray Rosenblatt, ed. New York: Wiley, 1963, p. 201-243.

Busby, J., Richardson, E.G., 1957, The absorption of sound in sediment: Geophys., v. 22, p. 821.

Cady, W.G., 1946, Piezoelectricity: McGraw and Hill, New York, p. 537-228.

Cohen, S.R., 1968, Measurement of the uncoelastic properties of water saturated clay sediments: Monterey, California, U.S. Naval Postgraduate School M.Sc. Thesis.

Cohen, T.J., 1970, Source-Depth determinations using spectral pseudo-autocorrelation and cepstral analysis: Geophys. J.R. Ash. Soc., v. 20, p. 223-231.

Cole, B.F., 1965, Marine sediment attenuation and ocean bottom reflected sound: J. Acoust. Soc. Am. v. 37, p. 211-297.

Darcy, 1856, Les fontaines publiques de la ville de Dijon: Dalmont, Paris.

Deresiewicz, H., Rice, J.T., 1962, The effect of boundaries on wave propagation in a liquid filled porous solid: III Reflection of plane waves at a free plane boundary (general case): Bull. Seis. Soc. Am., v. 52, No. 3, pp. 595-625.

Evans, P.E., Millman, R.S., 1964, The vibratory packing of powders: Powder Metallurgy, v. 7 (13), p. 50-63.

Faas, R.W., 1969, Analysis of the relationship between acoustic reflectivity and sediment porosity: Geophys., v. 34, No. 4, p. 546-553.

Fay, R.D., 1952, Waves in liquid filled cylinders: J. Acoust. Soc. Am., v. 24, p. 459-462.

Ferrero, M.A., Sacerdote, G.G., 1951, Acustica I, 137.

Fjell, P.O., 1976, Cross-correlation: J. Acoust. Soc. Am., v. 59, No. 2, p. 381-388.

Fry, J.C., Raitt, R.W., 1961, Sound velocities at the surface of deep sea sediments: J. Geophys. Res., v. 66, p. 589-597.

Gassman, F., 1951, Acoustical properties of aggregates of glass spheres: Geophys., v. 16, p. 673.

Geertsma, J., Smit, D.C., 1961, Some aspects of elastic wave propagation in fluid-saturated porous solids: Geophys., v. 26, p. 169-181

Glissen, T.H., Black, C.I., Sage, A.P., 1970, The digital computation of discrete spectra using the fast fourier transform: I.E.E.E. trans. aduio and Electroacoust., v. Au-18 (3), p. 271-287.

Hardin, B.O., Richart, F.E. Jnr., 1963, Elastic wave velocities in granular soils: J. Soil. Mech. and Foundations Div., Am. Soc. Civil Engin., S.M.I. p. 33-65 and discussions S.M.5. p. 103-118.

Hamilton, E.L., 1956, Low sound velocities in high porosity sediments: J. Acoust. Soc. Am., v. 28, p. 16.

Hamilton, E.L., 1963, Sound velocity measurements made in situ from Bathyscaph Trieste: J. Geophys. Res., v. 68, p. 5991-5998.

Hamilton, E.E., 1970a, Shear wave velocities in marine sediments (abstracts) Trans. Am. Geophys. Union. v. 51, No. 4, p.333

Hamilton, E.L., 1970b, Reflection coefficients and bottom losses at normal incidence computed from Pacific sediment properties: Geophys. v. 35, p. 995-1004.

Hamilton, E.L., 1971, Prediction of in situ acoustic and elastic properties of marine sediments: Geophys., v. 36, No. 2, p. 266-284.

Hamilton, E.L., 1972, Compressional wave attenuation in marine sediments: Geophys., v. 37, No. 4, p. 620-646.

Hamilton, E.L., 1976, Sound attenuation as a function of depth in the sea floor: J. Acoust. Soc. Am., v. 59, No. 3, P. 528-535.

Hamilton, E.L., Shumway, G., Menard, H.W. and Shipek, C.J., 1956, Acoustic and other physical properties of shallow water sediments of San Diego: J. Acoust. Soc. Am., v. 28, p. 1-15.

Hampton, L.D., 1966, Acoustic properties of sediments: Defence Research Laboratory, A.R.L. Report No. 254, University of Texas.

Hampton, L.D., 1967, Acoustic properties of sediments: J. Acoust. Soc. Am., v. 42, p. 882-890.

Hastrup, O.F., 1970, Digital analysis of acoustic reflectivity in the Tyrrhenian Abyssal Plain: J. Acoust. Soc. Am., v. 47, No. 1., Pt. 2.

Heuter, T.F., Bolt, R.H., 1955, Sonics: Wiley and Sons Inc., N.Y.

Hewitt, C., 1955, Seismic velocities from surface measurements: Geophys., v. 20., No. 1., p. 68-86.

Hodgkiss, W.S., Noue, L.W., 1976, Covariance between fourier coefficients representing the time waveforms observed from an array of sensors: J. Acoust. Soc. Am., v. 59, No. 3, p. 582-590.

Hopkins, J., Dyer, C., 1971, Internal report, University of Bath, Feasability study of sub-bottom profiling.

Horn, D.R., Horn, B.M., and Delach, M.N., 1968, Correlation between acoustical and other physical properties of deep sea cores: J. Geophys. Res., v. 73, p. 1939.

Hsieh, L., Yew, C.H., 1973, Wave motions in a fluid saturated porous media: J. App. Mech., v. 40, p. 657-661.

Hunter, A.N., Legg, R., and Malutawa, E., 1961, Measurements of acoustic attenuation and velocity in sand: Acustica v. 11, p. 26-31.

Iida, K., 1939, Velocity of elastic waves in a granual substance: Bull. Earthquake Res. Inst., v. XVLL, p. 783-807.

Inman, D.L., 1952, Measures for describing the size distribution of sediments: J. Sediment Petrol., v. 22 (3), p. 125-145.

Kanasewich, E.R., 1975, Time sequence analysis in Geophysics: The University of Alberta Press.

Kemerait, R.C., Childer, 1972, Signal detection and extraction by cepstrum techniques: I.E.E.E. Transactions on information theory, v. 1T-18, No. 6, p. 745-759.

Kinsler, L.E., Frey, A.R., 1962, Fundamentals of acoustics: Wiley and Sons, N.Y.

Knopoff, L., MacDonald, G.J.F., 1958, Attenuation of small amplitude stress waves in solids: Rev. Modern Physics, v. 65, p. 2191-2197.

Knopoff, L., 1965, Attenuation of elastic waves in the earth in physical acoustics: W.P. Mason, editor, New York Academic Press, v. IIIB, p. 287-324.

Laughton, A.S., 1957, Sound propagation in compacted ocean sediments: Geophys., v. 22, p. 233.

Lewis, L.F., 1971, An investigation of ocean sediments using the deep ocean sediment probe: Univ. of Rhode Island, Ph.D. thesis. p. 76.

Mackenzie, K.V., 1959, Reflections of sound from coastal bottoms: J. Acoust. Soc. Am., v. 32, (2), p. 221-231.

Mason, W.P., 1950, Piezoelectric crystals and their application to ultrasonics: Van Nostrand, New York.

McCann, D.M., 1972, Measurement of the acoustic properties of marine sediments: Acustica, v. 26, p. 55-66.

McCann, C., McCann, D.M., 1969, The attenuation of compressional waves in marine sediment: Geophys., v. 34, p. 882.

McDonald, F.J., Angona, F.A., Mills, R.L., Sengbush, R.L. Van Nostrand, R.G. and White, J.E., 1958, Attenuation of shear and compressional waves in Pierre shale: Geophys., v. 23, p. 421-439.

McLeroy, E.G., Deloach, A., 1968, Sound speed and attenuation from 15 to 1500 Kh measured in natural sea floor sediments. J. Acoust. Soc. Am., v. 44, p. 1148-1150.

McSkimin, H.J., 1961, Notes and references for the measurement of elastic moduli by means of ultrasonic waves: J. Acoust. Soc. Am. v. 33, p. 606-615.

McSkimin, H.J., 1964, Ultrasonic methods for measuring the mechanical properties of liquids and solids: Physical Acoustics I Part A, p. 272-330. Academic Press, New York.

Mifsud, J.F., 1953, Experimental study of acoustic properties of water filled sands: Univ. of Texas, D.R.L. A-72.

Mizikos, J.P., 1972, Attenuation of longditudinal sound waves in unconsolidated sediments with gravity dependent cohesion: Geophys. Prosp., in press.

Morgan, N.A., 1964, Geophysical studies in Lake Erie by shallow marine seismic methods: Unpublished Ph.D. dissertation. University of Toronto, Canada.

Morse, R.W., 1952, Acoustic propagation in granular media: J. Acoust. Soc. Am., v. 24, p. 696-700.

Mouselli, A., 1974, Experimental investigation of stress wave attenuation in gas-saturated rocks: Ph.D. dissertation, University of Texas, Austin, unpublished.

Neprochnov, Y.P., 1971, Seismic studies of the crustal structure beneath the seas and oceans: Oceanology II, p. 709-715.

Nolle, A.W., 1963, Acoustic properties of liquid filled sands - Defence Research Lab., Univ. of Texas - Public D.R.L. - A-63.

Nolle, A.W., Hoyer, W.A., Mifsud , J.F., Runyon, W.R., Ward, M.B., 1963, Acoustical properties of water filled sands: J. Acoust. Soc. Am., v. 35, p. 1394.

Pace, N.G., 1975, Sediment identification using acoustic impulse techniques: Proceedings Ultrasonics International, Imperial College, London. I.P.C. Science and Technology Press, p. 245-248.

Paterson, N.R., 1956, Seismic wave propagation in porous granular media: Geophys., v. 21, p. 691-714.

Peselnick, L., Outerbridge, W.F., 1961, Internal friction in shear and shear modules of solenhofen limestone over a frequency range of 10^7 cycles per second: J. Geophys. Res., v. 66, p. 581-588.

Press, F., 1966, Seismic velocities: Geol. Soc. Am. Memoir, v. 97, p. 195-218.

Ricker, N., 1953, Wavelet contraction, wavelet expansion, and the control of seismic resoltuion: Geophys., v. 18, p. 769-792.

Roderick, R.L., and Truell, R., 1952, The measurement of ultrasonic attenuation in solids by Pulse Technique and some results in steel: J. App. Physics., v. 23, No. 2, p. 267-279.

Schafer, R.W., 1968, Echo removal by discrete generalized linear filtering: Ph.D. Dissertation, Mass. Inst. Technol., Cambridge.

Schirmer, F., 1970, Schalleusbreitung im Schlick: Deut. Hydrogr. 2 Janr. 23, Heft 1, p. 24-30.

Schomer, P.D., 1972, Measurement of sound transmission loss by combining correlation and fourier techniques: J. Acoust. Soc. Am., No. 4 (I) p. 1127-1141.

Schreiber, B.C., 1968, Sound velocity in deep sea sediments: J. Geophys. Res., v. 73, p. 1259.

Shumway, G., 1956, A resonant chamber method for sound velocity and attenuation measurements in sediments: Geophys., v. 21, p. 305-319.

Shumway, G., 1958, Sound velocity versus temperature in water saturated marine sediments: Geophys., v. 23, p. 494-505.

Shumway, G., 1960, Sound, speed and absorption studies of marine sediments by a resonance method: Part I: Part II, Geophys., v. 25, p. 451-467, 659-682.

Salkield, A.P., 1975, Acoustic Backscattering from granular material: Unpublished Ph.D. thesis, University of Bath.

Shumway, G., and Igelman, K., 1960, Computed sediment grain surface areas: J. Sed. Petrology, v. 30, p. 486-489.

Sutton, G.H., Berckhemer, H., Nafe, J.E., 1957, The physical analysis of deep sea sediments: Geophys., v. 22, p. 779.

Swartz, R.L., Eggen, C.J., 1976, Simplified model of the spectral characterisitics of high frequency surface scatter: J. Acoust. Soc. Am., v. 59, No. 4.

Taylor Smith, D., 1975, Geophysical assessment of sea floor sediment properties: Proceedings oceanology International, p. 320-328.

Taylor Smith, D., Li, W.N., 1966, Echo sounding and sea floor sediments: Marine Geol., v. 4, p. 253.

Toulis, W.J., 1956, Thoery of a resonance method to measure the acoustic properties of sediments: Geophys., v. 21, p. 299-304.

Tucker, D.G., and Gazey, B.K., 1966, Applied underwater Acoustics: Pergamon Press Ltd., Oxford.

Tullos, F.N., and Reid, C., 1969, Seismic attenuation of Gulf Coast sediments: Geophys., v. 34, p. 516-528.

Ulonska, A., 1968, Versuche zur mersung der schaugeschwindigkeit und schalldampfund in sediment in situ: Deut. Hydrogr. Z Jahr. 21, Heft 2, p. 49-58.

Urick, R.J., 1947, The absorption of sound in suspensions of irregular particles: J. Acoust. Soc. Am., v. 20, p. 283 (1948) and J. App. Phys., v. 18, p. 983 (1947).

Walton, K., 1975, Elastic wave propagation in model sediments, Parts I and II and Effective elastic moduli of model sediments: Geophys. J.R. Soc., v. 43, p. 1-13.

Weston, D.E., Wood, A.B., 1964, Propagation of sound in muds: Acustica, v. 14, p. 157.

White, J.E., 1965, Seismic waves: radiation transmission and attenuation: New York: McGraw Hill Book Co. Inc.

Whitman, R.V., Holt, R.J., Murphy, V.J., 1969, Discussion of vibration modules of normally consolidated clay by B.O. Hardin and W.L. Black: J. Soil Mech. and Foundation Div., Am. Soc. Civil Engin. SM2, p. 656-659.

Wood, A.W., 1941, A textbook of sound: The Macmillan Company, New York.

Woods, J.P., 1956, The composition of reflections: Geophys., v. 21, p. 261.

Wyckoff, R., 1963, Crystal Structures: Univ. of Arizona, 2nd Ed., v. 1, Wiley and Sons.

Wyllie, M.R.J., Gregory, A.R., Gardner, G.H.F., 1956, Elastic wave velocity in heterogeneous and porous media: Geophys. XXI, p. 41-70.

Wyllie, M.R.J., Gardner, G.H.F., Gregory, A.R., 1962, Studies of elastic wave attenuation in porous media: Geophys., v. 27, p. 569-589. Addendum, Geophys. v. 28, p. 1074 (1963).

Yew, C.H, Jogi, P.N., 1976, Study of wave motions in fluid saturated porous rocks: J. Acoust. Soc. Am., v. 60., No. I.

Yong, R.N. and Warkertin, B.P., 1966, Introduction to soil behaviour: New York, The Macmillan Co.

Zemtsov, E.E., 1969, Effect of oil and gas deposits on dynamic characteristics of reflected waves: Int. Geology Rev., V.II, p. 504-509.

Zwikker, C., Kosten, C.W., 1949, Sound absorbing materials: Elsevier Publishing Company Inc., New York.